Electrochemical Energy Reviews (2021) 4:680–717
https://doi.org/10.1007/s41918-021-00100-y

REVIEW ARTICLE

Electrolyzer and Catalysts Design from Carbon Dioxide to Carbon Monoxide Electrochemical Reduction

Jingfu He[1] · Yuanli Li[2] · Aoxue Huang[3] · Qinghua Liu[4] · Changli Li[1]

Received: 24 June 2020 / Revised: 27 November 2020 / Accepted: 4 February 2021 / Published online: 15 April 2021

Abstract

Electrochemical CO_2 reduction reaction (CO_2RR) has attracted considerable attention in the recent decade for its critical role in the storage of renewable energy and fulfilling of the carbon cycle, and catalysts with varying morphology and modification strategies have been studied to improve the CO_2RR activity and selectivity. However, most of the achievements are focused on preliminary reduction products such as CO and HCOOH. Development and research on electrochemical CO reduction reaction (CORR) are considered to be more promising to achieve multicarbon products and a better platform to understand the mechanism of C–C formation. In this review, we introduce the current achievements of CO_2RR and emphasize the potential of CORR. We provide a summary of how electrolysis environment, electrode substrates, and cell design affect the performance of CORR catalysts in order to offer a guideline of standard operating conditions for CORR research. The composition–structure–activity relationships for CORR catalysts studied in H-cells and gas-phase flow cells are separately analyzed to give a comprehensive understanding of the development of catalyst design. Finally, the reaction mechanism, latest progress, major challenges and potential opportunities of CORR are also analyzed to provide a critical overview for further performance improvement of CORR.

Keywords Electrolysis · CO reduction · Flow cell design · Copper catalysts

1 Introduction

As the global energy supply continues to transition from fossil fuel toward carbon–neutral energy sources (e.g., electricity from solar energy or wind), it is imperative to develop an efficient electrochemical reaction to store the intermittent renewable electricity by means of produce fuels and feedstock chemicals [1–6]. Electrochemically converting carbon monoxide into valuable chemicals is one of the most attractive reactions because of its great potential for the storage of renewable electricity and the operation in relatively mild conditions, making it possible to replace the high-temperature and high-pressure Fischer–Tropsch reaction that relies on fossil energy [7, 8]. Great efforts have been devoted to the investigation of varying composition and morphology of catalysts for improvement of the CO_2RR activity and selectivity. After years of intense research, the electrochemical CO_2–to–CO technique is highly developed with high selectivity and energy conversion efficiency, while the electrochemical CO_2–to–$C_xH_yO_z$ conversion technique is far from mature [9–18]. There has been growing interest in this CORR process due to its emerging role as a sequential route for reducing CO_2 into multi-carbon products. From the techno-economic analysis, the sequential process of CO_2RR and CORR is more likely to overcome the barriers of chemical products to the market entry [19–21].

In the previous research, Cu is found to be the only catalyst that can reduce CO_2 to hydrocarbons with both high reaction rates and high selectivity [22]. By changing the

✉ Jingfu He
hejf27@mail.sysu.edu.cn

✉ Changli Li
lichli5@mail.sysu.edu.cn

1 School of Materials, Sun Yat-sen University, Guangzhou 510275, Guangdong, China

2 Fundamental Science on Nuclear Wastes and Environmental Safety Laboratory, Southwest University of Science and Technology, Mianyang 621010, Sichuan, China

3 Department of Chemistry, The University of British Columbia, Vancouver, BC V6T1Z1, Canada

4 National Synchrotron Radiation Laboratory, University of Science and Technology of China, Hefei 230029, Anhui, China

surface morphology, atomic structure, and electronic structure of Cu, the reaction path can be adjusted, and the reaction selectivity can be tuned toward special products such as ethylene, methane, and CO. The research of CORR is usually treated as a branch of CO_2RR research because CO is the key intermediate in the CO_2–to-hydrocarbon/oxygenate process on Cu catalysts [13, 23–25]. However, many recent pieces of research revealed that the selectivity of CORR is apparently different from CO_2RR on the copper catalyst, as CORR is preferable for oxygenate and C3 products [7, 26, 27]. For example, CORR on polycrystalline copper can produce > 70% oxygenate products in comparison with ~ 50% C_2H_4 and < 30% oxygenate for CO_2RR on copper [26, 27]. Moreover, the different solubility and acidity of CO_2 and CO result in their different interactions with electrolytes and, in turn, different electrolysis behaviors [28]. Therefore, we should consider CORR as an independent research field rather than the incidental of CO_2RR and develop its own test system, including the establishment of a standard testing environment, design of the flow reactor, and the development of CORR catalysts toward specific selectivity.

Only very recently has the uniqueness of CORR been concerned, and the effort has been devoted to exploring the different behaviors of catalysts for CORR and CO_2RR. Several factors may be responsible for the difference: (1) sufficient CO supplies near the surface of catalysts may benefit certain C2+ reaction pathway of CORR which is diminished in CO_2RR due to the insufficient surface coverage of adsorbed *CO (* for adsorbed groups) and a large activation barrier for C–C coupling. (2) The CO intermediate produced by CO_2 reduction would be further reduced at the same site, while free CO molecules would form an adsorption–desorption equilibrium with the catalysts and be reduced at different sites toward different products [29]. Nevertheless, the design of the catalyst for CORR is still in its infancy [7, 30, 31], and the information between the structure of catalytic sites and CORR performance is still lacking and requires intense research.

A key reason for the slow development of CORR catalysts is the low solubility of CO in aqueous solution. As most results achieved on non-gas diffusion electrodes in H-cells, the limited diffusion current density of CORR is below 1 mA cm^{-2} [32]. The low current density in such a system hindered the collection of minor intermediate products to explore the reaction pathway of CORR. The kinetic information from these low reaction rate experiments cannot necessarily transfer to the dynamic environment of an electrolyzer, which operates under a 0.5–1.0 A cm^{-2} reaction rate. The development of a CORR flow reactor, in which the mass transport limitations can be overcome by continuously circulating reactants and products, needs to be first considered for the benefit of guiding and comparing future research. In research areas such as fuel cells, water splitting, and CO_2 reduction, flow reactors have been systematically developed, resulting in a much in-depth understanding of catalyst behavior under a dramatic reaction environment [33–35]. However, the investigation of CORR in a flow reactor is still in its early stage [27, 36]. A fundamental understanding of the gas supply mode, electrode substrate design, whole-cell configuration, electrolyte concentration, and cation and anion composition is necessary to guide the construction of a highly efficient CORR system toward industrial application.

In this review, we focus on the reaction mechanism and the latest progress of carbon monoxide reduction, providing a critical overview regarding the current state and challenges in this system that is relevant to further performance improvement. The comparison between CO_2RR and CORR shows that the development of CORR would greatly contribute to the improvement of multicarbon products and mechanism understanding. A summary of how electrolysis environment, electrode substrates, and cell design affect the performance of CORR catalysts is discussed in order to offer a guideline of standard operation for CORR research. The composition–structure–activity relationships for CORR catalysts studied in H-cells and gas-phase flow cells are separately analyzed to give a comprehensive understanding of the development of catalyst design. Moreover, in situ and *operando* characterizations that help to clarify the reaction pathways and the dynamic evolution of catalysts during the reaction are also highlighted. Finally, we present the major challenges and potential opportunities that may exist for future CORR development.

2 The Current State of CO_2RR

The CO_2RR is of great interest to the renewable energy and environment research community and has been investigating for several decades. In particular, Hori and coworkers systematically analyzed the CO_2RR activity and selectivity on a series of different metal foils and in different electrolytes, which are still used as the standard reference in CO_2RR study nowadays [22, 37]. In the recent decade, an increasing global effort has been driven into this research topic due to the development of renewable energy electrochemistry.

Numerous CO_2RR catalysts with varying morphology and composition have been designed, fabricated, and studied in the last decade [9, 11, 38–51]. One sample modification method that needs to be specifically emphasized is the oxide-derived (OD) method for metal catalysts, which greatly enhances the catalytic geometric current density and suppresses the competing hydrogen evolution reaction (HER) [9, 38, 39]. According to the studies by Kanan and coworkers, the enhanced performance of OD catalysts mainly originated from the high surface area and high density of grain boundaries [52–54]. Another advantage of

these types of catalysts is that the synthesis process is facile and can be easily reproduced by other research groups as a standard comparison. Despite all these efforts, only CO and HCOOH products can be generated with near-100% faradaic efficiency, by using catalysts of Ag/Au and Sn/Bi/In, respectively. The formation of C_2H_4 with > 50% selectivity can be achieved on Cu catalysts by manipulating the morphology, but the controlling of other deep-reduced products is still very preliminary. On the other hand, a much deeper understanding of the influence of the environment on the behavior of catalysts is obtained during recent research [55]. High current densities and *FE* have been achieved for CO_2–to–CO, CO_2–to-HCOOH, and CO_2–to–C_2H_4 in a gas-phase flow cell [56–58].

2.1 Mechanism for CO_2RR

2.1.1 Initial Activation of CO_2 Molecules on Different Mono-Metals

Based on the CO_2RR selectivity, the mono-metal catalysts can be divided into four different groups. Group 1 of Pb, Hg, In, Sn, Cd, Tl, and Bi has high selectivities toward HCOOH; Group 2 of Au, Ag, Zn, Pd, and Ga favors the evolution of CO; Group 3 of Cu is the only metal that has high selectivity of hydrocarbon; other common transition metals such as Fe, Ni, Co, Mn, and Pt are categorized into Group 4 and dominated by the side reaction of HER. It is very interesting that the metals with similar CO_2RR selectivity are adjacent to each other in the periodic table, indicating that the CO_2RR selectivities are determined by electronic properties. A simple metal–CO adsorption model has been developed to explain the origination of selectivities by Hori and coworkers [22]. The CO_2RR reaction pathways can be categorized into the HCOOH pathway and the CO pathway, and the later one includes all the other three groups of metal except Group 1. For reaction following the CO pathway, the CO_2 would be absorbed on the surface of the catalyst and then quickly reduced to CO. After that, the adsorption strength (i.e., the CO heat of adsorption ΔH_{CO}) would determine the ultimate product. Au and Ag own low ΔH_{CO} and will release CO as the final product once it is produced, whereas Cu can bond CO much stronger so that CO can be further reduced to deep-reduced hydrocarbon products. Notably, the bonding strength between Cu and CO is strongly influenced by the surface facet and catalysts morphology, resulting in different CO_2RR selectivities. In the early research of Hori's group, the evolution of C_2H_4 is more favored on Cu(100) compared with the Cu(111) electrode, and the introduction of (111) steps to the Cu(100) basal plane can further promote C_2H_4 formation and suppress CH_4 formation [59]. Wang and coworkers reported that open facets such as (110) on Cu nanowires have strong activity for CO_2 reduction to CO at low overpotential (> − 0.5 V) [60]. Unfortunately, the ΔH_{CO} of transition metals such as Fe, Ni, Co, Mn, and Pt is too high. Thus, a CO monolayer would quickly be formed on the surface of the catalyst. The CO_2RR is therefore ceased, while the HER can still occur through the electron tunneling across the CO monolayer.

Under the CO_2RR environment, HCOOH cannot be further reduced. Therefore, the HCOOH pathway only corresponds to this single product. However, the reaction pathway for HCOOH formation is still under debate. Apparently, most of the HCOOH-producing catalysts are inert electrode materials in electrochemistry, which usually endow large work functions and can provide electrons for bonding. There are two types of hypotheses for the HCOOH formation. The first theory assumed that there is no bonding between CO_2 and metal, and electrons are directly injected into the CO_2 molecules dissolved in the electrolyte [37, 61]. The other hypothesis suggests that although those catalysts cannot provide electrons to form the M–C bond with CO_2, they can otherwise bond with the O atoms in CO_2 [62, 63]. The former hypothesis is not adopted in recent research, especially for Sn and In, because the theoretical electrode potential to form the CO_2^- intermediate structure is very negative (− 1.9 V vs. NHE) and cannot explain the onset potential (e.g., ~ − 1.0 V vs. NHE) observed in experiments.

The activation of CO_2 molecules was once considered to be very difficult, because of the forming of nonlinear intermediate CO_2^- from linear CO_2 molecules. However, the bonding between metal and the C center of the CO_2 molecule could stabilize the intermediate and greatly lower the overpotential for the reaction. As a two-electron electrochemical reaction normally has one intermediate structure, the overpotential can be minimized with optimal catalysts, as evidenced by the near-zero overpotential for CO_2RR on enzyme or biological catalysts [64]. Generally, the first step of CO_2–to–CO and CO_2–to–HCOOH reaction on catalysts would be proton-coupled electron transfer reaction, with *COOH to be the intermediate of CO evolution and *OCHO to be the intermediate of HCOOH formation, as shown in Fig. 1. The experiment from Jaramillo and coworkers on Sn and other metal electrodes further supports this theory [63]. Sn electrode can produce both CO and HCOOH as products, and this would be a promising candidate for the study of composition–activity relationship. In this experiment, the CO evolution activity of Sn, Ag, Au, Cu, Zn, Pt, and Ni is measured and plotted as the function of *COOH adsorption strength. Clearly, there is a volcano shape relationship between CO evolution rate and *COOH adsorption strength. From the volcano relationship, it is found that Au is the best catalyst, stronger bonding metals of Cu and Pt situated at the left side and weaker bonding metals of Ag and Sn located at the right side. However, this model cannot explain the activity for HCOOH formation, unless the *OCHO is

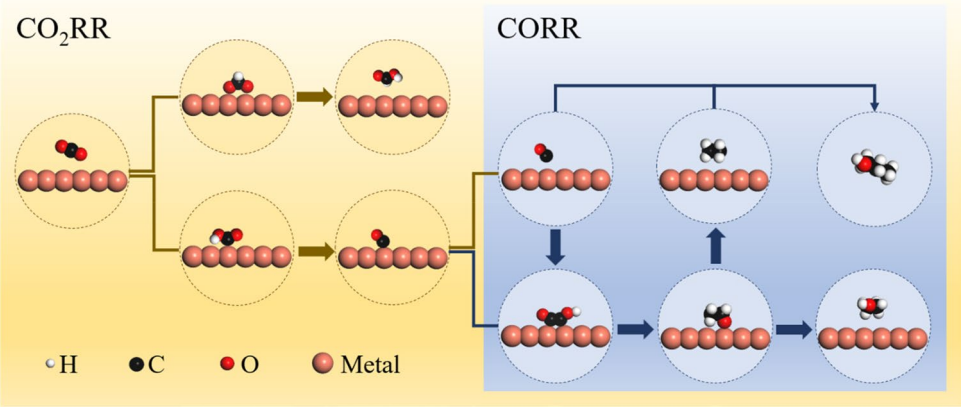

Fig. 1 The scheme of reaction pathways for CO_2RR and CORR. Black spheres, carbon; red spheres, oxygen; white spheres, hydrogen; orange spheres, the (metal) catalyst. CO_2 molecules can be bonded to metal by O–M bonds or C–M bonds, which lead to the formation of formate or CO, respectively. CORR starts from the adsorption of dissolved CO in the electrolyte or free CO molecules in the gas phase, while the key intermediate of CO in CO_2RR is bonded to the surface of catalysts and may not be released. Three attractive products of ethylene, ethanol and propanol can be produced by both CORR and CO_2RR but with different selectivities due to the different reaction sites

considered to be the critical intermediate structure instead. By plotting the HCOOH formation rate as the function of adsorption strength of *OCHO, for which intermediate is bonded with metal through two M–O bonds, a volcano shape relationship can be obtained. In this scheme, Sn is the best HCOOH formation catalyst, and the stronger bonding metals of Zn and Ni located at the left side and weaker bonding metals of Cu, Pt, Ag, and Au positioned at the right side. Notably, this mechanism cannot be applied to molecular catalysis of CO_2RR. For a typical molecular catalyst, such as cobalt-(proto)porphyrin, the metal center would be firstly reduced to a lower valence state, and then, it would adsorb and reduce the CO_2 molecule [65]. Proton transfer and electron transfer are thus decoupled.

2.1.2 Deep Reduction of CO_2 Molecule via C–C Bonds Formation

Compared with the understanding of CO and HCOOH formation, the model for deeply reduced products is much more preliminary. Considering the multi-carbon products of CO_2RR usually have higher energy density and commercial value, the investigation of C–C bond formation is of top priority in CO_2RR research. The CO_2RR performed on Cu (111) and (100) single crystalline orientation indicated that there are two different reaction pathways for C_2H_4 coupling. On the Cu (111) face, the C_2H_4 formation has a high overpotential and shares the same intermediate structure with CH_4, while on the Cu (100) face, the overpotential for C_2H_4 formation is low with few by-products. Notably, the C_2H_4 formation on Cu (100) is pH independent; thus, its selectivity compared with HER or CH_4 evolution can be promoted by increasing the pH value of the electrolyte or using a weak buffering electrolyte. The pH independent of C_2H_4 formation indicates that the rate-limiting step of C–C bonding is a decoupled proton–electron transfer process, which is proved by many DFT calculations [66, 67]. The critical intermediate structure of OCCOH was also observed in a recent operando IR experiment, which will be discussed in detail in 5.1.

Besides C_2H_4, ethanol and acetaldehyde are also the main C2 products from CO_2RR. These products are believed to share a common intermediate because they have similar pH dependency. The formation of acetate needs to be taken with caution because the disproportionation of acetaldehyde in the alkaline electrolyte can also produce acetate [68]. C3 products such as propanol are only reported in a small part of CO_2RR research, and the mechanism is not studied in-depth. A hypothesis is that propanol is formed through the coupling of CO and C_2H_4 on the catalyst surface. A series of catalysts have been designed in Sargent group based on this hypothesis and will be discussed in Sect. 4.2.2.

2.2 Catalysts development for CO_2RR

Based on the fundamental research of CO_2RR on traditional mono-metal catalysts, numerous catalysts with different metal/non-metal compositions, organic coordination, morphologies and space mixing patterns are designed and tested to realize high selectivity and energy conversion efficiency of CO_2RR, as shown in Fig. 2.

Kanan group was the first to systematically study the oxide-derived (OD) copper and gold catalysts for CO_2RR, which were synthesized by thermal or electrochemical oxidation and then reduced in situ in the electrochemical reduction process [7, 9, 38]. Their research showed that the OD catalysts could greatly suppress the hydrogen evolution

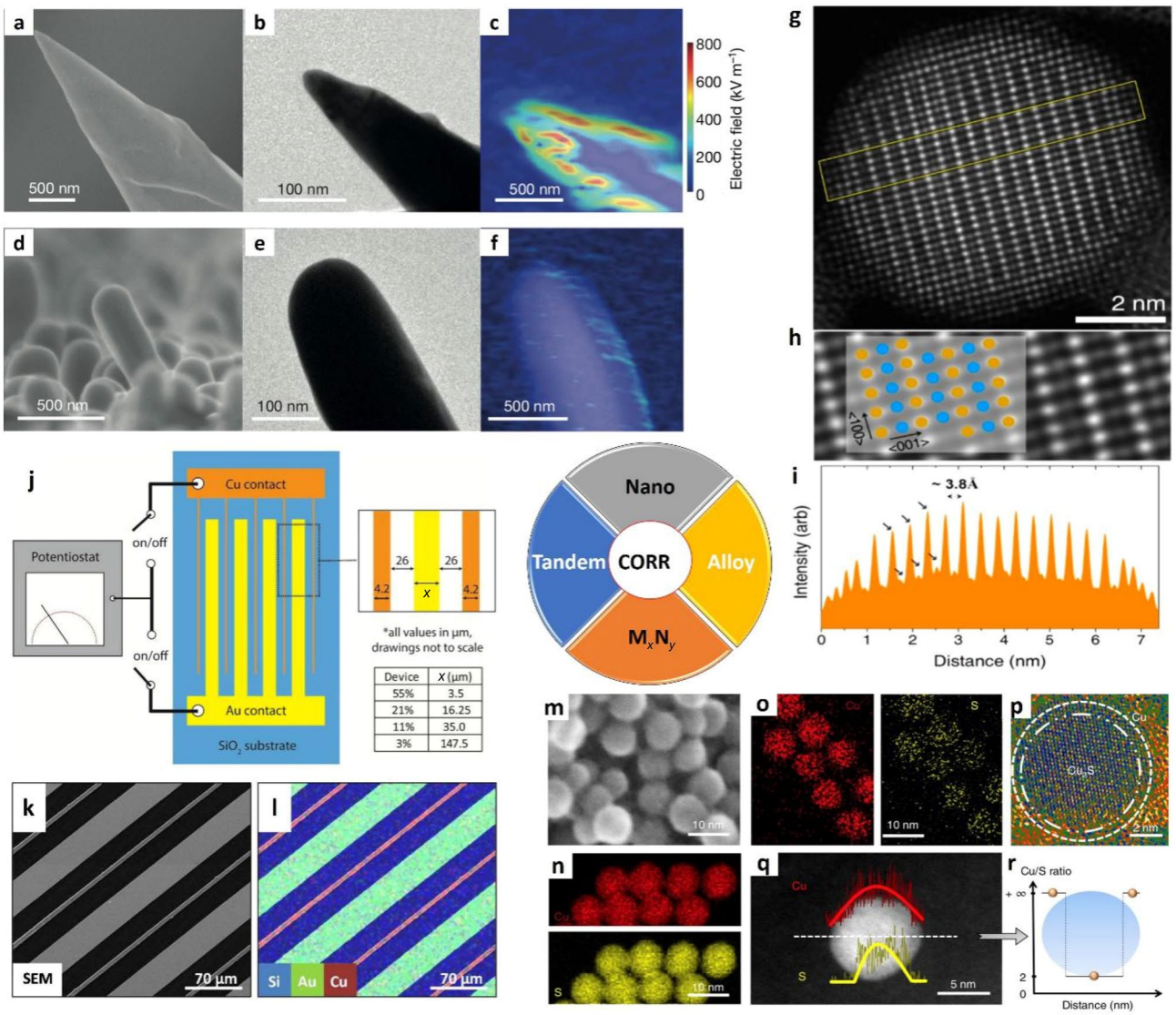

Fig. 2 **a**–**f** Typical nanostructured catalysts for CO_2RR. Adapted with permission from Ref. [10]. Copyright © 2016, Springer Nature. **a** Scanning electron microscopy (SEM) image. **b** TEM image and **c** electric field distribution of Au needles. **d** Scanning electron microscopy (SEM) image. **e** TEM image and **f** electric field distribution of Au rods. The sharp tip of electrodes would result in a high concentration of K^+ near the electrode and thus result in high CO_2RR activity. **g**–**i** AuCu alloy particles with ordered arrangement of two elements. Adapted with permission from Ref. [76]. Copyright © 2017, American Chemical Society. **g** Aberration-corrected HAADF-STEM image of AuCu nanoparticles. **h** Magnified STEM image of the center of the particle. Atoms in orange and blue colors represent gold and copper, respectively. **i** Intensity profile across the particle measured from the yellow box shown in **g**. Arrows indicate alternating high and low intensities, which represent gold and copper atoms, respectively. **j**–**l** Tandem design of AuCu bimetallic electrodes. Adapted with permission from Ref. [77]. Copyright © 2018, Royal Society of Chemistry. **j** Schematic of the interdigitated AuCu device. Externally connected on/off switches linked to a potentiostat can control the power supply on Au and Cu lines, separately. *X*% in table refers to the ratio of the geometric area of the Cu lines to the total metal area. **k** SEM and **l** EDX images of the 11% AuCu device with Si in blue, Au in green and Cu in red. **m**–**r** Typical metal–nonmetal compounds (M_xN_y) of Cu_2S for CO_2RR. Adapted with permission from Ref. [47]. Copyright © 2018, Springer Nature. **m** TEM and **n** EDS mapping of vacancy-rich Cu_2S nanoparticles. **o** EDS mapping, **p** high-resolution TEM, **q** EDS line scans and **r** the ratio of Cu/S concentration of vacancy-rich Cu_2S nanoparticles after electrochemical reduction, showing that S is removed from the nanoparticle surface

and enhance the CO_2RR geometric current densities at low overpotential. Later on, reports of other metal oxide-derived catalysts, such as AgO_x, SnO_x, ZnO_x, BiO_x, also exhibited much enhanced activity of CO_2RR compared with opponents that had not undergone this oxidation–reduction process [39, 69–71]. There is still a strong controversy on the origination of catalytic performance on these types of catalysts. One controversial issue is whether oxide contributes

to the performance of OD catalysts during operation. Theoretically, the aforementioned metal oxide is expected to be reduced at potential of CO_2RR due to their positive standard electrode potential of M/M^{n+}. However, many *operando* experiments show that a low remnant concentration of oxygen may remain in the crystal lattice even though the main body of catalysts is transferred from metal oxide to metal [72–74]. The remnant oxygen might change the electric structure of the metal center to influence the catalytic performance. Other outstanding features of OD catalysts are their extremely large surface area and special surface/interface structure that originates from the structure evolution during CO_2RR. For instance, Kanan group reported that OD catalysts have a high density of grain boundaries and assumed that grain boundaries could support reaction intermediate by providing a special distribution and construction of catalytic sites [53, 54]. Generally, the structure evolution of catalysts is very complex during the oxidation–reduction process, and the performance of OD catalysts may originate from comprehensive factors of composition, surface area and unique catalytic sites.

Other metal and nonmetal compounds, such as halogen compounds [45, 46], chalcogenides [47, 48, 51], and nitrides [49, 50] are recently studied in CO_2RR and exhibit promising CO_2RR activity. They also suffered from instability during CO_2RR, and the compound would be gradually converted into metal. However, the different bonding strength between metal and halide, chalcogen or nitrogen would result in different morphology, catalytic sites and electric structure compared with OD catalysts. Notably, these pre-catalysts provide an excellent parameter library for adjusting the performance of Cu-based catalysts, because Cu catalyst is very sensitive to tiny change of electric or atomic structure. Such as the case reported for Cu_2S nanoparticle catalysts (Fig. 2 m–r), the sulfur is indeed retained to a certain extent during operation, thus modifying the electronic structure of the catalyst toward higher selectivity for C2 products [47]. By controlling the composition of copper halide, the as-prepared catalyst microcrystals can be electrochemically transformed into three types of Cu nanostructures with completely different morphologies to optimize the CO_2RR selectivity toward C2 products [75].

Alloy catalysts are another group of catalysts that are systematically studied and some promising progress in mechanism understanding and performance are also achieved. It is assumed that by changing the composition of surface atoms, the bonding strength of catalyst with reactants or intermediates can be manipulated to boost the CO_2RR activity toward one certain product, such as CO, HCOOH or specific hydrocarbon compound. In view of this, the synthesis of the alloy catalysts is a mature way to selective produce CO and HCOOH.

The early research on alloy catalysts mainly focused on Au-based catalysts because Au is the catalyst that possesses a high CO_2 reduction current density and a high CO product selectivity [78]. Au-based alloy such as Au–Cu and Au–Fe [40, 79] exhibited even higher activity toward CO evolution (Fig. 2g–i) compared with the Au catalyst and at the same time reduce the usage amount of precious metals. In the research work of Yang and coworkers, this change in selectivity and activity of AuCu was believed to be directly related to the adjustment of the Fermi surface [40, 76], which in turn enhanced the CO evolution. The later research also found that the alloying of Cu with electrochemical inert metals such as In or Sn can realize excellent CO evolution catalysts, which is comparable to the performance achieved on Au and Ag [11, 41, 42]. It can be explained by a hypothesis that the alloy should have a CO adsorption heat ΔH_{CO} value in between of the two individual metals. In the above cases, the CO adsorption heat ΔH_{CO} value of typical Au and Ag catalysts are saddled by that of Cu and Sn/In, and thus, the mixing of Cu and Sn/In leads to the formation of highly efficient CO_2RR catalysts toward CO evolution. Mixing formic acid-producing metals with each other (e.g., Sn–Pb) [80], or combining the formic acid-producing metals with weakly adsorbed metals (e.g., Sn–Ag) [43], enables an efficient way to finely adjust the selectivity of formic acid. It is reported that Sn-Pd has achieved > 99% HCOOH selectivity under low overpotential [44]. These experiments emphasize that there is a synergistic effect in alloy catalysts that can be utilized to finely tune the selectivity of catalysts.

At present, the progress of alloy catalysts that can increase the yield of hydrocarbons clearly fell behind that of CO_2–to–CO and CO_2–to-HCOOH alloy catalysts. Many attempts to introduce a second metal into Cu can only slightly tune the selectivity for CO_2 to multicarbon products. Yeo and coworkers prepared a series of Cu–Zn alloys and found that selectivity of C_2H_5OH on copper can be increased from 11% to 29% at the expense of C_2H_4 [81]. Bell and coworkers reported that the strained CuAg surface alloys could shift the distribution of products to favor carbonyl-containing products at the expense of hydrocarbons [82]. The Cu–Al bimetallic catalysts reported by Sargent and coworkers can realize 80% C_2H_4 selectivity at 400 mA cm^{-2} [58]. On the other hand, there is not much progress for non-copper alloy for hydrocarbon evolution and alloys such as Ni-Ga can only produce < 3% of hydrocarbon products [83]. The development of this field urgently needs a deeper understanding of the mechanism of CO_2 reduction, especially the optimal intermediate structure.

Compared to alloys, bimetallic catalysts with a special spatial arrangement of metals may provide an efficient means to tune the selectivity of CO_2RR catalysts. Ager and coworkers reported Cu and Au wire electrodes deposited alternately in parallel on SiO_2 [77], as shown in Fig. 2j–l. Au

wires can only produce a mixture of H_2 and CO, while the Cu wires in this system can produce a series of multicarbon products similar to the standard copper foil. However, when voltage is applied to Cu and Au wires simultaneously, the *FE* of oxygenate can be increased from 21.4% to 41.4%. This is because the Au electrode can greatly increase the CO concentration on the Cu electrode surface, thereby changing the electrode selectivity. Meyer and coworkers mixed monodispersed 6-nm Cu and Ag nanoparticles on glassy carbon [84]. These catalysts also showed an increase of C2 selectivity with $FE_{acetate}$ of 21.2%.

Besides controlling catalysts composition, the design of the nanostructure is also widely used in the development of CO_2 reduction catalysts. The nanostructure morphology of catalysts can affect the performance of CORR from two aspects: surface catalytic sites [85] and local electrolyte environment[86, 87]. Compared with the planar electrode, nanostructured catalysts possess larger electroactive surface area and abundant unsaturated coordinated surface sites. For instance, the unsaturated coordinated metal sites in small Cu clusters are reported to have better catalytic activity for CO_2RR [85]. The unsaturated coordinated surface sites are also assumed to be the critical reason why catalysts derived from metal compounds have high selectivity for hydrocarbons [74, 85]. Nanostructure metal catalysts with regular polyhedron morphology can expose specific crystal facets. Due to their much larger electroactive surface area compared with single facet metal foil, they can act as better catalysts to regulate CORR selectivity and alternative platform for the mechanism study. For instance, cubic copper nanocrystal catalyst can produce ethylene at a high reaction rate and high selectivity because it exposes (100) faces with high surface area [88]. Nanowires and nanosheets are another widely studied morphologies in catalysis to expose certain surface orientation [89, 90].

From a more macroscopic perspective, the nanostructured electrode will also have a great impact on the solution environment near the electrode surface. The main reason is that the nanostructured electrode has a higher geometric current density than the planar electrode in a small voltage range, which consumes more protons and sequentially increases the surface pH value. The rough surface structure further limits the exchange of ions between the surface and the bulk solution and promotes this effect. The high local pH environment would greatly suppress the HER and favor CO_2RR. For instance, 10–30 times increase of the CO_2RR/HER ratio can be observed on mesostructured Ag and Au catalysts with increasing porous film thickness [86, 87]. On Cu catalysts, a high pH value is beneficial to increase the competitiveness of the series of reaction paths of C–C bond coupling, thereby increasing the selectivity of the C2 products. There is also a hypothesis that nanostructured electrodes can produce local high electric fields that concentrate the cations in the electrolyte (Fig. 2a–f) [10]. The CO_2RR activity and selectivity on nanostructured electrodes are therefore improved through the alkali metal cations enhanced CO_2RR. Based on this concept, Au needles with nanometer-sized tips realized a geometric current density for CO_2–to–CO of 22 mA cm^{-2} at − 0.35 V, which is an order of magnitude better than gold nanorods [10].

Molecular catalysts research actually started early in the CO_2RR area and mostly concentrated in mimic natural photosynthesis. In addition, this research area normally focused on reducing CO_2 into CO or HCOOH, which is the first step of CO_2 reduction in natural photosynthesis [91]. Although the molecular catalyst endows uniform structure and can provide precise reaction mechanisms from the structure and catalytic performance relationship, there are several drawbacks to molecular catalysts that hinder their further contribution to the scale-up of CO_2RR. First, most of the studies on molecular catalysts are focusing on preliminary reducing products rather than deep-reduced products, while for industrial electrochemical CO_2RR, C2+ products are more desired. Second, as mentioned above, the first electron transfer processes for heterogeneous catalysts and molecular catalysts are different. Thus, the information obtained from the mechanism studies on molecular catalysts cannot be directly transferred to the the design of heterogeneous catalysts. Finally, the long-term stability of molecular catalysts is still an issue during operation since the catalysts may decompose and deposit on the surface of the electrode [91]. Notably, sometimes the molecule-derived catalysts on the electrode can have superior performance compared with the molecule catalyst in solution, even though only a small proportion of molecular catalysts are converted [92]. This triggers the effort to deposit molecular catalysts on the surface of gas diffusion electrodes to mediate heterogeneous electrocatalysis. For instance, Berlingutte, Robert, and coworkers immobilized cobalt phthalocyanine on the gas diffusion layer and exposed it to gaseous CO_2 in a gas-phase flow cell architecture [93]. A current density of > 150 mA cm^{-2} with FE_{CO} > 90% can be achieved, which is comparable with the state-of-the-art Ag catalysts. Once the price of the molecular catalyst is decreasing to a considerably low level, it can be considered as a replacement of the current Ag catalyst. MOFs, on the other hand, can be considered as the mirror image of a molecular catalyst in heterogeneous catalysis. The MOF is a very new research area in the field of CO_2RR, and there are still relatively few related articles. However, according to the related research work of the Sargent group, Cu–MOF also suffers from a relatively strong degradation effect under the conditions of CO_2 reduction, as it eventually becomes metallic Cu [85]. Of course, due to the monodispersity of the metal in the MOF, the MOF-derived metal Cu obtained by degradation may also have a different dispersibility and thus have different catalytic properties.

2.3 Operation Environment and Cell Configurations for CO_2RR

Before diving into the synergistic effect of the reaction environment on catalysis, there is a top priority electrolyte environment issue for CO_2RR, which is the impurity. Compared with the water-splitting reaction, the CO_2 reduction reaction is greatly affected by impurities. Hori and coworkers showed in their early research that if ultra-pure reagents are not used, the performance of the metal thin film electrode will be completely attenuated and disappeared in about 1 h, while the Cu electrode is more sensitive to impurity than Au and Ag [94]. Common impurities in the general solution include Fe, Zn, and Mn, and these metals are active for hydrogen production. Under the CO_2 reduction potential, these metal ions can be deposited on the surface of the electrode, and complete coverage on the surface of the planar electrode can be achieved by the ppm-level impurities in the solution. Correspondingly, in the later research on porous electrodes, such as the research on oxide-derived electrodes, it was found that electrodes with a large specific surface area are more resistive to impurity contamination. The conventional methods to avoid impurity contamination in the experiment can be summarized as follows: (1) pre-electrodeposition method. By applying lower potential and current on double precious metal/carbon electrode in the solution, the impurities can be deposited on the electrode after a long time reaction of more than 12 h [94]. (2) A chelating agent-based ion exchange resin can be employed to replace the metal ions in the solution with protons [95]. (3) Adding chelate directly to the solution, the chelating agent can inhibit metal deposition on the electrode to a certain extent. In this case, the concentration of the chelating agent needs to match the concentration of impurities in the solution, and the chelating agent may have an etching effect on some metal electrodes [95, 96].

The choice of solution (aqueous phase/non-aqueous phase), pH, ion species, buffer capacity, and mass transfer conditions will all affect the activity and selectivity of the CO_2RR system. However, the impact of these factors on performance, which is very important for constructing reactors, has not been fully understood.

In an early-time standard CO_2RR reaction setup, 0.5 M (1 M = 1 mol L^{-1}) $NaHCO_3$ or 0.5 M $KHCO_3$ solution would be used as the electrolyte and CO_2 gas would be bubbled into the solution near the CO_2RR electrode. In the previous study based on this cell configuration, bicarbonate solution is proved to be the best supporting electrolyte for CO_2RR in terms of activity and selectivity. During the operation of CO_2RR, the protons near the electrode surface would be quickly consumed, resulting in a shift of CO_2/H_2CO_3, H_2CO_3/HCO_3^-, and HCO_3^-/CO_3^{2-} balance [97]. With different electrolyte composition and buffering capacities, the environment of the electrolyte–electrode interface would be dramatically different, leading to different selectivity and activity of CO_2RR. Most researchers believe that although dissolved CO_2 is an active substance, the bicarbonate–CO_2 complex in bicarbonate solution would greatly increase the CO_2 concentration on the electrode surface for a better CO_2RR environment. Recent research of FTIR and isotope labeling confirmed the role of carbonate as a reactant supplier [98, 99]. Non-buffer electrolytes cannot maintain the CO_2 concentration near electrode surface, and other buffer solutions, such as the phosphate buffer, are easier to provide protons than water, which would favor the HER and CH_4 production [97].

A large number of experiments have observed that large cations will lead to a high CO_2 reduction rate and a high C2/C1 ratio in the order of $CS^+ > K^+ > Na^+ > Li^+$ [100, 101]. Some studies believe that the hydration process of cations will help buffer the surface and increase the concentration of dissolved CO_2 on the surface. Another possible explanation is that cations make *OCCO and *OCCOH more stable than 2 *CO, which will be discussed more in Sect. 3.1.2. The research of influence of pH values in the aforementioned setup is considerably hindered by the buffering capacity of bicarbonate solution and the reaction between CO_2 gas and OH^- ions. Several experiments have investigated the pH region from 6–10 and found a positive correlation between C_2H_4 evolution and pH values, helping the development of the CO_2RR mechanistic model.

Due to the gradual understanding of the importance of local CO_2 concentration in CO_2RR, parameters besides electrolyte composition have been investigated to enhance the CO_2 supply for liquid-phase CO_2RR. Theoretically, the solubility of CO_2 in aqueous solution scales inversely with raising temperature. The solubility of CO_2 increases from 21 to 73 mM when temperature decreases from 42 °C to 2 °C [102]. It is observed that the hydrogen evolution on all metals was significantly suppressed at a lower temperature, resulting in better CO_2 reduction selectivity. However, the current density also decreased at a lower temperature, resulting in a lower CO_2 reduction rate [102–104]. Changing aqueous electrolytes to organic electrolytes could also increase the solubility of CO_2, but the CO_2 reduction rate was also lowered because of higher resistance and lower proton concentration [105, 106]. In the H-cell, the CO_2 injection position, solution stirring, and CO_2 partial pressure can also greatly influence the CO_2 supply on the catalyst surface. Based on these experiments, it becomes a consensus that increasing the CO_2 supply can reduce hydrogen production and improve the C–C bond formation.

Using the flow cell mode with gas diffusion layer as catalysts support and gas-phase CO_2 for mass transfer, the diffusion coefficient is three orders of magnitude greater than that of water-soluble CO_2, so the improvement in diffusion of CO_2 reactant is very obvious (Fig. 3). This is of great help

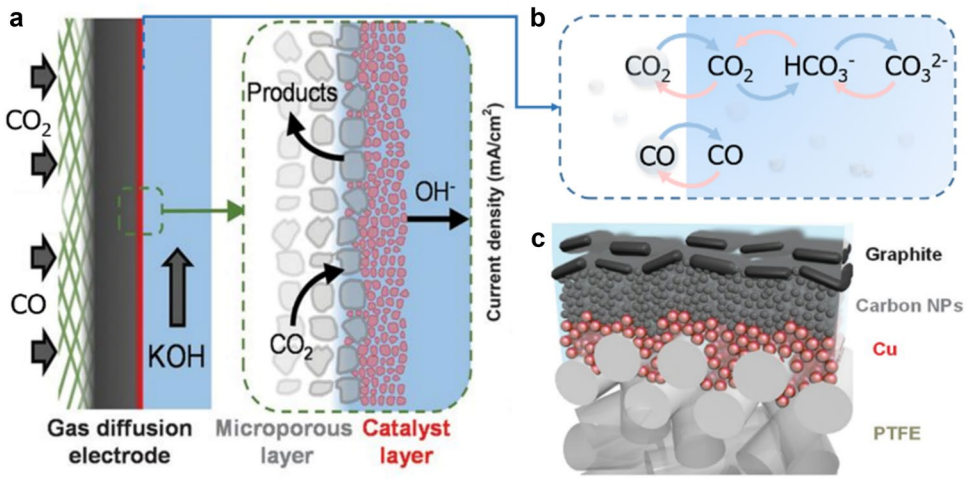

Fig. 3 **a** Typical design of the three-phase interface in CO_2RR and CORR flow cells. **b** Scheme of equilibrium of CO_2 and CO in gas–liquid phases. **c** Illustration of the graphite/carbon NPs/Cu/PTFE electrode. **a** and **c** adapted with permission from Ref. [55]. Copyright © 2018, Science Publishing Group

to the study of catalysts operating under large current density environments. For the clarity of the concepts in this review, the category labels of different electrochemical cell configurations are first demonstrated here. In general, the cell configurations can be divided into two large categories: H-cells and flow cells. The main difference is whether the electrolyte and gas reactants are kept flowing in and out of the reaction cell. In CO_2 and CO reduction area, the reactants in a flow cell are supplied by gas phase directly with the gas diffusion layer as pathways, that is why the flow cell discussed in this paper can be named "gas-phase flow cell" [33]. Notably, the gas diffusion electrode, as a basic feature of gas-phase flow cells, can also be used in an H-cell. According to the structure of the gas-phase flow cell, there are some further classification categories [33, 107]. In most research, membranes are used to separate anode and cathode chambers, so they can be labeled as membrane-based flow cells. Microfluidic electrolytic cells developed by Kenis and coworkers is membrane-less flow cells that replace the membrane with a thin space (< 1 mm in thickness) filled with flowing electrolyte stream to separate the anode and the cathode [108]. For membrane-based flow cells that press two electrodes together with an ion exchange membrane in between, it can be further categorized as membrane–electrode–assembly (MEA) flow cells or zero-gap flow cells [109, 110].

The information obtained by the above H-cell research, such as resistance of electrolytes and membranes, mass transfer, the overall balance of the system and the decay process of the catalyst usually, cannot be applied directly to that in a gas-phase flow cell with high current density. More importantly, the solution and the gas phase can be separated in a gas-phase flow cell mode, so that the electrolyte no longer takes the role of reactant supply. Thus, the bicarbonate solution is not necessarily the best choice of electrolytes, and the influence of the electrolyte on the reaction needs to be reconsidered. For example, the influence of pH on the CO_2RR reaction is greatly amplified when KOH can be used directly as a catholyte. In particular, alkaline flow cells have been widely used in CO_2RR research and result in a large improvement of catalysts performance. For instance, > 90% selectivity at current density > 150 mA cm^{-2} can be achieved for CO and HCOOH evolution on Ag/GDL and Sn/GDL, respectively [56, 57]. High C_2H_4 selectivity of > 70% can be realized at current density > 300 mA cm^{-2} with carefully designed Cu-based catalysts and gas-phase flow cells [55, 58]. There are also many problems in an alkaline CO_2RR gas-phase flow cell, such as the unavoidable crossover of HCO_3^- in a dual alkaline environment and the neutralization between KOH and CO_2, which need to be resolved before this system can be scaled up and industrialized.

Currently, there is no optimal method to investigate the detailed environment information in a gas-phase flow cell, because of the impermeable of gas-phase flow cell for most of the detection methods and the requirement of time and space resolution. The development and application of a multiphysics model provide a promising method to investigate the fundamental limitations of MEA designs. It can simulate the transport of neutral and ionic species, fluid flow through a porous medium, current and potential distribution, chemical and electrochemical reactions, and heat transfer [111–113]. Based on this method, interesting works have been accomplished, such as probing the surface ion diffusion on nanostructure catalysts, elucidating how local environment near the catalyst layer affects cell performance, and comparing the different MEA designs for high reaction rates and high selectivity.

2.4 From CO_2RR to CORR

2.4.1 An Economic Competitive Reaction Pathway

Producing highly reduced long-chain hydrocarbon products from CO_2RR attracts great attention because of the crucial role of long-chain hydrocarbon in the energy system and chemical industry. However, as mentioned above, the only CO_2RR products that can be produced exclusively are CO and HCOOH. Furthermore, only < 10% of C3 selectivity can be realized at current density > 100 mA cm^{-2} [27, 114]. From the perspective of the C–C coupling reaction mechanism, a high local concentration of CO should be very helpful for the formation of multi-carbon products. Therefore, if the reaction starts from CO, the selectivity of multi-carbon products will be improved. Starting from CO can also avoid the C1 reaction path in CO_2RR, such as the HCOOH reaction path.

Various ways to convert CO_2 into multi-carbon products have also been considered in depth technoeconomically [19, 20], including direct electrochemical reduction of CO_2 to multi-carbon products; electrochemical conversion of CO_2 to CO, and then electrochemical reduction of CO to multi-carbon products; chemically conversion of CO_2 to CO, and then conversion of CO into multi-carbon by Fischer–Tropsch reaction, etc. (Fig. 4). The fundamental challenge for the commercialization of all reaction pathways is that commercial profits cannot be realized under the current renewable electricity price. However, one can still seek the most likely path for commercialization. The reduction of CO_2 to CO has been able to achieve high *FE* and energy conversion efficiency under high current, and the reduction of CO is also prone to produce a large number of multi-carbon products. Unfortunately, the conversion efficiency from CO_2 to a single multi-carbon product is very low. Thus, CO_2–CO–C2+ pathway always has better energy conversion efficiency and lower product cost than the CO_2–C2+ pathway. Compared with the electrochemical conversion of CO into fuels, there is also a mature technology of Fischer–Tropsch reaction that can produce a large number of long-chain compounds from the feedstock of CO and H_2. In the current Fischer–Tropsch industry, the syngas feedstock comes from the coal gasification or steam-reforming natural gas [115, 116]. Thus, the whole Fischer–Tropsch industry is a net positive carbon emissions process. If the feedstock of the Fischer–Tropsch industry can be changed to CO and H_2 obtained by the electrochemistry process, it would be a strong competitor for renewable CORR. This is because the electrochemical hydrogen production is very mature with high energy conversion efficiency, and the products from the Fischer–Tropsch reaction have much longer chains compared with that of CORR. These are all challenges of CORR that need to be addressed urgently.

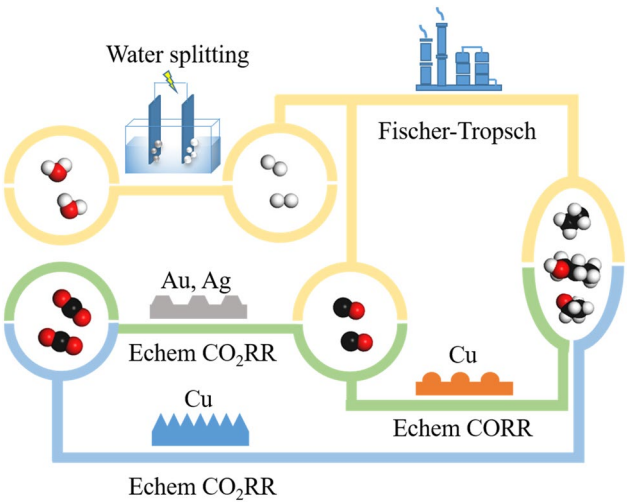

Fig. 4 Schematic of the three possible pathways for electrochemical CO_2 reduction to liquid products. The pathways are **a** CO_2 is electrochemically reduced to CO, and water is electrochemically reduced to H_2. The subsequent Fischer–Tropsch conversion of syngas can obtain long-chain hydrocarbon products. **b** CO_2 is first electrochemically reduced to CO and CO is subsequently reduced to multicarbon products. **c** CO_2 is directly electrochemically reduced to multicarbon products

2.4.2 A platform to Better Investigate the Reaction Mechanism

In addition to the commercial considerations, CORR also has its own special characteristics compared with CO_2RR. For CO_2RR, CO_2 will first be reduced to CO at one site, and then, it is likely to continue to be deeply reduced at the same site [29, 117]. However, for a catalysis process, efficient CO_2–to–CO reduction sites and CO–to–C2+ reduction sites are not necessarily the same. For instance, the best CO evolution catalyst of Au and the best hydrocarbon evolution catalyst of Cu have totally different electric properties. Moreover, the sequential reduction on a single site is likely lead to the scaling relationship effect. Since a large number of intermediate products of CO_2RR have similar structures, adjusting the catalyst structure to reduce the overpotential of some reaction steps will inevitably lead to an increase of the overpotential of other steps. By decoupling the CO_2–CO and CO–C2+ reaction steps, the optimization on the catalyst structure and the reaction system can be conducted independently, thus resulting in higher overall energy conversion efficiency. Related to this, research of CORR on the C–C coupling mechanism is also much more convenient and easier than CO_2RR because it has fewer intermediate products.

Another feature of CORR relative to CO_2RR is the interaction of reactants with water. Compared with the equilibrium of CO_2/HCO_3^-, H_2CO_3/HCO_3^- and HCO_3^-/CO_3^{2-} after CO_2 is dissolved in water, CO has less than one-tenth

solubility and does not form a complex ion balance. This greatly simplifies the experimental design of the catalytic system and the balance of the catalytic interface. Although the low solubility of CO will affect the research progress of the CORR system in H-cells (non-gas diffusion electrodes) to some extent, the current research in a gas-phase flow cell has solved this problem well. This part will be discussed more in Sect. 3.3.

3 Cell Design and Electrolyzer for CORR

A standard reaction cell is crucial to realize an efficient electrolysis reaction and make sure all the catalytic results can be reliably compared [118, 119]. Due to the low solubility of CO in aqueous solution, the investigation of CORR in H-cells is usually confined in a low current density region, where the catalytic performance is vulnerable to the tiny changes of the cell configuration. Moreover, to realize the industrialization of decarbonization, the ultimate goal of CORR research, the reaction rate of CORR should reach > 0.2 A cm^{-2} with > 80% *FE* [19, 33]. Thus, the construction of a standard test cell where the mass transport limit could be eliminated is the top priority in CORR research. For this purpose, the choice of electrolyte identity, the design of the gas diffusion layer (GDL) and the optimization of the membrane electrode assembly (MEA) must be carefully considered.

3.1 Choice of Electrolytes for CO Reduction

During the catalytic reduction process of CO, the adsorption of reactants and the bonding configuration of intermediates would be greatly influenced by the local atomic and electronic structures at the electrode interface, which is determined by both electrode materials and the liquid side of the reaction environment. The interaction of intermediates with the liquid side depends on the detail composition of the solution, i.e., the identity and concentration of the supporting electrolyte, and the pH value of the electrolyte.

3.1.1 Influence of pH Values on CORR

pH values can greatly influence an electrochemical reaction whose rate-determining step involves proton transfer. There are multi-steps of proton transfer in CORR, and for different products the proton transfer occurs at different stages of the reaction. Thus, changing the pH value of electrolytes can potentially lead to different trends for product generation in CORR. For instance, there is a significant difference in pH dependence between the C1 product of CH_4 and C2 products of C_2H_4 and C_2H_5OH in CORR on the Cu electrode. Two decades ago, Hori and coworkers first reported that a high pH value favored C_2H_4 and C_2H_5OH formation over CH_4 formation in CORR. The partial current of CH_4 generation was proportional to proton activity by analyzing the Tafel relationships on the SHE scale, whereas the Tafel relationships for C_2H_4 and C_2H_5OH formation were irrespective of pH values [97, 120]. Thus, it is indicated that the rate-determining step (RDS) of CH_4 production in CORR followed a concerted proton-electron transfer mechanism and the RDS of C_2H_4 production only involved an electron transfer. This hypothesis can be supported by the DFT calculations for the CORR on Cu (100) [66]. In the RDS step of CO coupling to *CO–COH, proton and electron transfer was decoupled, resulting in pH independence of C_2H_4 formation on the SHE scale. This decoupling phenomenon of proton and electron transfer is probably due to the high electron affinity of the intermediate C_2O_2, which leads to a much faster electron transfer than proton transfer. Notably, the phenomenon that C_2H_4 formation was more favored over CH_4 formation at high pH values only existed on the Cu (100) facet as reported by Koper [121]. On Cu (111), the onset potentials for the formation of C_2H_4 were close to the onset potentials of CH_4 formation from pH 7 to pH 12.

The pH dependence for other C2+ oxygenate products on copper is more difficult to investigate due to their low concentrations. Based on an electrochemical cell with a high ratio of electrode surface area to electrolyte volume, Jaramillo, Hahn, and coworkers proved that most of the C2+ oxygenate products were also irrespective of pH values [14, 122]. In this study, the major products were determined to be C_2H_4 and CH_3CH_2OH with a minor amount of CH_4, CH_3COO^-, C_3H_7OH, CH_3CHO, and CH_3CH_2CHO. On the SHE scale, the overpotentials for most C2+ products in CORR did not change with variation of pH values, indicating that the rate-limiting step for C2+ formation was pH-independent. CH_3COO^- was different from other C2+ products and showed a positive shift in onset potential on the SHE scale for CORR, suggesting that the rate-determining step was different for CH_3COO^- compared with other C2+ products. The reaction pathway of CH_4 was very complex as it shifted both on the SHE and on RHE scales. In summary, alkaline conditions indeed increase the energy conversion efficiency and selectivity of CORR to C–C coupled hydrocarbon/oxygenate products, which are more attractive from viewpoints of industry and fundamental science.

3.1.2 Influence of Cation Species on CORR

In an electrochemical reduction reaction, the cations are usually accumulated near the electrode surface due to the negative potential applied on the electrode. Cations in electrolytes have been observed to impact the selectivity of both CO_2RR and CORR greatly; however, the mechanism is still under debate [101, 123]. Hori and coworkers provided a

preliminary study on how Li^+, Na^+, K^+, Cs^+ impacted the CORR selectivity of a polycrystalline copper catalyst [123]. The general trend was that all C2+ compounds production, e.g., C_2H_4, CH_3CH_2OH, and C_3H_7OH, could be enhanced by larger cations (Cs^+ and K^+), while H_2 evolution and CH_4 evolution were more favored with small cations (Li^+ and Na^+). Thus, large cations such as Cs^+ and K^+ could greatly enhance the ratio of C2/C1. Notably, this promotion effect of large cations on C_2H_4 and CH_4 selectivities is different on different Cu facets. Koper and coworkers reported that the C_2H_4 evolution on the Cu (100) facet, which had the lowest overpotential among all CORR pathways in their study, showed the highest promotion effect by large cations in comparison with the C_2H_4 evolution on Cu (111) or CH_4 evolution on both facets [124]. They also found that although the polycrystalline copper showed a decreased overpotential of C_2H_4 products in the electrolyte with large cations of Rb^+ and Cs^+, the onset potential of C_2H_4 formation on Cu (111) or Cu (100) single-crystalline facets was actually independent of cation size. The decrease of overpotential of C_2H_4 products on polycrystalline copper could be attributed to the larger promotion of C_2H_4 evolution on Cu (100) facets compared with all other reaction pathways. In these studies, the role of cations in CORR was considered to be a catalytic promoter, which changed the free energy landscape of CO reduction and stabilized certain intermediates. The pathway with these intermediates was promoted more effectively by larger cations such as Cs^+ than the smaller cations.

The influence of cation on C2+ selectivity of CORR can be in part explained by the difference of outer Helmholtz plane potential (OHP). Cations tend to adsorb on the electrode and shift the potential of the outer Helmholtz plane in the positive direction. Large cations are easier to adsorb on the electrode because the hydration number from Li^+ to Cs^+ becomes smaller. In an electrolyte with larger cations, the positive shift of OHP would change the concentration of H^+ and results in higher pH values at the electrode surface, which benefits the production of C2 products. The above mechanism proposed for the influence of pH values and cation species on CORR is consistent with most of the research results; however, some recent results suggested that further development of this mechanism is needed. Lu and coworkers provided an interesting hypothesis that hydroxide was not a promoter of C2+ production in CORR on the Cu electrode, and the observed influence of pH on CORR selectivity was also coming from the distribution of cations [125]. In this study, the authors systematically studied the C2+ product generation in two kinds of electrolytes at both SHE and the RHE scales. The first electrolyte had an identical concentration of OH^- and different concentrations of Na^+, and the second electrolyte possessed a varying amount of OH^- and an equal amount of Na^+. The results demonstrated higher concentration of Na^+ instead of OH^-, resulting in a promotional effect on C2+ production during CORR. Their hypothesis was further supported by chelating the Na^+ in solution by 15-crown-5, leading to a drastic decrease in the partial current of C2+ generation.

The size effect of organic cations, however, cannot be considered the same as the alkaline cations, as reported by Waegele and coworker [126]. The CORR tested with alkyl$_4$N$^+$ cations showed that C_2H_4 was produced in small cation contained electrolytes, but not in large cation contained electrolytes. Surface-enhanced IR absorption spectra (SEIRAS) in attenuated total reflection (ATR) geometry proved that there was a significant difference in the O–D stretch band of interfacial heavy water in SEIRAS, indicating that the two large cations of propyl$_4$N+ and butyl$_4$N+ blocked the interaction between *CO and interfacial water. These water molecules were assumed to stabilize the key intermediate (CO dimer) in C_2H_4 formation by hydrogen bonding to the terminal oxygen of CO dimer.

3.2 Gas Diffusion Electrode in H-Cells for CORR

The sufficient supply of CO is the most important requirement of CORR experimental design. For CO_2RR, the solubility of CO_2 in aqueous solution is 34 mM, corresponding to > 10 mA cm^{-2} limited current density. However, the low solubility of CO in aqueous electrolytes (~1 mM) can only support limited current density lower than 1 mA cm^{-2} based on Fick's law (Fig. 5). This limitation was confirmed by Xu, Lu, and coworkers, who monitored the surface coverage ratio of linearly adsorbed CO (CO_L) under different mass transfer conditions by SEIRAS [32]. At a current density of ~1 mA cm^{-2}, the intensity of the IR band of CO_L dropped

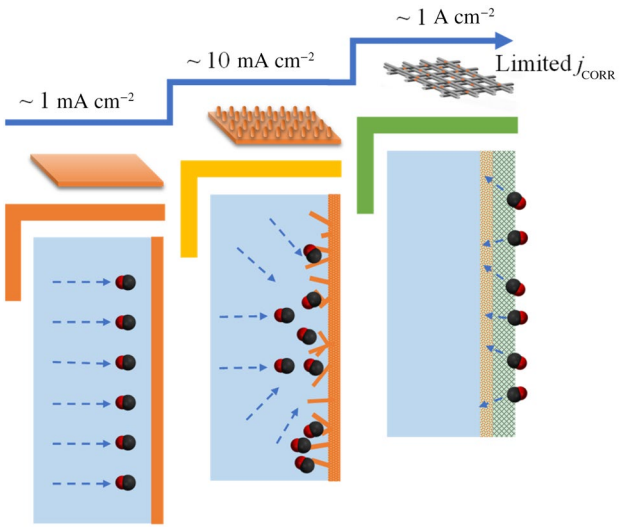

Fig. 5 The scheme of CO supply for planar electrodes, porous electrodes with nanostructure catalysts, and the gas diffusion substrate coated with catalysts

by ~70% once the stirring was turned off from 800 r min^{-1} and quickly recovered when the stirring rate was beyond 300 r min^{-1}. The insufficient supply of CO would result in a lower limited j_{CORR} current density due to the mass transport limitation and curtail the selectivity of CORR toward C2 and C3 products because the low coverage ratio of CO on the surface of catalysts would lower the chance of C–C bonds formation [122]. Higher CO partial pressure can benefit the production of C2+ products over CH_4, and there is a second-order dependence on the coverage of adsorbed CO for C2+ production in a wide pressure range. However, first-order reaction kinetics for CO–to–C2+ was observed at lower CO pressures [0.1 and 0.01 bar (1 bar = 100 kPa)] [32, 122]. This deviation can be explained by the fact that the adsorption sites of CO on copper are not evenly distributed. The step and kink sites are close to each other and bind CO stronger than terrace sites.

Replacing the planar electrode with a porous electrode is one way to levitate mass transport limitation [10, 127], probably due to the accumulation of gas bubbles on the surface and non-planar mass transport (Fig. 5). Wang and coworkers changed the morphology of copper catalysts from the planar substrate to a three-dimensional (3D) porous structure. They found 3D porous structure can benefit the transport of CO to realize a sixfold improvement in CORR geometric current density compared to the 2D counterpart with similar surface roughness factors in an H-cell test [127]. The optimized sample with 3D structure showed a high total current density of 2.7 mA cm^{-2} and *FE* of 51% at − 0.3 V (in this paper all voltages used are vs. RHE, unless specially noted) toward ethanol production. Nevertheless, the obtained CORR current density was still 1–2 orders of magnitude lower than that required for industrial applications.

Comparing to CO diffusion in aqueous solution, CO diffusion in the gas phase possesses > 1000 times higher diffusion coefficients and > 30 times higher concentrations, raising the theoretical diffusion limited current density to > 1 A cm^{-2}. Gas diffusion electrode (GDE) configurations is a promising structure to promote the supply of CO gas through the porous and continuous gas pathway inside the electrode itself (Fig. 5). Normally the GDE used in electrolysis consists of a dense array of carbon fibers and/or a densely packed carbon microporous layer. Catalysts are deposited on one side of the gas diffusion layer to form a three-phase interface of gas reactants, liquid electrolytes, and solid electrocatalysts. Unlike a planar electrode where CO gas needs to transport from the front side across a ~ 100 μm thickness liquid diffusion layer, in the GDE mode CO gas can directly flow to < 10 nm distance around the reaction sites, helping to enhance the up-limit current density to ~ 1 A cm^{-2}. A simple experimental comparison between CO gas flowing through and flowing by GDEs in H-cells exhibited more than 50 times difference of CORR production rates, strongly proving the important roles of direct gas feed configuration and construction of triple-phase interfaces in enhancing the reaction rates of the catalysts for CORR [128].

The hydrophobic property of GDLs is very important in the design and operation of GDEs because it determines whether the gas pathway is clear and not blocked by water flooding. In the pioneering work of CORR on GDEs from Xiang and coworkers, the GDE consisted of copper nanoparticles, C powders, and Teflon, which were not strictly hydrophobic [128]. A partial current density of 50.8 mA cm^{-2} and *FE* of 17.8% for CORR to C_2H_4 were achieved at − 0.85 and − 0.74 V in 10 M KOH, respectively. However, more than 70% of the current density corresponded to hydrogen evolution. The later CORR researches proved that enhancing the hydrophobic property of GDEs successfully suppressed the hydrogen evolution at high current densities and achieved high *FE* for CORR to hydrocarbons and multi-carbon oxygenates in an H-cell test [31, 129]. In the work of Lu and coworkers, the catalyst electrodes were prepared by depositing commercial dendritic polycrystalline Cu powders onto polytetrafluoroethylene (PTFE)-treated carbon fiber paper [31]. At the potential of − 0.94 V, the current density of dendritic Cu reached 180 mA cm^{-2} with *FE* > 80% for CORR. On the contrary, the dendritic Cu powders deposited on non-hydrophobic carbon support (i.e., non-PTFE-treated carbon fiber paper and glassy carbon) showed almost exclusive hydrogen evolution, indicating that the hydrophobicity of the catalyst support is the key to form triple-phase boundaries and achieve high reaction rates. Deng and coworkers further optimized the PTFE content of gas diffusion electrodes for CORR in an H-cell [129]. Three carbon papers (CP, without micro-porous layers) with different hydrophobicity (PTFE concentration of 5 wt%, 13 wt%, and 25 wt%) and one hydrophobic carbon paper with 25% PTFE treatment micro-porous layers (CP-MPL) were tested as the supports of Cu particles to optimize the CO diffusion to catalytic sites (Fig. 6). It was found that the *FE* for C_2H_4 formation increased from 2.46% to 52.7% when the hydrophobicity increased from CP-5% to CP-MPL. This result suggested that hydrophobic property of support carbon paper can benefit the CO supply to catalytic sites and in turn boost the C2 production.

3.3 Design of CORR Electrolyzers

There is a large body of work on flow cell design for other reactions (e.g., fuel cells, water splitting, and CO_2RR) besides CORR. Both acid and alkaline water splitting electrolyzers are quite mature and commercialized [130, 131]. The electrolyzer for fuel cells has been extensively investigated for many years, and the supply of the reactants is normally through the gas phase in both anode and cathode sides [132, 133]. For CO_2RR, the alkaline electrolyzer is the

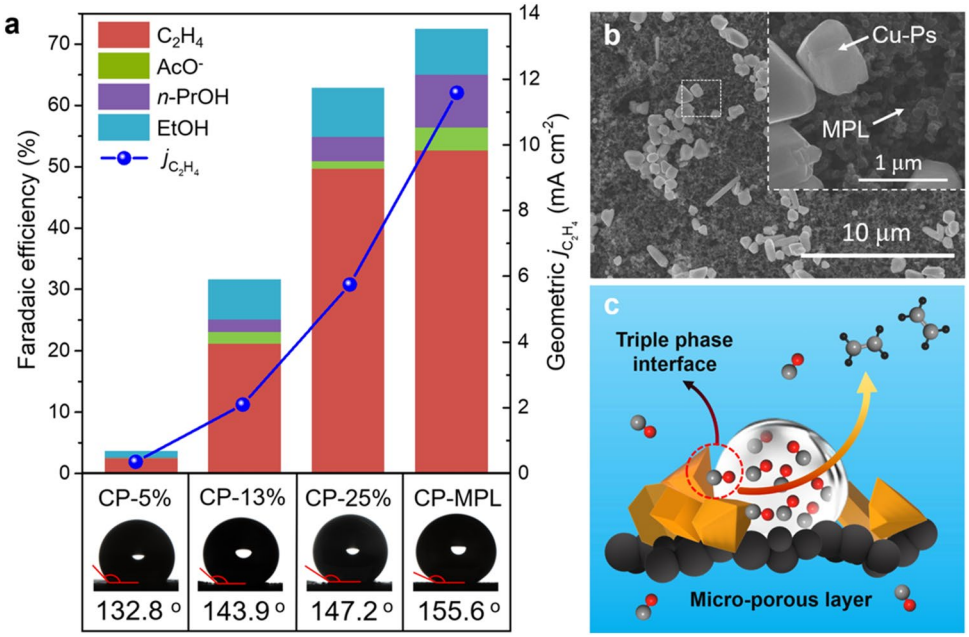

Fig. 6 **a** Faradaic efficiency and current density for CORR over Cu particles loaded on four types of carbon papers tested in 1 M KOH. Bottom pictures show contact angles of water droplets on carbon papers. **b** SEM images of Cu particles on the GDL electrode. **c** Schematic illustration for CORR processes on the Cu catalysts supported by hydrophobic microporous layers. Adapted with permission from Ref. [129]. Copyright © 2020, Wiley–VCH

most common setup, and CO_2 is supplied through the gas phase into the GDE [134, 135]. The current design of the CORR gas-phase flow cell largely takes advantage of these successful designs.

One key parameter of cell design is the choice of the membrane, which could be the proton exchange membrane (PEM), the anion exchange membrane (AEM), or the bipolar membrane (BPM). The choice of PEM and AEM does not result in a significant difference in energy conversion efficiency or ion flow efficiency in their most optimized design. The only thing that needs to keep in mind is that the PEM presents the best ion transport property for H^+, and the AEM shows the best ion transport property for OH^-. Other cations or anions such as K^+, Na^+, and NO_3^-, Cl^- can be used for ions transport in PEMs or AEMs, respectively, but require a much higher voltage. This fact recommends the use of PEMs in an acid environment and AEMs in an alkaline environment. BPMs can greatly hinder the ion exchange between anode and cathode sides; however, it requires 0.8 V extra activation energy to support the current [136]. The only case that BPM systems can have equal energy conversion efficiency compared with PEM and AEM systems is that employing acidity electrolytes in the cathode side and alkaline electrolytes in the anode side. In the CORR system, the BPM is not feasible because acidic catholytes would benefit the competitive reaction of hydrogen evolution. To ensure the sufficient supply of CO, gas-phase CO should be injected directly into GDEs. There are two different design principles for structure between GDEs and membranes. One can introduce an electrolyte layer to supply water and control the reaction environment, or GDEs can be directly pressed to the membrane and water is provided by humified CO. Eight different gas-phase membrane flow cell configurations can be proposed based on the above-analyzed factors that whether the liquid electrolyte is used in the anode side, whether PEMs or AEMs are used to separate cathode and anode sides, and whether the electrolyte layer is introduced between cathodes and membranes. The design scheme and the ion transport path of these eight cell configurations are shown in Fig. 7.

There is currently no research work that compares all these possible cell configurations. However, it is well known that the anionic products of CO_2RR such as $HCOO^-$ and CH_3COO^- could go across the AEM membrane [137–139]. Without catholytes to pull products away from the membrane, such as the cases of cell configurations 4 and 8, the crossover of liquid-phase anionic products would lead to the difficulty of collecting them or even loss of products via anodic oxidation. The design of "humified air|IrO_x–GDL|PEM|Cu–GDL|humified CO" in cell configuration 2 is highly suspected for its ability to support high current density because humified gas alone cannot provide sufficient water for the reaction [140]. In the previous study of CORR without catholytes, water supply for cathodic reaction actually came from the water transport from the anode side, as reported by Xiang and coworkers [141]. The relative humidity of the CO gas supply had little impact on the product selectivity and activity of CORR. It is also obvious that the only difference of cell configuration 5 and 7 is the choice of the membrane, and the AEM is apparently more compatible with alkaline electrolytes, suggesting cell configuration 7 is better than cell configuration 5. Thus, cell configurations 2, 4, 5, and 8 are not recommended for high current density CORR applications.

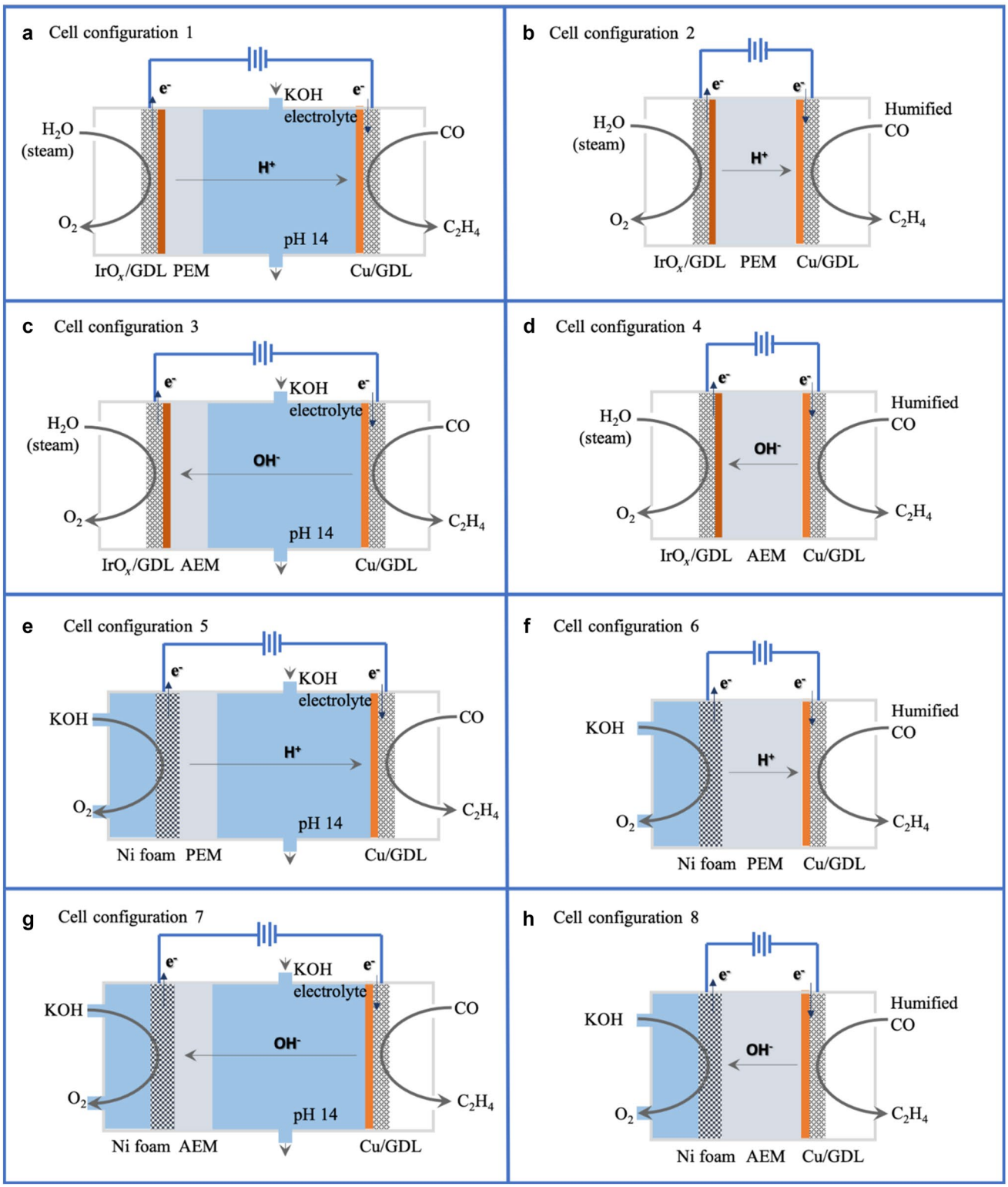

Fig. 7 The design scheme of eight different cell configurations. **a** "Humified air|IrO_x–GDL|PEM|KOH|Cu–GDL|CO", **b** "humified air|IrO_x–GDL|PEM|Cu–GDL|humified CO", **c** "humified air|IrO_x–GDL|AEM|KOH|Cu–GDL|CO", **d** "humified air|IrO_x–GDL|AEM|Cu–GDL|humified CO", **e** "KOH|Ni foam|PEM|KOH|Cu–GDL|CO", **f** "KOH|Ni foam|PEM|Cu–GDL|humified CO", **g** "KOH|Ni foam|AEM|KOH|Cu–GDL|CO", and **h** "KOH|Ni foam|AEM|Cu–GDL|humified CO"

For all cell configurations without electrolytes in anode sides (configurations 1–4), there is a potential shortcoming of high overall applied potential, because the acidic environment due to the loss of OH^- in the anode side requires an extra potential for both oxygen evolution reaction (OER) and compensation of pH differences between cathodes and anodes. This was confirmed in the research of Kanan and coworkers, in which they systematically analyzed the choice of the membrane, the catholyte, and the anolyte for CORR, as shown in Fig. 8 [142]. The performance of cell A (similar with cell configuration 1) was evaluated under the condition of 150 mL min^{-1} 1 M NaOH as the catholyte, 0.5 cm^3 min^{-1} of CO gas flow through Cu/GDE and 10 cm^3 min^{-1} of humidified N_2 through the anode. A crucial drawback of cell A was that a high total cell voltage was required for cell operation, e.g., − 3.4 V for j_{CORR} of 80 mA cm^{-2}. Although there is a shortcoming of high voltage, the selectivity of CORR in this cell configuration is not affected. The total *FE* for CORR ranged from 65% to 76% in the testing potential range. C_2H_4 was the only gas-phase CORR product detected in most potential ranges, and the liquid products included CH_3CH_2OH, CH_3COO^-, and $CH_3CH_2CH_2OH$. 65% of the CO flowing into the cell can be converted to reduced chemicals in a single pass. Changing the electrolyte from 1 M NaOH to 1 M NaCl did not seem to vary the CORR performance of the cell, including both the *j-V* relationship and product distribution.

With all other cell configurations excluded from the analysis above, only cell configurations 6 and 7 can meet the requirements of low applied voltage, minor products crossover and sufficient water supply. These two cell configurations have also been systematically studied by Kanan and coworkers (Fig. 8b–c). In cell B (cell configuration 7), the anolyte was changed to an alkaline medium, the anode was changed to Ni foam, and the membrane was changed to an alkaline-doped polybenzimidazole membrane. The CORR test showed that the products distribution in cell B was essentially identical to that of cell A; however, the cell voltage

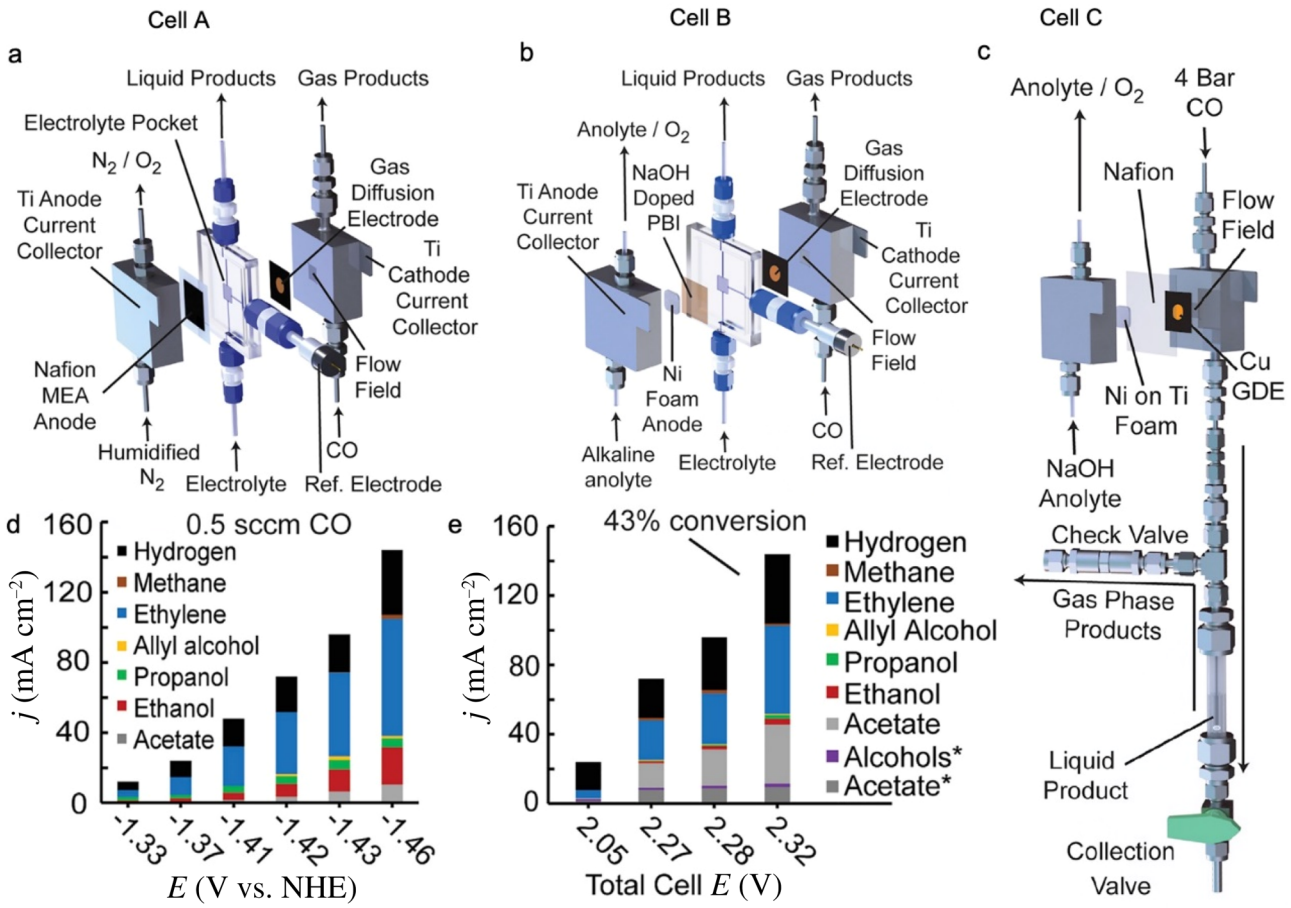

Fig. 8 Exploded view of the **a** cell A, **b** cell B, **c** cell C. **d** Product distributions and measured cathode potentials for CORR with the 1 M NaOH catholyte and 0.5 cm^3 min^{-1} CO flux in cell B; 1 sccm = 1 cm^3 min^{-1}. **e** Product distributions and measured total cell voltages for CORR with the 1 M NaOH recirculating anolyte and 1.0 cm^3 min^{-1} CO in cell C. The asterisks designate products found in the anolyte. Adapted with permission from Ref. [142]. Copyright © 2019, Elsevier

was lower by 0.8 V for the same current density, thanks to the introduction of alkaline environment for OER (Ni foam in 1 M NaOH). A j_{CORR} of 107 mA cm^{-2} was realized at a total cell voltage of 2.49 V, and 68% single-pass conversion was obtained. On the other hand, cell C (cell configuration 6) had the advantage of accumulating liquid products, in which the Nafion 117 membrane was used to separate the cathode and the anode, and the catholyte was removed. CORR in this cell configuration showed that C_2H_4 was the dominant gas-phase product, and a highly concentrated liquid-phase product of CH_3COO^- and alcohols could be obtained. A total current density of 144 mA cm^{-2} could be reached at 2.32 V, and 7.3 mL liquid product of 0.87 M CH_3COO^-, 0.07 M C2+ alcohols, and 2.75 M NaOH was produced after 24 h operation. A small amount of CH_3COO^- and alcohol products could be found in the NaOH anolyte, indicating that there was a crossover issue in this cell configuration. This work revealed critical design features for improving the current density, selectivity, and single-pass conversion simultaneously at moderate cell potentials.

'KOH|Ni foam|AEM|KOH|Cu–GDL|CO' design (cell configuration 7) is currently the most successful and frequently used design of CORR. Jiao and coworkers first reported a CORR catalyst study in this type of gas-phase membrane flow cell [27]. The j_{CORR} increased almost exponentially with respect to the applied potential, suggesting there was a sufficient supply of CO gas to the catalytic sites. A remarkable CO to C2+ partial current density of 830 mA cm^{-2} was achieved at − 0.72 V for OD–Cu catalysts. Hinrichsen and coworkers also confirmed the benefits of sufficient CO gas supply in their research of CORR in a similar microflow cell [143]. Total *FE* of 89% could be obtained for CORR toward C2+ product at 300 mA cm^{-2}, which was a twofold increase to C_2H_4 and a threefold increase toward CH_3CH_2OH and C_3H_7OH compared with CO_2RR. A series of copper catalysts with different morphology and performances were also studied in this type of flow cell by Sargent group, which will be further discussed in Sect. 4.2 and 4.4. Notably, multiphysics modeling could be important for CORR as well. Considering different solubility of reactants in the solvent, different buffer ability of the electrolyte to replenish the reactants, different distribution of liquid and gas products, a new model is required and some new phenomenon may be found.

4 Morphology and Composition of Catalysts for CORR

Besides electrolytes, the morphology and composition of catalysts also play important roles in determining the activity and selectivity of CORR. In this section, the performance of nanostructured catalysts measured both in the H-cell and in the flow reactor is classified and discussed to shed light on the design of highly efficient catalysts for CORR. The detailed CORR performance of some representative electrocatalysts is summarized in Table 1.

4.1 Single Crystal Facet Copper

For the research of catalysts, the single facet catalyst is the most fundamental and important starting point because a reliable relationship between structure and performance on single facets can be achieved due to the minimization of other structural factors. Based on online electrochemical mass spectra, Koper and coworkers revealed that the selectivity of CORR was very sensitive to the atomic configuration of the copper catalysts surface, and the production of C_2H_4 was more favored than CH_4 on the (100) facet [23]. On Cu (100), the onset potentials for C_2H_4 formation were − 0.4 V at pH 7 and − 0.3 V at pH 13. The corresponding maxima of C_2H_4 production exhibited at − 0.6 V and − 0.45 V, respectively, after which C_2H_4 production decreased and eventually stopped. At a potential of − 0.8 V at pH 7, the formation of C_2H_4 was again observed, accompanied by the formation of CH_4. Similarly, on Cu (111) with electrolytes of pH 7, both CH_4 and C_2H_4 were formed starting at − 0.8 V. At pH 13 and potential > − 1.0 V, the CH_4 and C_2H_4 production on the Cu (111) electrode was almost negligible. Based on these results, the authors proposed two separate pathways for the C_2H_4 evolution. One pathway shared an intermediate with the CH_4 evolution and required high overpotential, as observed on Cu (111) and Cu (100) with potentials < − 0.8 V at pH 7. Another pathway occurred only on Cu (100) and corresponds to the observed C_2H_4 evolution at low overpotential. In this case, the formation of CO dimer was suggested to be a key intermediate for C_2H_4 production. Koper and coworkers further confirmed that (100) terraces sites rather than (100) step sites were responsible for the C_2H_4 formation during CORR at low overpotentials, by investigating the reactivity of these sites on high index copper surfaces [24]. Two stepped Cu single crystals: Cu (322), with the [5(111) × (100)] orientation, and Cu (911), with the [5(100) × (111)] orientation were studied. On Cu (322) electrodes, the formation of CH_4 and C_2H_4 was detected at − 0.9 V, which was similar to the results obtained for CORR on Cu (111). This indicated that the CH_4 and C_2H_4 formation occurred at (111) terraces of Cu (322), but not at (100) steps. On Cu (911) electrodes, the selective formation of C_2H_4 was observed between − 0.5 and − 0.8 V, and no CH_4 was observed in this range. Moreover, the CH_4 and C_2H_4 formed at more negative potential simultaneously. This is consistent with the observations on Cu (100) electrodes. These results suggest the selective reduction of CO to C_2H_4 on copper electrodes at low overpotentials attribute

Table 1 The product distribution of CORR at a series of catalysts in H-cells or flow cells

Catalyst	Electrolyte	Potential vs. RHE	j_{total} (mA cm^{-2})	Faradaic efficiency (%)				Other products	References
				C_2H_4	Acetate	Ethanol	n-propanol		
H-cell									
Polycrystal–Cu	0.1 M KOH	−0.59	2.12	29.7	1.2	11.2	4.9	–	[26]
OD–Cu	0.1 M KOH	−0.3	0.285	0	13.6	42.9	0	–	[7]
Cu nanowire	0.1 M KOH	−0.3	0.22	0.66	14.5	49.8	0	–	[150]
Cu nanowire	0.1 M $KHCO_3$	−1.1	–	35	–	–	–	–	[151]
Cu nanoflower	0.1 M KOH	−0.33	0.78	1.78	21	60.37	0.65	–	[152]
Cu foam	0.1 M KOH	−0.3	2.69	0.4	24.2	51.6	0	–	[127]
Cu–Ag alloy	0.1 M KOH	−0.536	0.194	3.42	–	–	–	49.1% CH_3CHO	[169]
Co-phthalocyanine	0.1 M KOH	−0.64	4.77	–	–	–	–	14.3% CH_3OH	[162]
Cu–supermolecule	0.1 M KOH	−0.4	1.34	–	24	57	–	–	[163]
Cu–CP–MPL	1 M KOH	−0.7	21.8	52.7	3.7	7.4	8.7	–	[129]
Cu–PTFE–carbon fiber	0.1 M KOH	−0.83	100	35	19.8	13.2	9.3	–	[31]
Cu–GDE	10 M KOH	−0.74	260	17.8	–	–	–	–	[128]
Flow cell									
Micron–Cu	1 M KOH	−0.7	500	38.1	24.9	17.1	4.5	–	[27]
OD–Cu	1 M KOH	−0.42	10	19.2	7	15.6	25.6	–	[27]
		−0.72	1050	44.1	10.1	19.9	4.9	–	[27]
Cu nanosheet	2 M KOH	−0.736	200	16.3	48	2.4	2	–	[153]
Cu–adparticle	1 M KOH	−0.44	48	29.6	4.7	14.6	23	–	[155]
		−0.66	420	43.1	6.5	28	11.5	–	[155]
Cu nanocavity	1 M KOH	−0.56	37	21	7.8	12.5	21	–	[156]
Fragment Cu	1 M KOH	−0.45	42	22	5	12	20.3	–	[157]
Ag–Cu alloy	1 M KOH	−0.46	13.5	29.7	4.7	5.9	33.3	–	[170]

exclusively to Cu (100) terraces, whereas (100) step sites are not involved in this reaction.

Koper and coworkers later presented a mechanism study for the preferable production of C_2H_4, CH_3CH_2OH, and CH_3CHO from CORR on Cu (100) electrodes [66]. Using the computational hydrogen electrode model, the adsorption energy of all possible intermediates for the CORR to C_2H_4, CH_3CHO, and CH_3CH_2OH was calculated. The calculated onset potential of the reaction is the smallest applied potential U for all steps to be exergonic, and the rate-determining step is the last step to become exergonic when the overpotential is increased. For the first step of CO coupling, *COCHO was less stable than *COCOH by 0.16 eV, suggesting hydrogenation would happen on O rather than C atoms. The sequential hydrogenation would more prefer to form $*CCO + H_2O$, which was a precursor of C_2H_4 and CH_3CH_2OH instead of other C2 products. The subsequent hydrogenation processes were the α-carbon protonation (*CHCO), the protonation of the C atom in the carbonyl group (*CHCHO), then again protonation of α-carbon ($*CH_2CHO$). The next proton–electron transfer had two possible intermediates: $*CH_2CH_2O$ for C_2H_4 formation and $*CH_3CHO$ for CH_3CHO/CH_3CH_2OH formation. In this step, the reaction was inclined to C_2H_4 formation by approximately 0.2 eV. This can explain why C_2H_4 is the most abundant C2 product, followed by CH_3CH_2OH and CH_3CHO. Chen and coworkers theoretically studied the CORR process on another Cu facet: the (111) facet [144]. Based on their calculation, the presently defined CH_2O and CHOH pathways for hydrocarbon production might parallelly occur on the Cu (111) facet, and high overpotentials would favor the formation of CH_4. The RDS of the CORR process was very likely the CO–to–CHO step, which was dependent on the coverage of adsorbed $CO^{\delta-}$ species on Cu (111). With higher overpotential, the increasing surface CO coverage would lead to the weaker CO bonding with the Cu surface, which sequentially lower the activation barrier of further CO electroreduction into CHO. Goddard and coworkers as well as Rossmeisl and coworkers reexamined the CORR on copper with the water layer considered in DFT calculations [145, 146]. Both calculations showed that C_2H_4 formation dominated over CH_4 formation on Cu (100), because the energy

barrier of C–C bond coupling was much lower than that for *CHO formation. The protonation of *OCCO occurred at potentials prior to *H adsorption, explaining why C–C coupling was prior to HER on the Cu (100) facet.

4.2 Nanostructured Copper as Efficient Catalysts for CORR

Nanostructured catalysts have many advantages over bulk catalysts, such as large surface area, low coordinated sites and more compatible with the setup of gas-phase flow cells. The morphology of catalysts can be rationally designed to expose preferred catalytic sites or regulate the interface environment, thus controlling the activity and selectivity of CORR.

4.2.1 Nanostructured Catalysts Studied in H-Cells

The H-type electrolytic cell is used extensively in early research of CORR, which is convenient for fast measurement of the performance of catalysts. Based on H-cells, Kanan and coworkers tested the performance of OD–Cu and found that the OD–Cu electrodes greatly boost the CORR and CO_2RR selectivity and activity compared with the polycrystalline copper counterpart [7, 9]. OD–Cu exhibited total *FE* of 57% for CORR products at –0.3 V, with CH_3CH_2OH and CH_3COO^- as exclusive products at low overpotential and emerging C_2H_4 evolution at high overpotential. On the contrary, the commercial polycrystalline copper exhibited low FE_{CO} (< 6%) with products of CH_3COO^-, CH_3CH_2OH and C_2H_4. This improvement of CORR selectivity is assumed to be related to distinct grain boundaries between interconnected nanocrystallines observed in the TEM images of OD–Cu. This assumption is strongly supported by quantitative analysis between density of grain boundaries in Cu nanoparticles and their CO reduction activity [147]. By analyzing a series of Cu catalysts with different density of grain boundaries, the surface area normalized j_{CORR} was linearly proportional to their density of grain boundaries with intercepts very close to 0, suggesting that density of grain boundaries was the only factor in this research to influence the CORR activity (Fig. 9). Furthermore, when scanning electrochemical cell microscopy (SEC CM) was performed in CO_2 saturated electrolytes with low overpotential, the GB

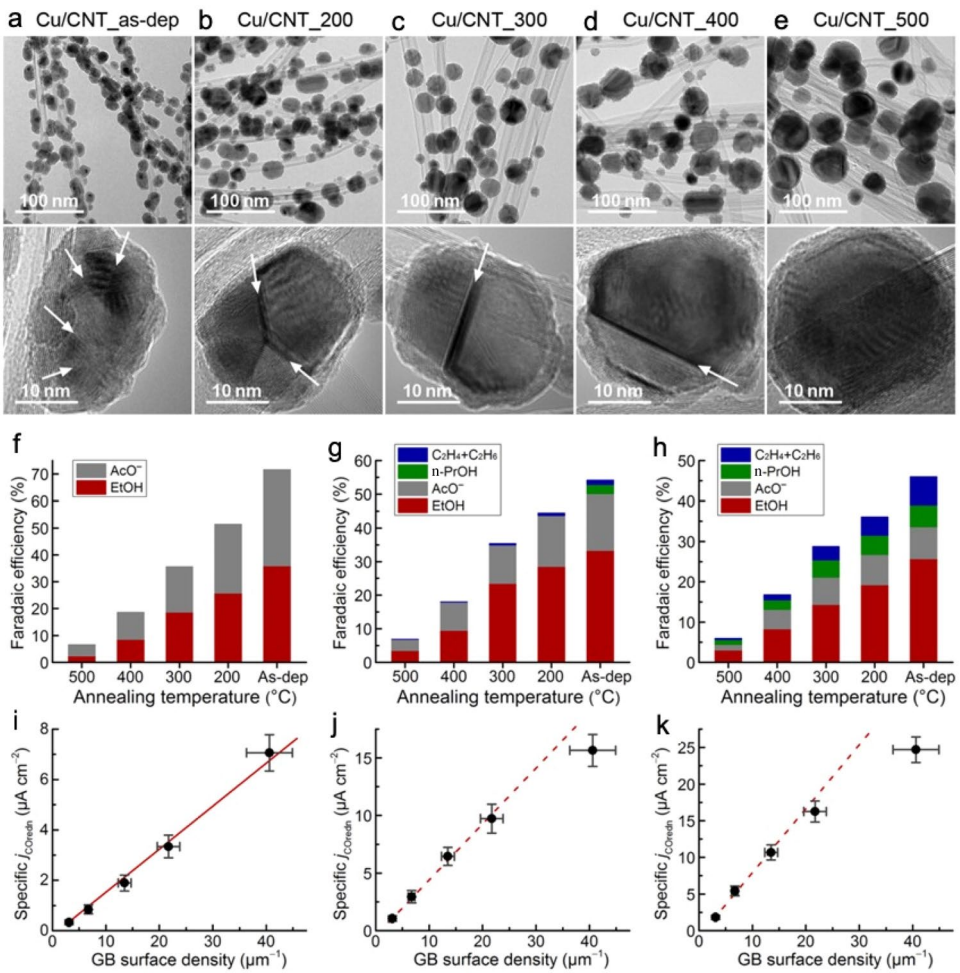

Fig. 9 **a**–**e** TEM characterization of Cu nanoparticles in the Cu/CNT electrodes. The five columns are the **a** as-deposited Cu/CNT electrode and the electrodes annealed under N_2 at **b** 200 °C, **c** 300 °C, **d** 400 °C, and **e** 500 °C. Top row—overview TEM images; the bottom row—representative high-resolution TEM images. The arrows indicate the gain boundaries. **f**–**k** *FE* for CORR on the five Cu/CNT electrodes. **h**–**j** Specific activity for CORR vs. the GB surface density. The potentials are – 0.3 V (**f**, **i**), – 0.4 V (**g**, **j**), and – 0.5 V (**h**, **k**) versus RHE. Adapted with permission from Ref. [147]. Copyright © 2016, American Chemical Society

region showed a steady reaction signal peak that was 2 to 2.5 times as large as the neighboring grains [54], whereas the HER between GB and grains does not show any difference.

An assumption for the effect of grain boundaries is that grain boundaries can support intermediate of C2 production by providing special catalytic sites with unique spatial distribution. This was confirmed by the temperature-programmed desorption (TPD) experiments on OD–Cu that extra binding sites with strong CO binding energy existed in comparison with polycrystalline copper foil, which was assumed to be the signal of grain boundaries [52]. The emerging new CO adsorption IR band at 2058 cm^{-1} during CORR for OD–Cu in comparison with polycrystalline Cu was another evidence that extra binding sites existed on OD–Cu surfaces [148]. Goddard and coworkers calculated the effects of grain boundaries on OD–Cu for CORR activity with DFT calculations [149]. The chemical vapor deposition of Cu NPs on a CNT was first simulated by the Molecular Dynamics simulations to establish a model of 10 nm Cu NPs (158555 atoms) on a CNT. The results showed that 9% of the surface sites have binding energy larger than three typical facets of (111), (100), and (211). This is consistent with the strong bonding sites reported by experimental TPD desorption [52]. Further calculation for the energy barrier of *OCCOH formation revealed that not all strong CO binding sites were active for C2 formation, but only the strong CO binding sites with at least one under-coordinated neighbor square site could promote C–C coupling. The active site presented in these studies may provide a prototype for future catalyst design.

The further development of OD–Cu is hindered by the relatively uneven morphology and surface structure distribution, which affects the determination of key active structures. Meanwhile, the sample preparation process of OD–Cu is relatively rough; thus, it is difficult to further optimize and adjust the structure. There are many successful cases in the synthesis of Cu catalysts with regular and uniform nanostructures by solvothermal methods, which expose special crystal faces. For example, cubic particles expose only (100) crystal faces, and octahedral particles expose only (111) crystal faces. The nanowire is well-studied morphology of Cu-based catalysts for CORR due to its high surface area and abundantly exposed facets. Wang and coworkers reported the synthesis of Cu nanowires by low-temperature (150 °C) thermal reduction of CuO nanowires under a hydrogen atmosphere and the obtained Cu nanowires exhibited high C2+-producing activity for CORR [150]. Particularly, the *FE* for CH_3COO^- and CH_3CH_2OH reached maxima of 21% and 50% at –0.25 V and –0.3 V, respectively. Other products, including C_2H_4 (up to 7%), C_2H_6 (up to 2.3%), and C_3H_7OH (up to 1.8%), were also observed at potentials more negative than –0.3 V. Increasing annealing temperature to 300 °C dramatically decreased the FE_{CORR} to < 10%. Using TPD analysis, a high (110) facet proportion of 14.3% was determined for the sample annealed at 150 °C, whereas the 300 °C-annealed sample showed a 3% (110) facet. Based on DFT calculations, the (110) facet is metastable and the most active for the selective reduction of CO to C2 species. Sun and coworkers also reported CORR properties on micrometer long Cu nanowires with a diameter of 50 nm [151]. The five-twinned structure of nanowires was assumed to expose five (100) planes, which favors the C–C coupling reaction for C_2H_4 evolution. The Cu nanowire exhibited *FE* of 60% for C_2H_4 and C_2H_6. Despite these discoveries, there is still a lot of areas to be explored in this research direction of utilizing nanostructured catalysts for CORR. Nanoparticles with special morphology may result in special catalytic selectivity of CORR. For example, cubic Cu nanoparticles have always been reported to increase the selectivity of CO_2 to ethylene by the exposed (100) faces [88]; however, it is yet to find out whether it has a similar improvement effect for CORR.

Notably, it is possible that in some cases the improved CORR selectivity observed from the nanostructure catalysts may not really attribute to the specific catalytic structure on the catalysts surface. Many studies have shown that multicarbon oxygenates tend to be produced at low overpotential (–0.25 to –0.50 V) [7, 122]. Jaramillo and coworkers proposed that high roughness factors might be the main reason for relatively high *FE* and producing rates of CORR observed on nanostructured Cu catalysts because electrodes with high roughness factors amplify the geometric CORR current density toward multi-carbon oxygenates at relatively low overpotential. Based on a hierarchical Cu nanoflower electrode with high surface areas, Jaramillo and coworkers realized nearly 100% selectivity of CORR toward multicarbon oxygenates at low overpotentials by suppressing hydrocarbon and hydrogen production (Fig. 10a, b) [152]. The nanoflakes were about 20–30 nm thick and 200–600 nm wide, with an average surface roughness factor (*RF*) of (390 ± 40). Strikingly, at –0.23 V, almost exclusively C2+ oxygenates were observed for CORR on nanoflower copper, including CH_3CHO, CH_3CH_2OH, and CH_3COO^- (Fig. 10c). With increasing overpotential, the selectivity shifts further from CH_3CHO to CH_3CH_2OH, which reaches maxima of 60% at only –0.33 V, indicating that CH_3CHO could be the reaction intermediate for CH_3CH_2OH formation. The authors also tested other documented nanostructured Cu-based electrodes with a different morphology and *RF*s, which proved the selectivity of CORR toward C2+ oxygenate was strongly determined by the *RF* but not the morphology (Fig. 10d). Notably, although the nanostructured Cu catalysts can increase the geometric current density of CORR, the intrinsic activity of CORR on copper does not change much. The FE_{CORR} on polycrystalline Cu is comparable with the FE_{CORR} of oxide-derived Cu, and the species of CORR products on polycrystalline Cu and oxide-derived Cu are almost the same [26]. The most significant selectivity

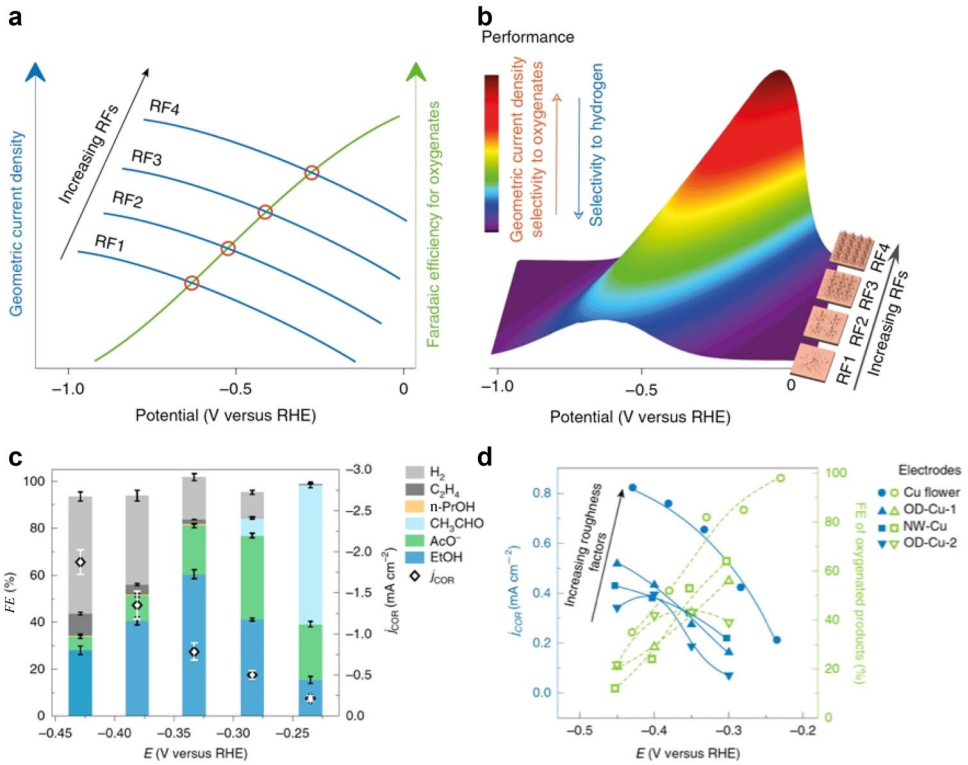

Fig. 10 **a** CORR performance dependences on overpotentials and the catalyst roughness factor. **b** Schematic of the CORR catalyst development strategy toward liquid oxygenates. **c** *FE* and geometric current densities for the CORR products vs. the electrode potential on Cu nanoflower electrodes. **d** Comparison of geometric CORR current densities (C2+ product current densities) and selectivity toward C2+ oxygenates for OD–Cu and Cu nanowires. Adapted with permission from Ref. [152]. Copyright © 2019, Springer Nature

difference between these two catalysts is the distribution of C2+ products. While nanostructured Cu favors alcohols, polycrystalline Cu produces more aldehydes and ethylene. Authors attributed this difference to the strong-binding under-coordinated sites on nanostructured Cu that can bind intermediate products stronger for further reduction. Moreover, the porous structure of nanostructured Cu could enhance the retention of aldehydes in near-surface space for a better chance to further reduce aldehydes to alcohol.

4.2.2 Nanostructured Catalysts Studied in a Gas-Phase Flow Cell

The studies in H-cells were mainly based on Cu catalysts with tailored micro-/nanostructures on Cu foil substrates, and many strategies have been employed to improve the CORR performance, including engineering the oxidation state of a metal catalyst, the selective formation of desired facets, the introduction of grain boundaries and the increase of roughness factors. However, although many studies of Cu catalysts showed enhanced C2+ *FE* of > 55%, the reaction rates were very low [7, 152]. This can be ascribed to the low solubility of CO in solution and the operation in batch-type cells. The recent investigation of CORR catalysts in gas-phase flow cells exhibited a dramatic difference in activity and selectivity compared to CORR in H-cells.

Jiao and coworkers reported CORR on OD–Cu and micrometer copper nanoparticles in a three-compartment flow electrolyzer [27]. Both the OD–Cu and micrometer copper nanoparticles showed a similar C2+ selectivity at high overpotentials, with total C2+ *FE* of 80%, indicating that the CO–to–C2+ activity of copper was not determined by morphology in this configuration (Fig. 11a, b). This observation is dramatically different from the aforementioned OD–Cu research in H-cells [7]. Furthermore, the CORR on OD–Cu exhibited 26% of $FE_{\text{n-propanol}}$ at − 0.42 V, much higher than the 2%–10% for OD–Cu tested in H-cells. The pH value of the electrolyte had a strong impact on the C2+ production, and the C2+ (especially for CH_3COO^-) partial current density and *FE* increased as the KOH concentration increased from 0.1 to 2.0 M (Fig. 11c, d). In 2.0 M KOH, total C2+ *FE* of 91% was achieved at − 0.67 V with a partial current density of 635 mA cm^{-2}. The reaction rates of a Cu catalyst combined with a GDL and tested in gas-phase flow cells were about two orders of magnitude higher than that tested in H-cells without the utilization of GDLs, and the difference can be even three orders of magnitude for the formation of C3 products.

A follow-up research from the same group further explored in gas-phase flow cells the relationship between CO reduction selectivity and copper exposed facets through studying the freestanding high-quality Cu nanosheets [153]. The average edge length and thickness of the 2D nanosheets were ~ (1.7 ± 0.5) μm and ~ 5 nm, respectively, with 99% of the exposed surface be (111). This provided a perfect platform to study the CORR performance on nanostructured

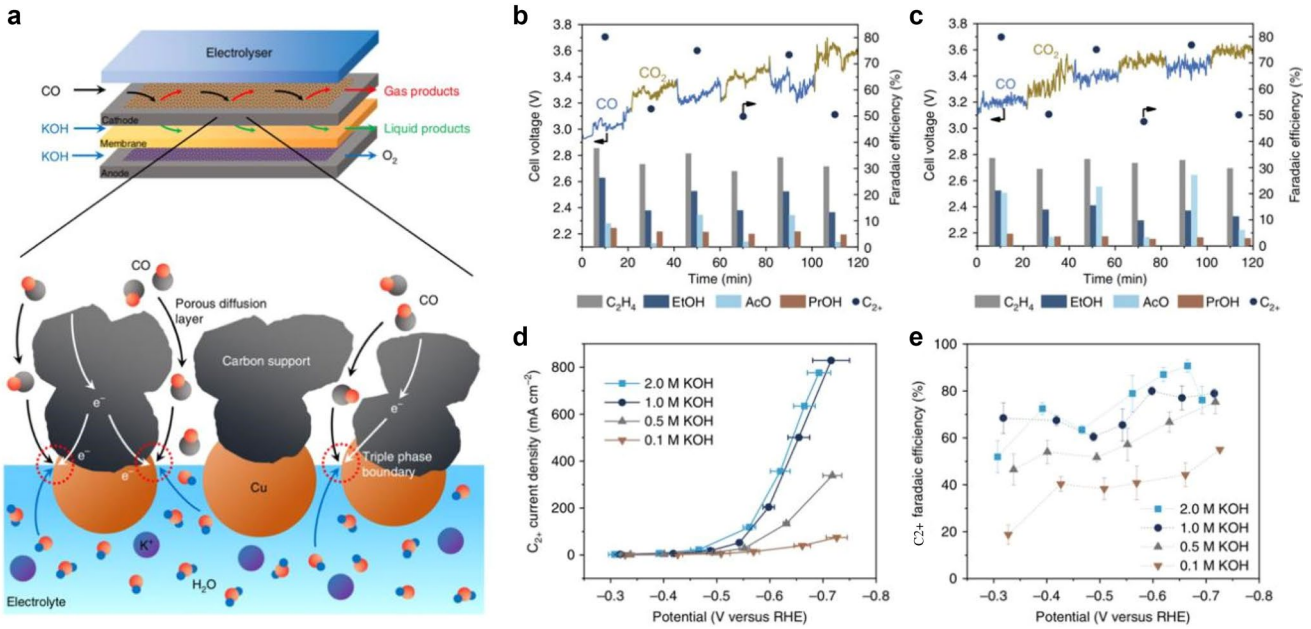

Fig. 11 **a** Top: schematic of the three-compartment microfluidic CO flow electrolyzer. Bottom: schematic of the well-controlled electrode–electrolyte interface for CO reduction at high current densities. The C2+ product distribution of CO/CO_2 reduction on **b** OD–Cu and **c** micrometer copper at 300 mA cm^{-2} in 1 M KOH. **d** Partial current density and **e** associated *FE* for C2+ products for CO reduction in varying concentrations of KOH. Adapted with permission from Ref. [27]. Copyright © 2018, Springer Nature

(111) facets in gas-phase flow cells. The maximum $FE_{CH_3COO^-}$ of 48% and $j_{CH_3COO^-}$ up to 131 mA cm^{-2} are achieved in 2 M KOH. The selectivity of CORR toward C_2H_4 and CH_3CH_2OH was greatly suppressed on Cu nanosheets compared to commercial Cu nanoparticles. This can be ascribed to the reduction of exposed (100) and (110) surfaces for 2D Cu nanosheets, because it was well known that (100) and (110) facets favored C_2H_4 and CH_3CH_2OH evolution. Interestingly, the $C^{18}O$ labeling studies on Cu nanosheets showed that only one oxygen of the CH_3COO^- originated from the CO feeding and the other oxygen came from the water. This phenomenon can be explained by the hydration of important intermediates CH_3CHO to ethane-1,1-diol, which would result in isotopic scrambling with water [154]. The CH_3CH_2OH further reduced from CH_3CHO would also contain oxygen derived from solvent water.

The platform of gas-phase flow cell emphasizes the C3 yield in CORR, thus providing a better platform for studying the relationship between catalyst structure and its C3 selectivity. Realizing long-chain products from CORR is also of interest to both the future industrial application and fundamental science research. Sargent and Sinton group proposed a hypothesis that C3 formation can proceed via C–C coupling between C2 and C1 intermediates. To this end, they designed several different types of copper catalysts with special morphology and performed the CORR in gas-phase flow cells with sufficient CO supply [155–157].

Copper adparticles were proposed as efficient catalysts for CORR due to high density of under-coordinated atoms and could serve as preferential sites for the formation of n-propanol [155]. Based on DFT prediction, the adparticles on metallic Cu surfaces could increase *CO/*C2 surface coverage and decrease the energy barriers toward intermolecular C–C coupling between *CO and *C2. The Cu adparticle structures were synthesized by in situ electroreduction of the copper oxide precursor under a CO-rich condition, which would weaken the interaction of the Cu–Cu bond and result in surface reconstruction. High-resolution scanning electron microscopy clearly showed the presence of adparticles with an average size of ~ 3.2 nm on the Cu backbone. These copper adparticles catalysts exhibited maximum FE_{C2+} of 89% reached at − 0.66 V. The production of n-propanol dramatically increased from 2.8% at − 0.32 V to a peak of 23% at both − 0.44 V and − 0.47 V and then gradually dropped to ~ 11% at − 0.66 V. The highest $j_{n\text{-propanol}}$ of 11 mA cm^{-2} was achieved at − 0.47 V. The control samples of commercial Cu nanoparticles and in situ reduced copper oxide under nitrogen gas conditions, which did not form adparticles, can only deliver peak $FE_{n\text{-propanol}}$ of 12% and 16%, respectively.

Another strategy was the introduction of nanocavity structure to promote C2:C1 coupling via the nanoconfinement and concentrating of C2 intermediates, which thereby promotes C3 formation [156]. The nanocavity structure was synthesized by gentle acidic etching of Cu_2O nanoparticles and sequential electrochemical reduction to the metallic

state. By finite-element method simulations, the nanocavity with an optimized open angle of 45°–90° was a benefit to both the C2 production and confinement, thus resulting in the best C3/C2 selectivity. The experimental results of a series of nanocavity catalysts with different opening angles consist with the finite-element method simulations. The cavity II nanocatalyst with an opening angle of ~ 90° showed higher $FE_{C_3H_7OH}$ but smaller $FE_{CH_3COO^-}$ and $FE_{CH_3CH_2OH}$ over the entire potential range compared to all other samples, consistent with the finite-element method simulations (Fig. 12). At − 0.56 V, $FE_{C_3H_7OH}$ reached its maximum of (21 ± 1)%, and the corresponding $j_{C_3H_7OH}$ was (7.8 ± 0.5) mA cm^{-2}.

Besides nanocavity structure, Sargent, Sinton, and coworkers reported highly fragmented (HF) copper catalysts can also bring C1 and C2 binding sites together to produce C3 product of C_3H_7OH [157]. It is well known that C2 production is more favored on Cu (100) than Cu (111); however, the first principle calculation shows that the C3 formation on Cu (100) is much slower than the reaction on Cu (111). Thus, it is interesting if one can restrict the CORR process in the interface between Cu (111) and Cu (100) and take advantage of active sites on both facets. Synthesis of HF copper catalysts was realized by replacing cupric salts in precursor solution with less reactive cuprous salt to slow down the nucleation and growth rates. Two control copper samples were prepared by annealing the as-synthesized CuO pre-catalyst or using a commercial CuO nanoparticle as the pre-catalyst, which were labeled as medium- and low-fragmented copper (MF–Cu and LF–Cu, respectively). The density of the Cu (111):(100) interface was measured by the high-resolution TEM (HR-TEM) and scanning transmission electron microscopy (STEM), and the density order was HF–Cu > MF–Cu > LF–Cu. HF–Cu showed the maximum $FE_{C_3H_7OH}$ of (20.3 ± 0.1)% at − 0.45 V, and corresponding energy conversion efficiency was 10.8%. The $FE_{C_3H_7OH}$ could keep at (19 ± 0.7)% at a potential as high as − 0.66 V to reach maximum $j_{C_3H_7OH}$ of (33 ± 0.6) mA cm^{-2}. On the contrary, MF–Cu and LF–Cu could only realize maximum $FE_{C_3H_7OH}$ of 17.5% and 11.5%, in agreement with the density of the Cu (111):(100) facet interface.

Notably, the investigation of CORR catalysts in gas-phase flow cells also requires us to reexamine the relationship of operating parameters and overall CORR catalysis

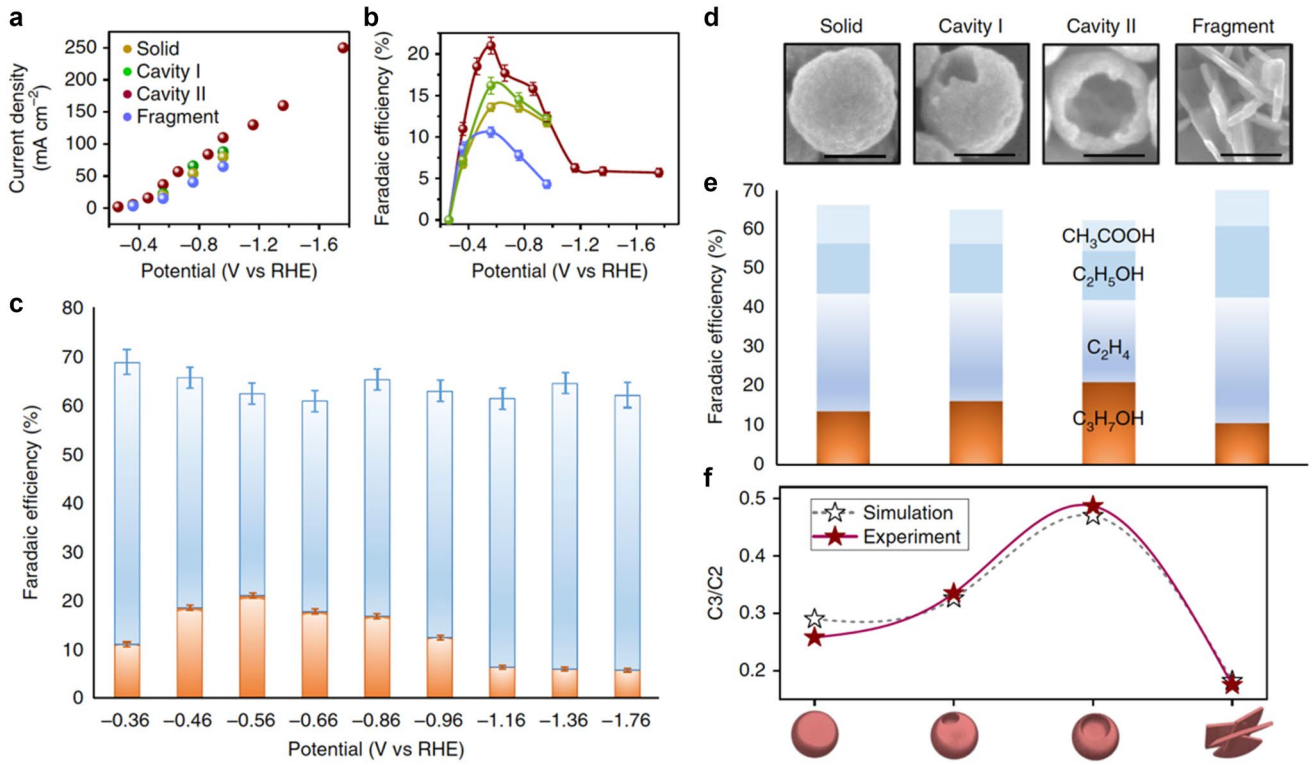

Fig. 12 **a** Plot of *j-V* curves on Cu-based catalysts with different morphology structures of solid, cavity I, cavity II, and fragment. **b** $FE_{C_3H_7OH}$ on the catalysts at different applied potentials. **c** *FE* of C2 products (CH_3COO^-, CH_3CH_2OH, and ethylene) (blue) and C3 propanol (orange) on the cavity II Cu catalyst under a range of applied potentials. **d** SEM images of these catalysts. Scale bars, 100 nm. **e** *FE* of C2 and C3 products on the catalyst morphology at the applied potential of − 0.56 V versus RHE. **f** The experimental and finite-element method simulation results of the C3/C2 product selectivity on different catalysts show a good agreement. Adapted with permission from Ref. [156]. Copyright © 2018, Springer Nature

performance. The pH value and CO supply in a gas-phase flow cell have a strong impact on the selectivity between C2+ products, and these parameters can be controlled to guide the formation of certain products. In Jiao's research, by introducing 2 M KOH electrolyte and pure CO gas in the gas-phase flow cell system, high C_2H_4 *FE* of 40% and cathodic energy efficiency of ~ 20% were achieved for CORR [27]. Sargent and coworkers further found that highly alkaline electrolytes actually favor the CORR to acetate rather than C_2H_4 [36]. It was found that when the concentration of KOH increased from 1 to 5 M, the $FE_{C_2H_4}$ gradually decreased and the formation of CH_3COO^- increased, indicating that concentrated hydroxide ions can react with the CORR intermediates that are relevant to C_2H_4, CH_3CH_2OH, and C_3H_7OH. The local CO availability was also found to be a key factor for high C_2H_4 selectivity, which can be tuned by CO concentration and reaction rates. Figure 13 shows the CORR performance of Cu catalysts tested in 1 M KOH with different concentrations of CO. By varying the incoming CO concentration from 2.5% to 100%, an overall increase of both the total current density and the CORR partial current density was observed. With 2.5% CO, peak $FE_{C_2H_4}$ of 51% was reached at − 0.53 V. For the operation condition with 5% and 10% CO, peak $FE_{C_2H_4}$ of 72% was reached at − 0.52 V. Further increasing the CO concentration to 50% and 100% leads to peak $FE_{C_2H_4}$ of ~ 70% at − 0.66 V and − 0.72 V, respectively, and the C_2H_4 partial current density corresponded to 509 and 808 mA cm^{-2}. High cathodic energy efficiency

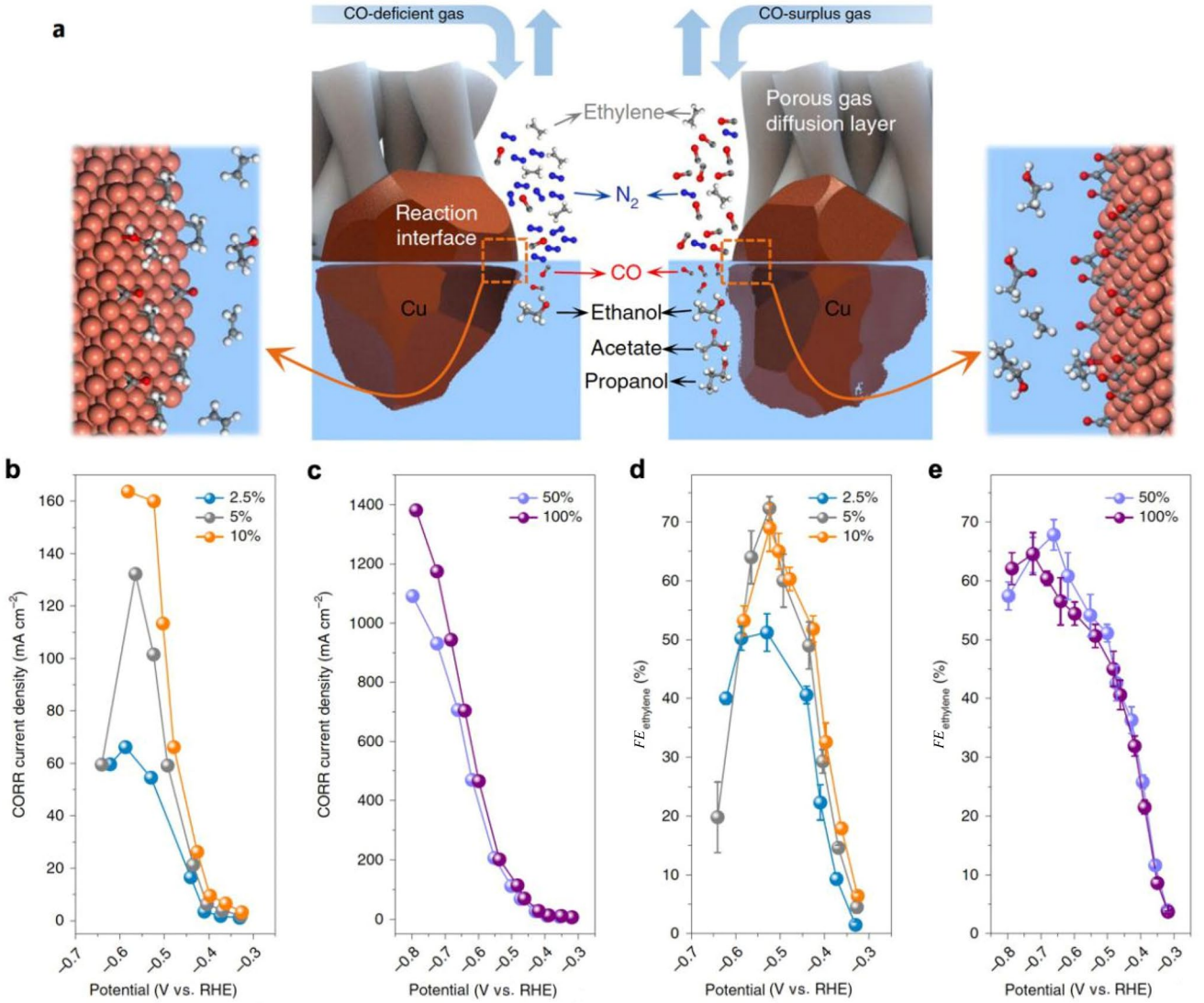

Fig. 13 **a** Schematic illustration of porous gas diffusion electrodes with CO reduction at the catalyst–electrolyte interface. The CORR partial current densities (**b**, **c**) and $FE_{C_2H_4}$ (**d**, **e**) at low (**b**, **d**) and high (**c**, **e**) CO concentrations in 1 M KOH. Adapted with permission from Ref. [36]. Copyright © 2019, Springer Nature

of 44% was achieved for C_2H_4 production under the condition of 5% CO. DFT calculations revealed the relationship between CO concentration and CORR selectivity. The lower CO coverage stabilized the C_2H_4-relevant intermediates and thus benefited the C_2H_4 pathway both thermodynamically and kinetically, whereas higher CO coverage favored oxygenate production.

The utilization of flow cells will play a very important role in future CORR catalyst research. However, this does not mean that the research in H-type cells can be completely replaced. In the H-type cell with the planar electrode system, the surface mass transfer model of the electrode is simpler, and the reaction interface is easy to define and model, so it is easier for the electroanalytical study of the catalysts. Furthermore, the membrane electrode assembly in a gas-phase flow cell based on gas diffusion electrodes is relatively difficult to combine with current in situ methods. Most of the mature in situ detection technologies are still based on the structure of the H-type electrolytic cell or one compartment cell.

4.3 Metal–Organic Catalysts

The CORR activity and selectivity of metal catalytic sites are strongly related to the local chemical environment. One promising strategy to control the structure of the active site is via the construction of metal organic ligands, which is proved to be effective in previous CO_2RR and water-splitting electrocatalysis [158–160]. Robert and coworkers demonstrated that cobalt phthalocyanine(CoPc), a well-known catalyst for the CO_2RR [93, 161], could also catalyze the reaction from CO to CH_3OH in aqueous electrolytes [162]. In this study, CH_3OH was produced with *FE* of 1%–2% and a partial current density of 0.06 mA cm^{-2} at pH of 7.2 and an applied potential of − 0.68 V. Upon increasing the pH value to 13, the *FE* and partial current density of CH_3OH increased to 14.3% and 0.68 mA cm^{-2}, respectively. CH_2O production was also observed with *FE* of 3.3%. However, further increasing the pH value to 14 resulted in the cease of CH_3OH production, probably due to the stabilization problem of CH_2O under ultra-high pH values, which is the intermediate of CH_3OH production. By combining the CO–to–CH_3OH system sequentially with the previous CO_2–to–CO system by using the same catalyst, theoretical global *FE* of 19.5% and chemical selectivity of 7.5% are expected for CO_2–to–CH_3OH.

Chang and coworkers demonstrated a molecular–materials interfaces strategy by self-assembly of supramolecular cages on the copper catalyst to promote the C–C coupling during electrochemical CO reduction [163]. The α,α,α,α-atropisomers was chosen to provide a rigid platform for face-to-face arrangement between the porphyrin molecule and the copper catalyst surface (Fig. 14a). Thiol-terminated legs built off of the porphyrin scaffold can strongly bind to the copper electrode material. The underpotential deposition proved that porphyrins with down orientation legs did not affect the accessibility of copper surfaces for electrolysis. The CORR test showed that surface-tethered porphyrins could significantly enhance the oxygenate formation on copper. By the introduction of a second metal site (e.g., Fe, Ni, Zn) in porphyrins, the CORR efficiency was further enhanced to an order of magnitude higher than unfunctionalized copper electrodes (Fig. 14b). The Fe-porphyrin derivative on Cu realized a j_{CORR} of 1.34 mA cm^{-2} and FE_{C_2} of 83%, in which $FE_{CH_3CH_2OH}$ was 57% and $FE_{CH_3COO^-}$ was 24% (Fig. 14c).

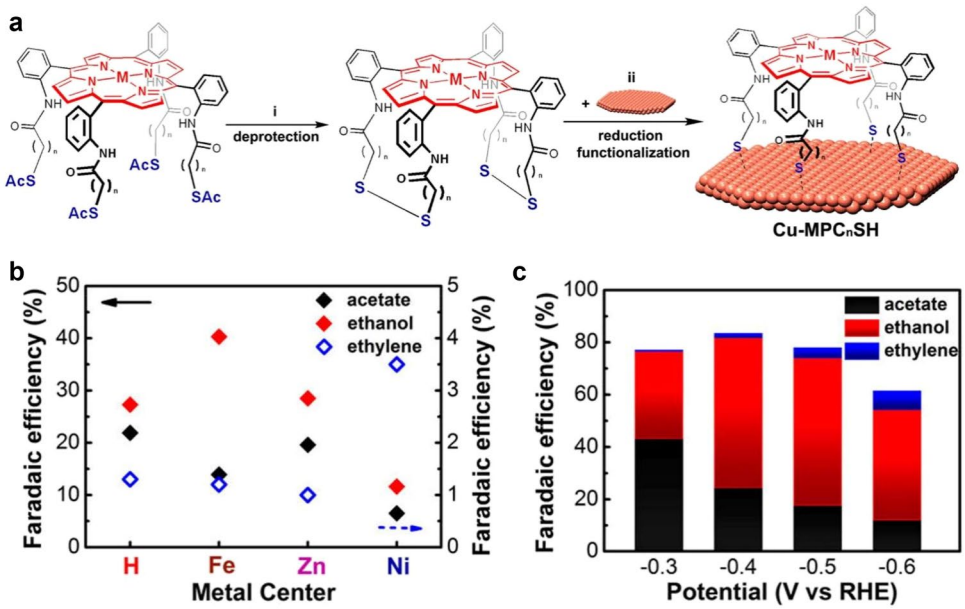

Fig. 14 **a** Schematic illustration of the functionalization of Cu surfaces with porphyrin cages. **b** FE_{CORR} on Cu foils functionalized with metalloporphyrins (Cu-MPC_2SH) at − 0.55 V in CO-saturated 0.1 M KOH. **c** *FE* on electrodeposited Cu functionalized with iron porphyrins ($FePC_2SH$). Adapted with permission from Ref. [163]. Copyright © 2017, American Chemical Society

More possible metal–organic CORR catalysts were predicted based on DFT calculations. For instance, a Mott–Schottky catalyst composed of a copper trimer and a holey C_2N semiconductor was designed, which can stabilize the $Cu^{\delta+}$ sites to promote the production of n-propanol [164]. By binding the Cu_3 cluster to the semiconducting C_2N substrate, the electron transferred from the Cu_3 to C_2N could retain the oxidation state of the Cu trimer. The calculation showed that the CO binding energy was relatively strong, and the CO dimerization energy barrier was much lower on the $Cu_3@C_2N$ catalyst than on traditional Cu (111), Cu (100) and Cu (211) surfaces. Double metal atoms anchored on carbon nitride (C_2N) may also efficiently produce C2 chemicals over CH_4 from CORR [165]. The calculated C–C coupling energy on the V-Mo dimer was found to smaller than Cu (100) (0.54 eV). Moreover, the CH_4 formation was greatly suppressed on the V-Mo dimer because the critical intermediate of *CH was not stable on V-Mo, resulting in a high C2/C1 products ratio on the V-Mo@C_2N catalyst. Although there are many reports for combining metals and semiconductors such as modified graphene, carbon tubes or C_3N_4 for CO_2RR [166, 167], which dramatically changed their selectivities compared with their mono-metal opponents, the experimental research on CORR molecular catalysts is still relatively limited. More experimental results are needed to verify the theoretical predictions.

4.4 Alloy Catalysts

Alloys provide a handle to tailor the geometric and electronic environments of active sites on the catalyst. The research on alloy catalysts in CORR basically revolves around Cu, because it is the only metal that can catalyze CORR with high selectivity. One of the alloy catalysts showing a very promising performance for CO_2RR toward C2+ was AgCu [82, 168]. Jaramillo and coworkers demonstrated AgCu alloy could also realize almost single selectivity for carbon product of CORR [169]. In their research, CuAg alloy was synthesized by the galvanic replacement approach, in which a polycrystalline Cu foil was immersed into a dilute $AgNO_3$ solution. The final electrode exhibited a Cu:Ag atomic ratio of 7:1 at the surface. The planar CuAg electrode favored the CH_3CHO production and achieved *FE* of 50% at − 0.5 V, which accounts for 90% of all carbon basis products. By increasing the *RF* of CuAg electrodes, the FE_{CH_3CHO} can further increase to 70%. The selectivity of CORR toward CH_3CHO would gradually shift to C_2H_4 and eventually, CH_3CH_2OH with more negative electrode potential. The origination of CH_3CHO selectivity was studied by comparing the activities of CH_3CHO reduction on Cu and CuAg. The result showed that CuAg was much less active to further reduce CH_3CHO to CH_3CH_2OH, which might be ascribed to weaker binding of the key intermediate, $*CH_3CH_2O$, on Cu than Ag ad-atoms.

Sargent, Sinton, and coworkers also proposed that Ag-doped Cu exhibited the highest activity for C1–C1 and C1–C2 coupling among different M-doped Cu candidates (M = Ag, Au, Ru, Rh, and Pd), due to the strain and ligand effects of Ag doping on neighboring Cu atoms [170]. Based on DFT calculations, it was revealed that two adjacent Cu atoms with and without neighboring Ag atoms have different electronic structures and atomic structures, thus promoting the C1–C2 coupling between asymmetric C1 and C2 intermediates (Fig. 15a). Ag-doped Cu nanocatalysts were fabricated by a galvanic replacement approach, in which the Cu GDE was immersed in 5 μmol L^{-1} $AgNO_3$ aqueous solution to obtain the Ag-doped Cu GDE. The total *FE* of CORR in a gas-phase flow cell toward C2+ reached 80% on the Ag-doped Cu GDE at − 0.56 V, in comparison with 60% on pristine Cu. In particular, the Ag-doped Cu GDE realized high n-propanol *FE* of (33 ± 1)%, whereas $FE_{propanol}$ on pristine Cu was (22 ± 1)% (Fig. 15b, c). Besides galvanic replacement approaches, the Cu–Ag alloy catalysts can also be realized by reduction of Ag–Cu oxides. Schmid and coworkers reported that $Ag_2Cu_2O_3$ can be used as starting template material for CORR to C2+ products [171]. The separate-phase CuAg bimetallic material was in situ formed during the first 2 min of electrolysis. The resulted catalysts showed *FE* for C2+ products during CORR of ca. 92% at 600 mA cm^{-2}, with dominant products of ethylene, ethanol, and acetate. The differences in the selectivity of these experiments of AgCu catalysts also indicate that the actual local atomic structure of Cu–Ag and the test environment have a great influence on the performance of the catalyst.

Besides traditional alloy catalysts, high-entropy alloys have also been proposed as efficient CORR catalysts based on the DFT calculations [172]. The analysis of Rossmeisl and coworkers was focused on CoCuGaNiZn and AgAuCuPdPt high-entropy alloys because these elements were previously used as CO_2RR catalysts. Locally optimal composition of Cu, $Co_9Ga_{42}Ni_7Zn_{42}$, $Ga_{83}Ni_{17}$, $Ag_{69}Cu_{31}$, and $Ag_{84}Pd_{16}/Au_{84}Pd_{16}$ was found for CORR, if activity and selectivity are equally considered. Considering that a > 10% ratio of each element may be the requirement to access high-entropy alloys, other optimized composition of $Co_{10}Cu_{10}Ga_{60}Ni_{10}Zn_{10}$ and $Ag_{30}Au_{33}Cu_{17}Pd_{10}Pt_{10}$ was proposed. A high-entropy alloy of AgAuCuPdPt with an equal amount of each metal was then synthesized experimentally by melting and cryogrinding for the test of CO_2RR [173]. All metals were homogeneously distributed in fcc-facet crystalline structures. A dramatically different selectivity of this high-entropy alloy compared with mono Cu metal was realized as CO_2 was 100% converted to gaseous products at a low voltage (− 0.3 V). The effect of novel types of alloy catalysts, including high-entropy alloys, in CORR remains to

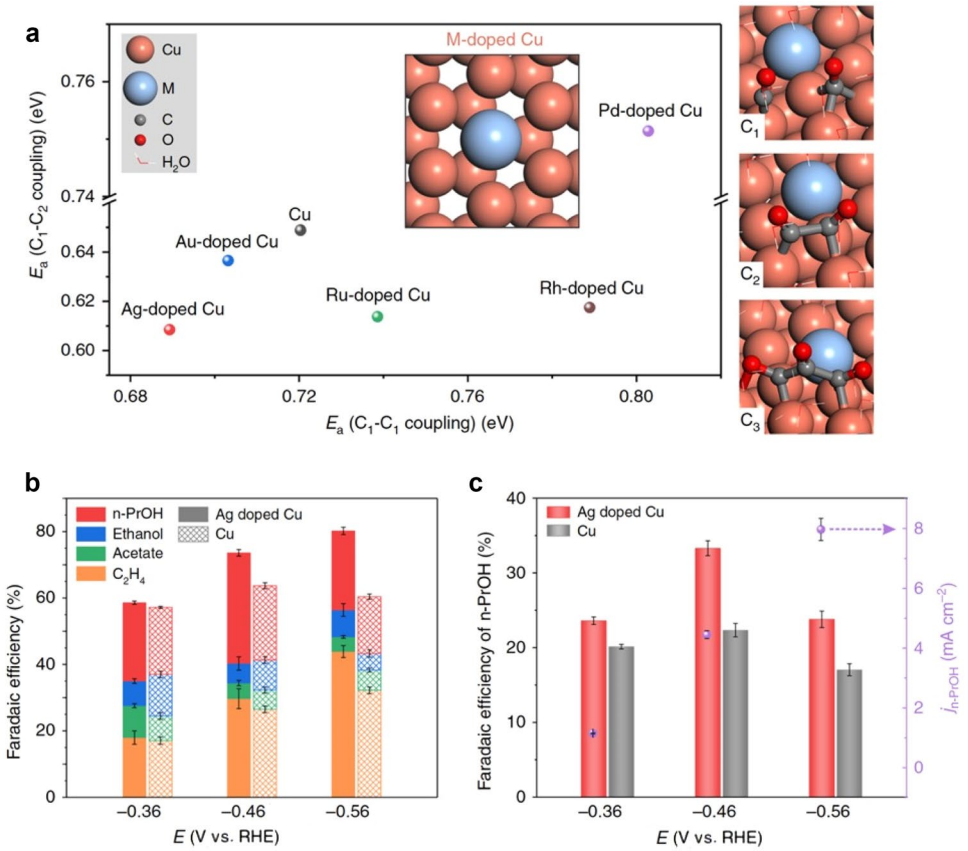

Fig. 15 **a** DFT calculations on reaction barriers (E_a) for C1–C1 and C1–C2 coupling on screened M-doped Cu systems (M = Ag, Au, Ru, Rh, and Pd). **b** *FE* of n-propanol, CH_3CH_2OH, CH_3COO^-, and C_2H_4 on Ag-doped Cu and pristine Cu catalysts under different potentials. **c** $FE_{n\text{-propanol}}$ on Ag-doped Cu and Cu GDEs under different potentials, as well as $j_{n\text{-propanol}}$ formation on Ag-doped Cu GDEs. Adapted with permission from Ref. [170]. Copyright © 2019, Springer Nature

be studied in order to provide new mechanism understanding and performance.

5 In situ and Operando Studies

Before any technical consideration on the implementation of electrolyzers for CORR is made, the fundamental problem of the electrocatalysis selectivity and activity must be solved. The key step toward optimizing the CORR performance is the formulation of the reaction mechanism that can explain the observed selectivity and onset potential for different products. The elucidation of the relationship between catalysis and reaction environment is also important. The common route for the development of electrolytic catalysts is the long feedback loops of synthesis, testing, and analyzing the catalyst in order to form an optimization roadmap. In situ and *operando* tests can greatly accelerate the feedback loops by directly providing the structure information of reaction sites. In particular, infrared (IR) spectra can provide the information of C-based intermediates on the catalyst surface, scanning tunneling microscope (STM) can show the surface structure of the catalysts, and X-ray absorption fine structure spectra (XAFS)/ X-ray diffraction (XRD) and Raman spectra can provide information of the evolution process of the metal center during catalysis.

5.1 Operando IR Techniques for Determining Key Intermediates During CORR

Operando IR spectroscopy is a noninvasive technique that is sensitive to the functional groups, and it can recognize signals for even ~ 3 molecular monolayers on the interface. For CORR, *operando* IR spectroscopy can provide evident fingerprints and structural characteristics for the intermediates such as adsorbed CO (2052–2083 cm^{-1}), adsorbed COOH (1379–1402 cm^{-1}, 1720 cm^{-1}), adsorbed CO_3^{2-} (1517–1544 cm^{-1}) and other intermediates on the interface or in the electrolyte [98]. The most significant challenge for the *operando* IR detection of CORR and other aqueous electrochemical reactions is the strong absorption of IR by water. To this end, attenuated total reflection infrared (ATR-IR) spectroscopy has been developed as the most common detection mode for aqueous electrochemical reactions [174].

It has been proposed that a negatively charged CO dimer should be the first C–C coupled intermediate [66, 175, 176]. However, the existence of the dimer was usually deduced

from experimental and computational results. Direct experiment evidence confirming the CO dimerization in the liquid electrolyte during CORR on the Cu electrode was absent. *Operando* IR has been employed in many pieces of research to monitor the information of CO coverage and binding sites on different kinds of Cu electrodes [32, 148]. Koper and coworkers further developed an *operando* IR experiment to provide experimental evidence for the formation of a hydrogenated CO dimer (OCCOH) at low overpotentials during CORR on Cu (100) electrodes in LiOH electrolytes [177]. Comparing the absorption spectra taken under Argon atmosphere and CO atmosphere, bands originated from CO introduction could be found. Based on the combined experimental data obtained in H_2O and D_2O, two bands (1191 and 1584 cm^{-1}) coming from C containing species were identified at low overpotentials on Cu (100) only. Notably, these bands emerged at the potential range where no CORR reduction products existed, suggesting that the bands should be ascribed to the vibrations of adsorbed intermediates of CORR rather than to species in electrolytes. The IR absorption band positions of C1 species of CHO and COH, and C2 species of the CO dimer, the lithiated dimer, the hydrogenated CO dimer, and the adsorbed acetylenediol were all calculated by DFT methods to identify the intermediate structure. It was found that the bands at 1191 and 1584 cm^{-1} can be attributed to C–O–H and C=O stretching vibrations and originated from a simple hydrogenated dimer (OCCOH), providing direct evidence to prove that the C–C coupling to C2 species on Cu (100) occurred through a reductive dimerization step at the early stage of the reaction mechanism. Koper and coworkers then reported an IR absorption study of the influence of cations on the different copper facets for CORR [124]. On Cu (100), two common bands existed for all alkaline electrolytes. The first band located in the range of 1635–1600 cm^{-1}, corresponded to the O−H bending mode of H_2O. The second band located in the range of 1730–1670 cm^{-1}, corresponded to the C–O stretching of CO adsorbed on hollow sites on Cu (100). However, the band at 1191 cm^{-1} attributed to the C–O stretching of a hydrogenated dimer (OCCOH) was only observed in Li, Na, and K hydroxides, but not in Rb and Cs hydroxides. This could be explained by DFT calculations, which indicated that the potential required for coupling of 2 *CO to *OCCOH was − 0.10 eV for Li^+, − 0.16 eV for Na^+, and − 0.28 eV for Cs^+. Therefore, the hydrogenated dimer could only be observed in Li and Na hydroxides, but not in Cs hydroxides at low overpotential (> − 0.2 V). The spectra obtained for CORR on Cu (111) only show apparent band signals at 1407 cm^{-1}, consistent with the dramatic selectivity difference on Cu (111) and Cu (100).

5.2 Operando X-Ray Techniques for Monitoring Catalyst Structure Evolution During CORR

The monitoring of the dynamic change of the atomic structure of the electrode under CORR is necessary to obtain reliable structure–property relationships and guide the development of more active and selective catalysts. X-ray detection methods such as XRD and XAFS endowed the high penetration ability in aqueous solution and are sensitive to the long-range and short-range structure change of Cu catalysts. One challenge for X-ray research on liquid-phase electrochemical catalysts is that X-rays can penetrate the sample by a depth of several microns and are not only sensitive to interface signals. To overcome this challenge, the grazing incidence method needs to be used for the detection of planar samples, and the scale of nanostructured samples should be small enough to ensure a high surface ratio.

In the previous study, oxidation of Cu was believed to improve the CO_2RR performance of Cu toward C2+ products; however, the presence of subsurface oxygen in Cu electrodes during the electrolysis is under debate [18, 74]. Recently, Chorkendorff, Jaramillo, and coworkers studied the structure change of Cu_2O during CORR by in situ grazing incidence X-ray diffraction (GIXRD) with synchrotron radiation [178]. It was clearly showed that the broad Cu_2O (111) peak centered at $2\theta = 16.9°$ disappeared after electrochemical reduction (Fig. 16b). The in situ tests confirmed that the time required for the total reduction was merely 40 s, when the potential was applied between 0.4 and 0.3 V (Fig. 16c). The reduction process would be slightly different with CO atmosphere compared with Ar atmosphere, due to the role of CO as a chemical reductant. In particular, a surface reconstruction of the copper catalyst was observed with the CO atmosphere as the Cu (200)/Cu (111) intensity ratio increased after electrochemical reduction of Cu_2O (Fig. 16e). This helps to explain the high selectivity for CO reduction to ethylene on oxidized polycrystalline Cu, because (200) is similar to the stepped (100) surfaces. Compared with Raman spectroscopy, GIXRD can be more surface-sensitive and has high time resolution, providing a powerful means to probe the surface structure during the chemical reaction. Although in situ X-ray absorption spectroscopy has been employed in the research of CO_2RR and provides many useful information of structure evolution, its application in CORR is yet to perform.

5.3 Operando STM for Monitoring Catalyst Surface Reconstruction During CORR

Due to the high mobility of the surface atoms of Cu, the polycrystalline Cu surface is also susceptible and easy to be reconstructed during operation. Notably, the electrochemically prepared Cu(*hkl*) surfaces would easily be oxidized

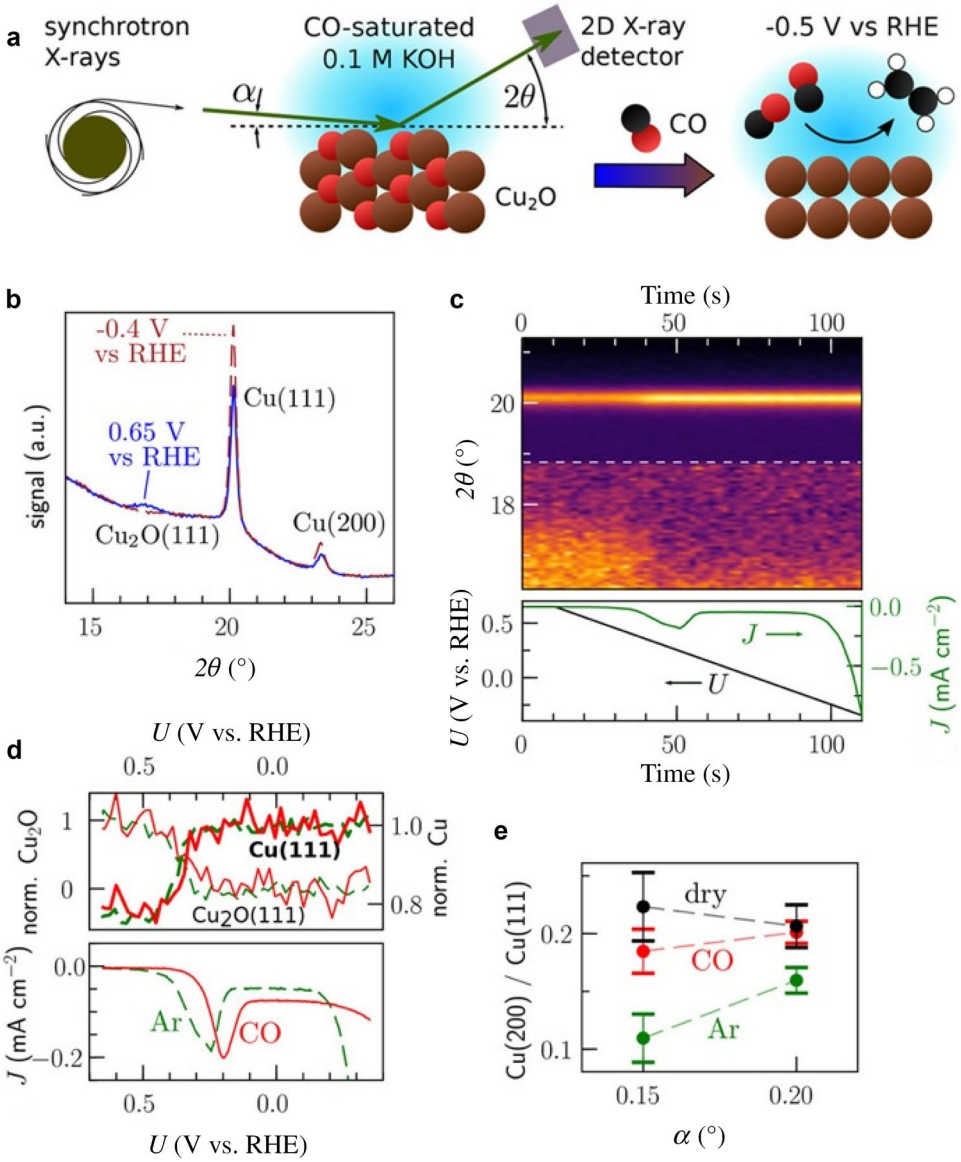

Fig. 16 **a** Scheme of in situ GIXRD of polycrystalline Cu electrodes. **b** Diffractograms of a Cu sample at an incident angle $\alpha = 0.15°$ in CO-saturated 0.1 M KOH. **c** *Operando* monitoring of diffraction signals during the reduction of a sample in Ar-saturated electrolytes. **d** Normalized integrated Cu (111) and Cu_2O (111) Bragg peaks during the reduction of samples in Ar-saturated or CO-saturated electrolytes. **e** The ratio of the integrated Cu (200) to Cu (111) peaks for dry samples and reduced samples as a function of incident angles. Adapted with permission from Ref. [178]. Copyright © 2019 American Chemical Society

once it is removed from the influence of the applied potential in solution, resulting in the difficulty to understand the real connection between surface facets and the CORR performance. The STM method can probe the atomic arrangement on the catalysts surface and has been developed to immerse the STM probe into the liquid media for electrochemistry applications, namely electrochemical scanning tunneling microscopy (EC-STM) [179]. By combining this method with differential electrochemical mass spectrometry, the relationship between surface facets and selectivity can be better understood.

Based on the *operando* EC-STM method, Soriaga group first reported that the polycrystalline Cu electrode underwent a stepwise surface reconstruction under − 0.9 V vs. SHE in 0.1 M KOH [180]. The polycrystalline Cu surface was first transformed to Cu (111) within 30 min and then converted to Cu (100) after another 30 min. The obtained Cu (100) was stable, and no further transformations occurred with prolonged operation time. This is important information to avoid the misunderstanding of the origination of selectivity on polycrystalline Cu.

This method also provides a promising opportunity to understand and steer the selectivity of Cu electrodes by reconstructing the surface. Normally, at low overpotential, pristine Cu (100), Cu (111) or Cu (100) surface structure by Cu(pc)–to–Cu(100) reconstruction did not produce ethanol. Interestingly, a subsequent $Cu \leftrightarrow Cu_2O$ oxidation–reduction cycle between − 0.9 and 0.1 V vs. SHE converted the reconstructed region to a stepped Cu(S)-[3(100) × (111)], or the Cu (511) surface [181, 182]. The obtained Cu (511) surface

exhibited an excellent selectivity for ethanol at a low overpotential of − 1.06 V vs. SHE; the *FE* for CO toward ethanol was almost 100%.

Further studies based on *operando* polarization-modulation IR reflection–absorption spectroscopy (PMIRS) revealed that on the reconstructed Cu (511) surface, the surface coverage of CO increased from 0 to 0.5 as the potential was stepped from − 0.80 V to − 0.85 V vs. SHE and fixed at 0.5 at even more negative potential, indicating that all available surface coordination (adsorption) sites have already been taken up [183]. The peak position of ν_{CO} was ~ 2025 cm^{-1}, which can be ascribed to the adsorbed molecule with fully vertical orientation at an atop site (ν_{CO} for top-site bonding is in the range of 2000–2130 cm^{-1}; twofold and threefold bridge coordinations have been marked by the ranges 1860–2000 cm^{-1} and 1800–1920 cm^{-1}). Interestingly, only signals corresponded to terrace-bound CO adsorbates were apparent in this study because the vibrational characteristics of CO are evidently different from that on stepped surfaces, suggesting that under-coordinated step sites may not be involved in the production of ethanol. *Operando* STM results, on the other hand, provided information on the CO adsorption pattern. When the Cu (100) surface was immersed in 0.1 M KOH with saturated CO under a potential more negative than − 0.8 V, the CO adlayer structure from EC-STM detection was Cu (100)-*c*(2 × 2)–CO or Cu (100)-($\sqrt{2} \times \sqrt{2}$)–CO, with a coverage θ_{CO} of 0.5.

6 Summary and Perspectives

CORR with high selectivity and energy conversion efficiency toward high-value products is crucial for the realization of large-scale industrial applications. The ideal CORR system should provide C2+ with > 80% purity and > 70% energy efficiency at > 200 mA cm^{-2} [19, 20]. The system should be stably operated for more than one year. The realization of pure C2+ products is still limited due to the lack of understanding between the structure and function of catalysts. In addition, the energy efficiency for CORR is still below 50% at > 200 mA cm^{-2} [19, 20, 142]. The performance of CORR in early studies operated in H-cells has been severely limited by the sluggish mass transport of the reactants in the electrolyte, obliging the urgent development of the CORR flow reactor. In this review, we emphasized the difference between CO_2RR and CORR and then summarized the current strategies of optimizing electrolyzers for efficient CORR, highlighting the importance of designing a standard test platform for highly efficient CORR and reliable results comparison. The effect of electrolyte composition, pH, catalyst surface facets, and nanostructuring on the performance of CORR was discussed as efficient methods to steer the activity and selectivity of CORR. The development of surface-sensitive in situ and *operando* techniques such as STM, PMIRS, GIXRD for CORR has been emphasized for their potential to provide valuable insights into the evolution of catalytic structure and intermediate products of CORR.

Although the oxide-derived and nanostructured copper catalysts showed promising high performance for CORR, a deep understanding of the C–C coupling toward multiple-carbon products in the flow reactor was not complete. The different experimental parameters used in different research works and the difficulty of identifying active catalytic sites due to the instability or non-uniform catalysts are the major obstructions. This requires a full elucidation of the relationship between the structure of catalytic sites, reaction environment, and reaction pathways, in order to manipulate the interaction between reactant and catalytic sites. Thus, the following challenges should be considered and addressed to push the CORR technique toward industrial applications.

6.1 Optimizing the Operation Parameters for a Standard Gas-Phase Flow Cell

The large CORR performance differences observed for different catalysts tested in H-cells may become negligible when they are tested under the quasi-practical condition in a gas-phase flow cell because of the different reaction interfaces and reactant supply modes[27]. To provide a suitable catalyst for the future CORR industry, it is necessary to calibrate the performance of the catalyst under a high current density (> 200 mA cm^{-2}) in a gas-phase flow cell with sufficient reactant supply. To fairly compare the performance of catalysts reported in different research groups, the critical factors that influence the CORR in a gas-phase flow cell need to be determined and a standard testing environment needs to be established. Compared with the more mature CO_2 gas-phase flow cells, there are some similarities and differences in the CORR gas-phase flow cells. For instance, the selectivities of CO_2–to–C2+ and CO–to–C2+ can both be enhanced by larger cations and higher pH values of electrolytes [121, 124]. However, for CORR, the situation may be more complex due to the large amount of liquid oxygenate products. Generally, the formation of ethylene from CORR is more favored in the 1 M KOH electrolyte and a much higher concentration (> 1 M) is believed to favor the oxygenate production over ethylene due to the influence of OH^- on the intermediate structure [36, 153]. CORR products of ethylene, ethanol and propanol are assumed to share the same C–C coupling rate-limiting step. The selectivity is tuned mostly by the design of the catalyst rather than the environment. If a more in-depth understanding of the intermediate structures and rate-limiting steps that determine the selectivity of these products (ethylene, ethanol and propanol) can be realized, it may be possible to fine-tune the C2+ selectivity of CORR by changing the reaction environment.

Notably, the interaction of reactant with electrolytes and products distribution of CORR are totally different from that of CO_2RR. The membrane–electrode interface and the three-phase interface in GDLs need to be specially optimized. The parameters, including CO concentration, gas flow rates, GDL structure, hydrophobic property, membrane property and so on can all potentially impact the whole-cell performance. A non-optimized cell configuration may result in high voltage consumption and low faradaic efficiency and cause the sudden shutdown of the electrolyzer due to flooding of electrolytes, drying up of membrane interfaces or crystallization of salts [27, 140]. Multiphysics theoretical simulation will play a very important role in constructing and optimizing the CORR reaction cell, and more research for such simulation is highly desired.

6.2 Design Nanostructured Catalysts with Varying Morphology and Composition for CORR in Gas-Phase Flow Cells

Currently, the investigation of the relationship between the morphology of catalysts and multicarbon selectivity of CORR is still at an early stage. There is still a controversy about whether simply increasing the surface area of copper catalysts can really change the intrinsic catalytic property of surface bonding sites [26, 152]. Nevertheless, the research on single-crystalline Cu facets of (100) and (111) clearly showed the surface atomic arrangement could influence the selectivity of CORR [23, 24], and there were successful examples where the fine-tuning of the local structure of copper without a dramatic change of whole morphology could significantly improve the selectivity toward C2 and C3 oxygenate products in a gas-phase flow cell [156, 157]. Many catalysts with well-designed morphology have been studied in CO_2RR, such as nanocube copper [88, 184], nanowires [89], Cu rhombic dodecahedra with (110) facets [185]. In specific, nanocube copper with exposed 100 facets was able to reach 60% *FE* for C_2H_4 at 140 mA cm^{-2}. However, the study of well-designed nanoparticles with a single exposed facet is still lacking in CORR, and it is very interesting to find out whether this kind of nanoparticles can realize even higher C2+ selectivity when subjected to CORR. Besides regular polyhedral nanostructured copper, there are also many other catalysts that can be further explored in CORR. For instance, copper halogen compounds [45], copper chalcogenides [47], copper nitrides [49, 50], etc., are recently studied in CO_2RR and exhibit promising CO_2RR activity. Their potential as efficient CORR catalysts needs to be investigated. The study of alloy catalysts for CORR is also very little compared with CO_2RR, and there is a huge opportunity to design novel composition for efficient CORR.

6.3 Advanced In Situ and Operando Techniques for Mechanism Study

Besides the selectivity challenges mentioned above, there is also an energy conversion efficiency challenge for CORR. The start of CORR in a gas-phase flow cell usually required > 400 mV overpotential, which greatly hindered the achievement of high energy conversion efficiency. The high overpotential may be attributed to the complex multiple reaction steps of CORR and the linear scale relationship between these reaction steps. To overcome these selectivity and activity challenges, the reaction pathways and intermediate structures of CORR to different products should be established with the help of *operando* techniques.

The mechanism studies of C–C coupling are more often performed on CORR than on CO_2RR because it can avoid the influence of side reaction and spectra signals from dissolved CO_2 and bicarbonate, while amplifying the production rate of the product. In situ and *operando* techniques are powerful technologies for the investigation of the CORR process by providing the important information of intermediate structure and reaction pathways toward different products. Furthermore, the dynamic change of the structure and surface morphology can be in situ monitored to give the structure–composition–activity relationships. The *operando* research by IR, XRD, and STM methods already provided many promising results for the nano-/microstructure catalyst change and the information of C-based intermediates during electrolysis, as described in Sect. 5.

Further expanding related *operando* research in the flow cell will be a major challenge in the future. The fast reaction environment of the flow cell places high requirements on the mass transfer channel, which limits the design of the detection light path, such as IR light and X-ray. The components of the flow cell should have a low absorption ratio of detection light, including the reactant transport channel, the GDL and external supports. Although there is no mature CO_2RR and CORR flow cell specifically used for *operando* detection, the related *operando* cell design in the fuel cell field is relatively mature and can be used as an important reference [186, 187].

6.4 The Stability and Structure Evolution of CORR Catalysts in Gas-Phase Flow Cells

Although a high CORR current has been achieved in the gas-phase flow cell and the corresponding *FE* toward certain C2+ products was promising, the investigation of long-term stability of the system is elusive. Usually, a few hours of operation was reported for the CORR under high current in a gas-phase flow cell, which is inferior to the case of CO_2RR. For a practical application, the CORR should be operated at

a high reduction current for a long time (> 1 year), which required a system design and optimization.

A part of the reason for the short operation time is the instability of the gas-phase flow cell, which would be terminated by flooding, dehydration or salts crystallization and thus require the optimizing of operation parameters as discussed in Sect. 6.1. Another important reason is that the morphology and the oxidation state of Cu catalysts were sensitive to the applied voltage and reaction environment, leading to a change of selectivity and even degradation after long time testing. Thus, other novel and stable catalysts should be designed to be against structural/morphology change during CORR and keep the activity and selectivity for a long time. The impurity existed in the electrolyte that may poison the catalysts should be eliminated by chemical methods such as the addition of EDTA [96].

6.5 Other Issues for the Economic Challenges of Practical Application

It is worth noting that the current research on CORR is under ideal, small-scale, and short-term conditions. For the requirement of actual industrialization, there are many specific problems needing to be resolved to reduce the capital cost of electrolyzer components and feedstock materials and to increase the economic value of products per unit of electricity. (1) For example, to reduce the cost, CO gas used in industry may contain a lot of impurities, such as O_2, CO_2 and sulfide. The industrial electrochemical system also prefers low-grade electrolytes and easily constructed metal electrolytic cells. How we can enhance the endurance of fragile and sensitive Cu catalysts will be a big challenge [94]. (2) A large amount of Cu with special structures under current research requires complicated preparation steps. It is important to develop high-efficiency catalysts suitable for large-scale applications with low prices. (3) The membrane consumes a huge voltage drop in the electrolytic cell. It would be interesting to find out whether a membraneless CORR electrolytic cell is feasible. (4) The half-reaction of oxygen evolution consumes a lot of electricity but provides no commercial value. It may be able to be replaced by an anode reaction that produces chemicals with commercial values and a large market. (5) When the system is scaled up toward industrial application, the pressure distribution of the gas–liquid flow and the resistance of the current collection will change greatly; thus, the whole-cell design needs to be further optimized.

Acknowledgements Changli Li acknowledges financial funding from National Natural Science Foundation of China (No. 22002191). Qinghua Liu acknowledges funding from the National Natural Science Foundation of China (U1932212 and 11875257).

References

1. Lewis, N.S., Nocera, D.G.: Powering the planet: chemical challenges in solar energy utilization. Proc. Natl. Acad. Sci. USA **103**, 15729–15735 (2006). https://doi.org/10.1073/pnas.0603395103
2. Walter, M.G., Warren, E.L., McKone, J.R., et al.: Solar water splitting cells. Chem. Rev. **110**, 6446–6473 (2010). https://doi.org/10.1021/cr1002326
3. Blankenship, R.E., Tiede, D.M., Barber, J., et al.: Comparing photosynthetic and photovoltaic efficiencies and recognizing the potential for improvement. Science **332**, 805–809 (2011)
4. Chu, S., Cui, Y., Liu, N.: The path towards sustainable energy. Nat. Mater. **16**, 16–22 (2016). https://doi.org/10.1038/nmat4834
5. Davis, S.J., Lewis, N.S., Shaner, M., et al.: Net-zero emissions energy systems. Science **360**, 1419–1428 (2018)
6. Feng, C., Faheem, M.B., Fu, J., et al.: Fe-based electrocatalysts for oxygen evolution reaction: progress and perspectives. ACS Catal. **10**, 4019–4047 (2020). https://doi.org/10.1021/acscatal.9b05445
7. Li, C.W., Ciston, J., Kanan, M.W.: Electroreduction of carbon monoxide to liquid fuel on oxide-derived nanocrystalline copper. Nature **508**, 504–507 (2014). https://doi.org/10.1038/nature13249
8. Yang, J., Ma, W.P., Chen, D., et al.: Fischer–Tropsch synthesis: a review of the effect of CO conversion on methane selectivity. Appl. Catal. A: Gen. **470**, 250–260 (2014). https://doi.org/10.1016/j.apcata.2013.10.061
9. Li, C.W., Kanan, M.W.: CO_2 reduction at low overpotential on Cu electrodes resulting from the reduction of thick Cu_2O films. J. Am. Chem. Soc. **134**, 7231–7234 (2012). https://doi.org/10.1021/ja3010978
10. Liu, M., Pang, Y.J., Zhang, B., et al.: Enhanced electrocatalytic CO_2 reduction via field-induced reagent concentration. Nature **537**, 382–386 (2016). https://doi.org/10.1038/nature19060
11. He, J.F., Dettelbach, K.E., Salvatore, D.A., et al.: High-throughput synthesis of mixed-metal electrocatalysts for CO_2 reduction. Angew. Chem.-Int. Edit. **56**, 6068–6072 (2017). https://doi.org/10.1002/anie.201612038
12. He, J., Johnson, N.J.J., Huang, A., et al.: Electrocatalytic alloys for CO_2 reduction. Chemsuschem **11**, 48–57 (2018). https://doi.org/10.1002/cssc.201701825
13. Birdja, Y.Y., Pérez-Gallent, E., Figueiredo, M.C., et al.: Advances and challenges in understanding the electrocatalytic conversion of carbon dioxide to fuels. Nat. Energy **4**, 732–745 (2019). https://doi.org/10.1038/s41560-019-0450-y
14. Kuhl, K.P., Cave, E.R., Abram, D.N., et al.: New insights into the electrochemical reduction of carbon dioxide on metallic copper surfaces. Energy Environ. Sci. **5**, 7050 (2012). https://doi.org/10.1039/c2ee21234j
15. Schreier, M., Yoon, Y., Jackson, M.N., et al.: Competition between H and CO for active sites governs copper-mediated electrosynthesis of hydrocarbon fuels. Angew. Chem.-Int. Edit. **57**, 10221–10225 (2018). https://doi.org/10.1002/anie.201806051
16. De Luna, P., Quintero-Bermudez, R., Dinh, C.T., et al.: Catalyst electro-redeposition controls morphology and oxidation state for selective carbon dioxide reduction. Nat. Catal. **1**, 103–110 (2018). https://doi.org/10.1038/s41929-017-0018-9
17. Xie, M.S., Xia, B.Y., Li, Y.W., et al.: Amino acid modified copper electrodes for the enhanced selective electroreduction of carbon dioxide towards hydrocarbons. Energy Environ. Sci. **9**, 1687–1695 (2016). https://doi.org/10.1039/C5EE03694A
18. Lum, Y., Ager, J.W.: Stability of residual oxides in oxide-derived copper catalysts for electrochemical CO_2 reduction investigated

with 18 O labeling. Angew. Chem.-Int. Edit. **57**, 551–554 (2018). https://doi.org/10.1002/anie.201710590
19. De Luna, P., Hahn, C., Higgins, D., et al.: What would it take for renewably powered electrosynthesis to displace petrochemical processes? Science **364**, 1 (2019). https://doi.org/10.1126/science.aav3506
20. Spurgeon, J.M., Kumar, B.: A comparative technoeconomic analysis of pathways for commercial electrochemical CO_2 reduction to liquid products. Energy Environ. Sci. **11**, 1536–1551 (2018). https://doi.org/10.1039/c8ee00097b
21. Jouny, M., Hutchings, G.S., Jiao, F.: Carbon monoxide electroreduction as an emerging platform for carbon utilization. Nat. Catal. **2**, 1062–1070 (2019). https://doi.org/10.1038/s41929-019-0388-2
22. Hori, Y.: Electrochemical CO_2 Reduction on Metal Electrodes: Modern Aspects of Electrochemistry (pp 89–189). Springer, New York. (1959). https://doi.org/10.1007/978-0-387-49489-0_3
23. Schouten, K.J.P., Qin, Z.S., Pérez Gallent, E., et al.: Two pathways for the formation of ethylene in CO reduction on single-crystal copper electrodes. J. Am. Chem. Soc. **134**, 9864–9867 (2012). https://doi.org/10.1021/ja302668n
24. Schouten, K.J.P., Pérez Gallent, E., Koper, M.T.M.: Structure sensitivity of the electrochemical reduction of carbon monoxide on copper single crystals. ACS Catal. **3**, 1292–1295 (2013). https://doi.org/10.1021/cs4002404
25. Zhang, H.C., Li, J., Cheng, M.J., et al.: CO electroreduction: Current development and understanding of Cu-based catalysts. ACS Catal. **9**, 49–65 (2019). https://doi.org/10.1021/acscatal.8b03780
26. Bertheussen, E., Hogg, T.V., Abghoui, Y., et al.: Electroreduction of CO on polycrystalline copper at low overpotentials. ACS Energy Lett. **3**, 634–640 (2018). https://doi.org/10.1021/acsenergylett.8b00092
27. Jouny, M., Luc, W., Jiao, F.: High-rate electroreduction of carbon monoxide to multi-carbon products. Nat. Catal. **1**, 748–755 (2018). https://doi.org/10.1038/s41929-018-0133-2
28. Pinsent, B.R.W., Pearson, L., Roughton, F.J.W.: The kinetics of combination of carbon dioxide with hydroxide ions. Trans. Faraday Soc. **52**, 1512 (1956). https://doi.org/10.1039/tf9565201512
29. Lum, Y., Ager, J.W.: Evidence for product-specific active sites on oxide-derived Cu catalysts for electrochemical CO_2 reduction. Nat. Catal. **2**, 86–93 (2019). https://doi.org/10.1038/s41929-018-0201-7
30. Hori, Y., Murata, A., Takahashi, R., et al.: Electroreduction of carbon monoxide to methane and ethylene at a copper electrode in aqueous solutions at ambient temperature and pressure. J. Am. Chem. Soc. **109**, 5022–5023 (1987). https://doi.org/10.1021/ja00250a044
31. Li, J., Chang, K., Zhang, H.C., et al.: Effectively increased efficiency for electroreduction of carbon monoxide using supported polycrystalline copper powder electrocatalysts. ACS Catal. **9**, 4709–4718 (2019). https://doi.org/10.1021/acscatal.9b00099
32. Malkani, A.S., Li, J., Anibal, J., et al.: Impact of forced convection on spectroscopic observations of the electrochemical CO reduction reaction. ACS Catal. **10**, 941–946 (2020). https://doi.org/10.1021/acscatal.9b03581
33. Weekes, D.M., Salvatore, D.A., Reyes, A., et al.: Electrolytic CO_2 reduction in a flow cell. Acc. Chem. Res. **51**, 910–918 (2018). https://doi.org/10.1021/acs.accounts.8b00010
34. Speck, F.D., Dettelbach, K.E., Sherbo, R.S., et al.: On the electrolytic stability of iron-nickel oxides. Chem **2**, 590–597 (2017). https://doi.org/10.1016/j.chempr.2017.03.006
35. Xu, D.Y., Stevens, M.B., Cosby, M.R., et al.: Earth-abundant oxygen electrocatalysts for alkaline anion-exchange-membrane water electrolysis: effects of catalyst conductivity and comparison with performance in three-electrode cells. ACS Catal. **9**, 7–15 (2019)
36. Li, J., Wang, Z.Y., McCallum, C., et al.: Constraining CO coverage on copper promotes high-efficiency ethylene electroproduction. Nat. Catal. **2**, 1124–1131 (2019). https://doi.org/10.1038/s41929-019-0380-x
37. Hori, Y., Wakebe, H., Tsukamoto, T., et al.: Electrocatalytic process of CO selectivity in electrochemical reduction of CO_2 at metal electrodes in aqueous media. Electrochim. Acta **39**, 1833–1839 (1994). https://doi.org/10.1016/0013-4686(94)85172-7
38. Chen, Y.H., Li, C.W., Kanan, M.W.: Aqueous CO_2 reduction at very low overpotential on oxide-derived Au nanoparticles. J. Am. Chem. Soc. **134**, 19969–19972 (2012). https://doi.org/10.1021/ja309317u
39. Ma, M., Trześniewski, B.J., Xie, J., et al.: Selective and efficient reduction of carbon dioxide to carbon monoxide on oxide-derived nanostructured silver electrocatalysts. Angew. Chem.-Int. Edit. **55**, 9748–9752 (2016)
40. Kim, D., Resasco, J., Yu, Y., et al.: Synergistic geometric and electronic effects for electrochemical reduction of carbon dioxide using gold-copper bimetallic nanoparticles. Nat. Commun. **5**, 1–8 (2014). https://doi.org/10.1038/ncomms5948
41. Rasul, S., Anjum, D.H., Jedidi, A., et al.: A highly selective copper-indium bimetallic electrocatalyst for the electrochemical reduction of aqueous $CO_2$to CO. Angew. Chem.-Int. Edit. **54**, 2146–2150 (2015). https://doi.org/10.1002/anie.201410233
42. Sarfraz, S., Garcia-Esparza, A.T., Jedidi, A., et al.: Cu–Sn bimetallic catalyst for selective aqueous electroreduction of CO_2 to CO. ACS Catal. **6**, 2842–2851 (2016). https://doi.org/10.1021/acscatal.6b00269
43. Luc, W., Collins, C., Wang, S.W., et al.: Ag-Sn bimetallic catalyst with a core-shell structure for CO_2 reduction. J. Am. Chem. Soc. **139**, 1885–1893 (2017). https://doi.org/10.1021/jacs.6b10435
44. Bai, X.F., Chen, W., Zhao, C.C., et al.: Exclusive formation of formic acid from CO_2 electroreduction by a tunable Pd-Sn alloy. Angew. Chem.-Int. Edit. **56**, 12219–12223 (2017). https://doi.org/10.1002/anie.201707098
45. Ma, W.C., Xie, S.J., Liu, T.T., et al.: Electrocatalytic reduction of CO_2 to ethylene and ethanol through hydrogen-assisted C–C coupling over fluorine-modified copper. Nat. Catal. **3**, 478–487 (2020). https://doi.org/10.1038/s41929-020-0450-0
46. He, S., Ni, F., Ji, Y., et al.: The p-orbital delocalization of main-group metals to boost CO_2 electroreduction. Angew. Chem. Int. Ed. Engl. **57**, 16114–16119 (2018). https://doi.org/10.1002/anie.201810538
47. Zhuang, T.T., Liang, Z.Q., Seifitokaldani, A., et al.: Steering post-C–C coupling selectivity enables high efficiency electroreduction of carbon dioxide to multi-carbon alcohols. Nat. Catal. **1**, 421–428 (2018). https://doi.org/10.1038/s41929-018-0084-7
48. Zhang, A., He, R., Li, H.P., et al.: Nickel doping in atomically thin tin disulfide nanosheets enables highly efficient CO_2 reduction. Angew. Chem.-Int. Edit. **57**, 10954–10958 (2018). https://doi.org/10.1002/anie.201806043
49. Liang, Z.Q., Zhuang, T.T., Seifitokaldani, A., et al.: Copper-on-nitride enhances the stable electrosynthesis of multi-carbon products from CO_2. Nat. Commun. **9**, 1–8 (2018). https://doi.org/10.1038/s41467-018-06311-0
50. Yin, Z.Y., Yu, C., Zhao, Z.L., et al.: Cu3N nanocubes for selective electrochemical reduction of CO_2 to ethylene. Nano Lett. **19**, 8658–8663 (2019). https://doi.org/10.1021/acs.nanolett.9b03324
51. Asadi, M., Kim, K., Liu, C., et al.: Nanostructured transition metal dichalcogenide electrocatalysts for CO_2 reduction in ionic liquid. Science **353**, 467–470 (2016). https://doi.org/10.1126/science.aaf4767
52. Verdaguer-Casadevall, A., Li, C.W., Johansson, T.P., et al.: Probing the active surface sites for CO reduction on oxide-derived copper electrocatalysts. J. Am. Chem. Soc. **137**, 9808–9811 (2015). https://doi.org/10.1021/jacs.5b06227

53. Feng, X.F., Jiang, K.L., Fan, S.S., et al.: Grain-boundary-dependent CO_2 electroreduction activity. J. Am. Chem. Soc. **137**, 4606–4609 (2015). https://doi.org/10.1021/ja5130513
54. Mariano, R.G., McKelvey, K., White, H.S., et al.: Selective increase in CO_2 electroreduction activity at grain-boundary surface terminations. Science **358**, 1187–1192 (2017). https://doi.org/10.1126/science.aao3691
55. Dinh, C.T., Burdyny, T., Kibria, M.G., et al.: CO_2 electroreduction to ethylene via hydroxide-mediated copper catalysis at an abrupt interface. Science **360**, 783–787 (2018). https://doi.org/10.1126/science.aas9100
56. Yang, H.Z., Kaczur, J.J., Sajjad, S.D., et al.: Electrochemical conversion of CO_2 to formic acid utilizing Sustainion™ membranes. J. CO_2 Util. **20**, 208–217 (2017). https://doi.org/10.1016/j.jcou.2017.04.011
57. Dinh, C.T., García de Arquer, F.P., Sinton, D., et al.: High rate, selective, and stable electroreduction of CO_2 to CO in basic and neutral media. ACS Energy Lett. **3**, 2835–2840 (2018). https://doi.org/10.1021/acsenergylett.8b01734
58. Zhong, M., Tran, K., Min, Y., et al.: Accelerated discovery of CO_2 electrocatalysts using active machine learning. Nature **581**, 178–183 (2020). https://doi.org/10.1038/s41586-020-2242-8
59. Hori, Y., Takahashi, I., Koga, O., et al.: Selective formation of C2 compounds from electrochemical reduction of CO_2 at a series of copper single crystal electrodes. J. Phys. Chem. B **106**, 15–17 (2002). https://doi.org/10.1021/jp013478d
60. Cao, L., Raciti, D., Li, C.Y., et al.: Mechanistic insights for low-overpotential electroreduction of CO_2 to CO on copper nanowires. ACS Catal. **7**, 8578–8587 (2017). https://doi.org/10.1021/acscatal.7b03107
61. Paik, W., Andersen, T.N., Eyring, H.: Kinetic studies of the electrolytic reduction of carbon dioxide on the mercury electrode. Electrochim. Acta **14**, 1217–1232 (1969). https://doi.org/10.1016/0013-4686(69)87019-2
62. Baruch, M.F., Pander, J.E., White, J.L., et al.: Mechanistic insights into the reduction of CO_2 on tin electrodes using *in situ* ATR-IR spectroscopy. ACS Catal. **5**, 3148–3156 (2015). https://doi.org/10.1021/acscatal.5b00402
63. Feaster, J.T., Shi, C., Cave, E.R., et al.: Understanding selectivity for the electrochemical reduction of carbon dioxide to formic acid and carbon monoxide on metal electrodes. ACS Catal. **7**, 4822–4827 (2017). https://doi.org/10.1021/acscatal.7b00687
64. Armstrong, F.A., Hirst, J.: Reversibility and efficiency in electrocatalytic energy conversion and lessons from enzymes. Proc. Natl. Acad. Sci. U. S. A. **108**, 14049–14054 (2011). https://doi.org/10.1073/pnas.1103697108
65. Shen, J., Kolb, M.J., Göttle, A.J., et al.: DFT study on the mechanism of the electrochemical reduction of CO_2 catalyzed by cobalt porphyrins. J. Phys. Chem. C **120**, 15714–15721 (2016). https://doi.org/10.1021/acs.jpcc.5b10763
66. Calle-Vallejo, F., Koper, M.T.: Theoretical considerations on the electroreduction of CO to C2 species on Cu(100) electrodes. Angew. Chem.-Int. Edit. **52**, 7282–7285 (2013). https://doi.org/10.1002/anie.201301470
67. Montoya, J.H., Shi, C., Chan, K.R., et al.: Theoretical insights into a CO dimerization mechanism in CO_2 electroreduction. J. Phys. Chem. Lett. **6**, 2032–2037 (2015). https://doi.org/10.1021/acs.jpclett.5b00722
68. Birdja, Y.Y., Koper, M.T.M.: The importance of cannizzaro-type reactions during electrocatalytic reduction of carbon dioxide. J. Am. Chem. Soc. **139**, 2030–2034 (2017). https://doi.org/10.1021/jacs.6b12008
69. Geng, Z.G., Kong, X.D., Chen, W.W., et al.: Oxygen vacancies in ZnO nanosheets enhance CO_2 electrochemical reduction to CO. Angew. Chem.-Int. Edit. **130**, 6162–6167 (2018). https://doi.org/10.1002/ange.201711255
70. Chen, Y.H., Kanan, M.W.: Tin oxide dependence of the CO_2 reduction efficiency on tin electrodes and enhanced activity for tin/tin oxide thin-film catalysts. J. Am. Chem. Soc. **134**, 1986–1989 (2012). https://doi.org/10.1021/ja2108799
71. Gong, Q.F., Ding, P., Xu, M.Q., et al.: Structural defects on converted bismuth oxide nanotubes enable highly active electrocatalysis of carbon dioxide reduction. Nat. Commun. **10**, 1–10 (2019). https://doi.org/10.1038/s41467-019-10819-4
72. Eilert, A., Cavalca, F., Roberts, F.S., et al.: Subsurface oxygen in oxide-derived copper electrocatalysts for carbon dioxide reduction. J. Phys. Chem. Lett. **8**, 285–290 (2017). https://doi.org/10.1021/acs.jpclett.6b02273
73. Firet, N.J., Blommaert, M.A., Burdyny, T., et al.: Operando EXAFS study reveals presence of oxygen in oxide-derived silver catalysts for electrochemical CO_2 reduction. J. Mater. Chem. A **7**, 2597–2607 (2019). https://doi.org/10.1039/c8ta10412c
74. Mistry, H., Varela, A.S., Bonifacio, C.S., et al.: Highly selective plasma-activated copper catalysts for carbon dioxide reduction to ethylene. Nat. Commun. **7**, 1–9 (2016). https://doi.org/10.1038/ncomms12123
75. Wang, H., Matios, E., Wang, C.L., et al.: Rapid and scalable synthesis of cuprous halide-derived copper nano-architectures for selective electrochemical reduction of carbon dioxide. Nano Lett. **19**, 3925–3932 (2019). https://doi.org/10.1021/acs.nanolett.9b01197
76. Kim, D., Xie, C.L., Becknell, N., et al.: Electrochemical activation of CO_2 through atomic ordering transformations of AuCu nanoparticles. J. Am. Chem. Soc. **139**, 8329–8336 (2017). https://doi.org/10.1021/jacs.7b03516
77. Lum, Y., Ager, J.W.: Sequential catalysis controls selectivity in electrochemical CO_2 reduction on Cu. Energy Environ. Sci. **11**, 2935–2944 (2018). https://doi.org/10.1039/C8EE01501E
78. Kuhl, K.P., Hatsukade, T., Cave, E.R., et al.: Electrocatalytic conversion of carbon dioxide to methane and methanol on transition metal surfaces. J. Am. Chem. Soc. **136**, 14107–14113 (2014). https://doi.org/10.1021/ja505791r
79. Sun, K., Cheng, T., Wu, L.N., et al.: Ultrahigh mass activity for carbon dioxide reduction enabled by gold–iron core–shell nanoparticles. J. Am. Chem. Soc. **139**, 15608–15611 (2017). https://doi.org/10.1021/jacs.7b09251
80. Choi, S.Y., Jeong, S.K., Kim, H.J., et al.: Electrochemical reduction of carbon dioxide to formate on tin–lead alloys. ACS Sustain. Chem. Eng. **4**, 1311–1318 (2016). https://doi.org/10.1021/acssuschemeng.5b01336
81. Ren, D., Ang, B.S.H., Yeo, B.S.: Tuning the selectivity of carbon dioxide electroreduction toward ethanol on oxide-derived Cu_xZn catalysts. ACS Catal. **6**, 8239–8247 (2016). https://doi.org/10.1021/acscatal.6b02162
82. Clark, E.L., Hahn, C., Jaramillo, T.F., et al.: Electrochemical CO_2 reduction over compressively strained CuAg surface alloys with enhanced multi-carbon oxygenate selectivity. J. Am. Chem. Soc. **139**, 15848–15857 (2017). https://doi.org/10.1021/jacs.7b08607
83. Torelli, D.A., Francis, S.A., Crompton, J.C., et al.: Nickel–gallium-catalyzed electrochemical reduction of CO_2 to highly reduced products at low overpotentials. ACS Catal. **6**, 2100–2104 (2016). https://doi.org/10.1021/acscatal.5b02888
84. Wang, Y., Wang, D.G., Dares, C.J., et al.: CO_2 reduction to acetate in mixtures of ultrasmall (Cu)n, (Ag)m bimetallic nanoparticles. Proc. Natl. Acad. Sci. USA. **115**, 278–283 (2018). https://doi.org/10.1073/pnas.1713962115
85. Nam, D.H., Bushuyev, O.S., Li, J., et al.: Metal–organic frameworks mediate Cu coordination for selective CO_2 electroreduction. J. Am. Chem. Soc. **140**, 11378–11386 (2018). https://doi.org/10.1021/jacs.8b06407
86. Yoon, Y., Hall, A.S., Surendranath, Y.: Tuning of silver catalyst mesostructure promotes selective carbon dioxide conversion into

fuels. Angew. Chem.-Int. Edit. **55**, 15282–15286 (2016). https://doi.org/10.1002/anie.201607942
87. Hall, A.S., Yoon, Y., Wuttig, A., et al.: Mesostructure-induced selectivity in CO_2 reduction catalysis. J. Am. Chem. Soc. **137**, 14834–14837 (2015). https://doi.org/10.1021/jacs.5b08259
88. Roberts, F.S., Kuhl, K.P., Nilsson, A.: High selectivity for ethylene from carbon dioxide reduction over copper nanocube electrocatalysts. Angew. Chem.-Int. Edit. **54**, 5179–5182 (2015). https://doi.org/10.1002/anie.201412214
89. Li, Y.F., Cui, F., Ross, M.B., et al.: Structure-sensitive CO_2 electroreduction to hydrocarbons on ultrathin 5-fold twinned copper nanowires. Nano Lett. **17**, 1312–1317 (2017). https://doi.org/10.1021/acs.nanolett.6b05287
90. García de Arquer, F.P., Bushuyev, O.S., de Luna, P., et al.: 2D metal oxyhalide-derived catalysts for efficient CO_2 electroreduction. Adv. Mater. **30**, 1802858 (2018). https://doi.org/10.1002/adma.201802858
91. Boutin, E., Merakeb, L., Ma, B., et al.: Molecular catalysis of CO_2 reduction: recent advances and perspectives in electrochemical and light-driven processes with selected Fe, Ni and Co aza macrocyclic and polypyridine complexes. Chem. Soc. Rev. **49**, 5772–5809 (2020). https://doi.org/10.1039/d0cs00218f
92. Wasylenko, D.J., Palmer, R.D., Schott, E., et al.: Interrogation of electrocatalytic water oxidation mediated by a cobalt complex. Chem. Commun. **48**, 2107 (2012). https://doi.org/10.1039/c2cc16674g
93. Ren, S.X., Joulié, D., Salvatore, D., et al.: Molecular electrocatalysts can mediate fast, selective CO_2 reduction in a flow cell. Science **365**, 367–369 (2019). https://doi.org/10.1126/science.aax4608
94. Hori, Y., Konishi, H., Futamura, T., et al.: "Deactivation of copper electrode" in electrochemical reduction of CO_2. Electrochimi. Acta **50**, 5354–5369 (2005). https://doi.org/10.1016/j.electacta.2005.03.015
95. Wuttig, A., Surendranath, Y.: Impurity ion complexation enhances carbon dioxide reduction catalysis. ACS Catal. **5**, 4479–4484 (2015). https://doi.org/10.1021/acscatal.5b00808
96. He, J.F., Huang, A.X., Johnson, N.J.J., et al.: Stabilizing copper for CO_2 reduction in low-grade electrolyte. Inorg. Chem. **57**, 14624–14631 (2018). https://doi.org/10.1021/acs.inorgchem.8b02311
97. Hori, Y., Murata, A., Takahashi, R.: Formation of hydrocarbons in the electrochemical reduction of carbon dioxide at a copper electrode in aqueous solution. J. Chem. Soc. Faraday Trans. **85**, 2309 (1989). https://doi.org/10.1039/f19898502309
98. Zhu, S.Q., Jiang, B., Cai, W.B., et al.: Direct observation on reaction intermediates and the role of bicarbonate anions in CO_2 electrochemical reduction reaction on Cu surfaces. J. Am. Chem. Soc. **139**, 15664–15667 (2017)
99. Dunwell, M., Lu, Q., Heyes, J.M., et al.: The central role of bicarbonate in the electrochemical reduction of carbon dioxide on gold. J. Am. Chem. Soc. **139**, 3774–3783 (2017). https://doi.org/10.1021/jacs.6b13287
100. Resasco, J., Chen, L.D., Clark, E., et al.: Promoter effects of alkali metal cations on the electrochemical reduction of carbon dioxide. J. Am. Chem. Soc. **139**, 11277–11287 (2017). https://doi.org/10.1021/jacs.7b06765
101. Singh, M.R., Kwon, Y., Lum, Y., et al.: Hydrolysis of electrolyte cations enhances the electrochemical reduction of CO_2 over Ag and Cu. J. Am. Chem. Soc. **138**, 13006–13012 (2016). https://doi.org/10.1021/jacs.6b07612
102. Ahn, S.T., Abu-Baker, I., Palmore, G.T.R.: Electroreduction of CO_2 on polycrystalline copper: Effect of temperature on product selectivity. Catal. Today **288**, 24–29 (2017). https://doi.org/10.1016/j.cattod.2016.09.028
103. Kaneco, S., Hiei, N.H., Xing, Y., et al.: Electrochemical conversion of carbon dioxide to methane in aqueous $NaHCO_3$ solution at less than 273 K. Electrochim. Acta **48**, 51–55 (2002). https://doi.org/10.1016/s0013-4686(02)00550-9
104. Azuma, M., Hashimoto, K., Hiramoto, M., et al.: Electrochemical reduction of carbon dioxide on various metal electrodes in low-temperature aqueous $KHCO_3$ media. J. Electrochem. Soc. **137**, 1772–1778 (1990). https://doi.org/10.1149/1.2086796
105. Kaneco, S., Iiba, K., Katsumata, H., et al.: Effect of sodium cation on the electrochemical reduction of CO_2 at a copper electrode in methanol. J. Solid State Electrochem. **11**, 490–495 (2007). https://doi.org/10.1007/s10008-006-0185-0
106. Murugananthan, M., Kumaravel, M., Katsumata, H., et al.: Electrochemical reduction of CO_2 using Cu electrode in methanol/$LiClO_4$ electrolyte. Int. J. Hydrog. Energy **40**, 6740–6744 (2015). https://doi.org/10.1016/j.ijhydene.2015.04.006
107. Fan, L., Xia, C., Yang, F.Q., et al.: Strategies in catalysts and electrolyzer design for electrochemical CO_2 reduction toward C^{2+} products. Sci. Adv. **6**, 3111 (2020). https://doi.org/10.1126/sciadv.aay3111
108. Hoang, T.T.H., Ma, S.C., Gold, J.I., et al.: Nanoporous copper films by additive-controlled electrodeposition: CO_2 reduction catalysis. ACS Catal. **7**, 3313–3321 (2017). https://doi.org/10.1021/acscatal.6b03613
109. Li, Y.C., Zhou, D.K., Yan, Z.F., et al.: Electrolysis of CO_2 to syngas in bipolar membrane-based electrochemical cells. ACS Energy Lett. **1**, 1149–1153 (2016). https://doi.org/10.1021/acsenergylett.6b00475
110. Salvatore, D., Berlinguette, C.P.: Voltage matters when reducing CO_2 in an electrochemical flow cell. ACS Energy Lett. **5**, 215–220 (2020). https://doi.org/10.1021/acsenergylett.9b02356
111. Raciti, D., Mao, M., Wang, C.: Mass transport modelling for the electroreduction of CO_2 on Cu nanowires. Nanotechnology **29**, 044001 (2018). https://doi.org/10.1088/1361-6528/aa9bd7
112. Weng, L.C., Bell, A.T., Weber, A.Z.: Towards membrane-electrode assembly systems for CO_2 reduction: a modeling study. Energy Environ. Sci. **12**, 1950–1968 (2019). https://doi.org/10.1039/C9EE00909D
113. Weng, L.C., Bell, A.T., Weber, A.Z.: Modeling gas-diffusion electrodes for CO_2 reduction. Phys. Chem. Chem. Phys. **20**, 16973–16984 (2018). https://doi.org/10.1039/c8cp01319e
114. Wang, X., Wang, Z.Y., García de Arquer, F.P., et al.: Efficient electrically powered CO_2–to-ethanol via suppression of deoxygenation. Nat. Energy **5**, 478–486 (2020). https://doi.org/10.1038/s41560-020-0607-8
115. Staffell, I., Scamman, D., Velazquez Abad, A., et al.: The role of hydrogen and fuel cells in the global energy system. Energy Environ. Sci. **12**, 463–491 (2019). https://doi.org/10.1039/c8ee01157e
116. Dry, M.E.: The Fischer–tropsch process: 1950–2000. Catal. Today **71**, 227–241 (2002). https://doi.org/10.1016/s0920-5861(01)00453-9
117. Wang, X.L., Araújo, J.F., Ju, W., et al.: Mechanistic reaction pathways of enhanced ethylene yields during electroreduction of CO_2–CO co-feeds on Cu and Cu-tandem electrocatalysts. Nat. Nanotechnol. **14**, 1063–1070 (2019). https://doi.org/10.1038/s41565-019-0551-6
118. Clark, E.L., Resasco, J., Landers, A., et al.: Standards and protocols for data acquisition and reporting for studies of the electrochemical reduction of carbon dioxide. ACS Catal. **8**, 6560–6570 (2018). https://doi.org/10.1021/acscatal.8b01340
119. Pander, J.E., III., Ren, D., Yeo, B.S.: Practices for the collection and reporting of electrocatalytic performance and mechanistic information for the CO_2 reduction reaction. Catal. Sci. Technol. **7**, 5820–5832 (2017). https://doi.org/10.1039/C7CY01785E

120. Hori, Y., Takahashi, R., Yoshinami, Y., et al.: Electrochemical reduction of CO at a copper electrode. J. Phys. Chem. B **101**, 7075–7081 (1997). https://doi.org/10.1021/jp970284i
121. Schouten, K.J.P., Pérez Gallent, E., Koper, M.T.M.: The influence of pH on the reduction of CO and CO_2 to hydrocarbons on copper electrodes. J. Electroanal. Chem. **716**, 53–57 (2014). https://doi.org/10.1016/j.jelechem.2013.08.033
122. Wang, L., Nitopi, S.A., Bertheussen, E., et al.: Electrochemical carbon monoxide reduction on polycrystalline copper: effects of potential, pressure, and pH on selectivity toward multicarbon and oxygenated products. ACS Catal. **8**, 7445–7454 (2018). https://doi.org/10.1021/acscatal.8b01200
123. Murata, A., Hori, Y.: Product selectivity affected by cationic species in electrochemical reduction of $CO_2$and CO at a Cu electrode. Bull. Chem. Soc. Jpn. **64**, 123–127 (1991). https://doi.org/10.1246/bcsj.64.123
124. Pérez-Gallent, E., Marcandalli, G., Figueiredo, M.C., et al.: Structure- and potential-dependent cation effects on CO reduction at copper single-crystal electrodes. J. Am. Chem. Soc. **139**, 16412–16419 (2017). https://doi.org/10.1021/jacs.7b10142
125. Li, J., Wu, D.H., Malkani, A.S., et al.: Hydroxide is not a promoter of C_{2+} product formation in the electrochemical reduction of CO on copper. Angew. Chem. **132**, 4494–4499 (2020). https://doi.org/10.1002/ange.201912412
126. Li, J.Y., Li, X., Gunathunge, C.M., et al.: Hydrogen bonding steers the product selectivity of electrocatalytic CO reduction. Proc. Natl. Acad. Sci. U. S. A. **116**, 9220–9229 (2019). https://doi.org/10.1073/pnas.1900761116
127. Wang, Y.X., Raciti, D., Wang, C.: High-flux CO reduction enabled by three-dimensional nanostructured copper electrodes. ACS Catal. **8**, 5657–5663 (2018). https://doi.org/10.1021/acscatal.8b00902
128. Han, L.H., Zhou, W., Xiang, C.X.: High-rate electrochemical reduction of carbon monoxide to ethylene using Cu-nanoparticle-based gas diffusion electrodes. ACS Energy Lett. **3**, 855–860 (2018). https://doi.org/10.1021/acsenergylett.8b00164
129. Chen, R.X., Su, H.Y., Liu, D.Y., et al.: Highly selective production of ethylene by the electroreduction of carbon monoxide. Angew. Chem.-Int. Edit. **59**, 154–160 (2020). https://doi.org/10.1002/anie.201910662
130. King, L.A., Hubert, M.A., Capuano, C., et al.: A non-precious metal hydrogen catalyst in a commercial polymer electrolyte membrane electrolyser. Nat. Nanotechnol. **14**, 1071–1074 (2019). https://doi.org/10.1038/s41565-019-0550-7
131. Xiang, C.X., Papadantonakis, K.M., Lewis, N.S.: Principles and implementations of electrolysis systems for water splitting. Mater. Horiz. **3**, 169–173 (2016). https://doi.org/10.1039/C6MH00016A
132. Ramaswamy, N., Mukerjee, S.: Alkaline anion-exchange membrane fuel cells: challenges in electrocatalysis and interfacial charge transfer. Chem. Rev. **119**, 11945–11979 (2019). https://doi.org/10.1021/acs.chemrev.9b00157
133. Kraytsberg, A., Ein-Eli, Y.: Review of advanced materials for proton exchange membrane fuel cells. Energy Fuels **28**, 7303–7330 (2014). https://doi.org/10.1021/ef501977k
134. Yin, Z.L., Peng, H.Q., Wei, X., et al.: An alkaline polymer electrolyte CO_2 electrolyzer operated with pure water. Energy Environ. Sci. **12**, 2455–2462 (2019). https://doi.org/10.1039/c9ee01204d
135. Salvatore, D.A., Weekes, D.M., He, J.F., et al.: Electrolysis of gaseous CO_2 to CO in a flow cell with a bipolar membrane. ACS Energy Lett. **3**, 149–154 (2018). https://doi.org/10.1021/acsenergylett.7b01017
136. Vermaas, D.A., Wiegman, S., Nagaki, T., et al.: Ion transport mechanisms in bipolar membranes for (photo)electrochemical water splitting. Sustain. Energy Fuels **2**, 2006–2015 (2018). https://doi.org/10.1039/c8se00118a
137. Larrazábal, G.O., Strøm-Hansen, P., Heli, J.P., et al.: Analysis of mass flows and membrane cross-over in CO_2 reduction at high current densities in an MEA-type electrolyzer. ACS Appl. Mater. Interfaces **11**, 41281–41288 (2019). https://doi.org/10.1021/acsami.9b13081
138. Zhang, J., Luo, W., Züttel, A.: Crossover of liquid products from electrochemical CO_2 reduction through gas diffusion electrode and anion exchange membrane. J. Catal. **385**, 140–145 (2020). https://doi.org/10.1016/j.jcat.2020.03.013
139. Li, Y.C., Yan, Z.F., Hitt, J., et al.: Bipolar membranes inhibit product crossover in CO_2 electrolysis cells. Adv. Sustain. Syst. **2**, 1700187 (2018). https://doi.org/10.1002/adsu.201700187
140. Wheeler, D.G., Mowbray, B.A.W., Reyes, A., et al.: Quantification of water transport in a CO_2 electrolyzer. Energy Environ. Sci. **13**, 5126–5134 (2020). https://doi.org/10.1039/d0ee02219e
141. Sullivan, I., Han, L.H., Lee, S.H., et al.: A hybrid catalyst-bonded membrane device for electrochemical carbon monoxide reduction at different relative humidities. ACS Sustain. Chem. Eng. **7**, 16964–16970 (2019). https://doi.org/10.1021/acssuschemeng.9b04959
142. Ripatti, D.S., Veltman, T.R., Kanan, M.W.: Carbon monoxide gas diffusion electrolysis that produces concentrated C2 products with high single-pass conversion. Joule **3**, 2581 (2019). https://doi.org/10.1016/j.joule.2018.10.007
143. Romero Cuellar, N.S., Wiesner-Fleischer, K., Fleischer, M., et al.: Advantages of CO over CO_2 as reactant for electrochemical reduction to ethylene, ethanol and n-propanol on gas diffusion electrodes at high current densities. Electrochim. Acta **307**, 164–175 (2019). https://doi.org/10.1016/j.electacta.2019.03.142
144. Ou, L.H., Chen, J.X.: Theoretical insights into the effect of the overpotential on CO electroreduction mechanisms on Cu(111): Regulation and application of electrode potentials from a CO coverage-dependent electrochemical model. Phys. Chem. Chem. Phys. **22**, 62–73 (2020). https://doi.org/10.1039/C9CP05043D
145. Cheng, T., Xiao, H., Goddard, W.A., III.: Full atomistic reaction mechanism with kinetics for CO reduction on Cu(100) from ab initio molecular dynamics free-energy calculations at 298 K. Proc. Natl. Acad. Sci. USA **114**, 1795–1800 (2017). https://doi.org/10.1073/pnas.1612106114
146. Bagger, A., Arnarson, L., Hansen, M.H., et al.: Electrochemical CO reduction: A property of the electrochemical interface. J. Am. Chem. Soc. **141**, 1506–1514 (2019). https://doi.org/10.1021/jacs.8b08839
147. Feng, X.F., Jiang, K.L., Fan, S.S., et al.: A direct grain-boundary-activity correlation for CO electroreduction on Cu nanoparticles. ACS Central Sci. **2**, 169–174 (2016). https://doi.org/10.1021/acscentsci.6b00022
148. Malkani, A., Dunwell, M., Xu, B.J.: Operando spectroscopic investigations of copper and oxide-derived copper catalysts for electrochemical CO reduction. ACS Catal. **9**, 474–478 (2019). https://doi.org/10.1021/acscatal.8b04269
149. Cheng, T., Xiao, H., Goddard, W.A.: Nature of the active sites for CO reduction on copper nanoparticles; suggestions for optimizing performance. J. Am. Chem. Soc. **139**, 11642–11645 (2017). https://doi.org/10.1021/jacs.7b03300
150. Raciti, D., Cao, L., Livi, K.J.T., et al.: Low-overpotential electroreduction of carbon monoxide using copper nanowires. ACS Catal. **7**, 4467–4472 (2017). https://doi.org/10.1021/acscatal.7b01124
151. Zhang, H.Y., Zhang, Y.J., Li, Y.Y., et al.: Cu nanowire-catalyzed electrochemical reduction of CO or CO2. Nanoscale **11**, 12075–12079 (2019). https://doi.org/10.1039/C9NR03170G
152. Wang, L., Nitopi, S., Wong, A.B., et al.: Electrochemically converting carbon monoxide to liquid fuels by directing selectivity

with electrode surface area. Nat. Catal. **2**, 702–708 (2019). https://doi.org/10.1038/s41929-019-0301-z
153. Luc, W., Fu, X.B., Shi, J.J., et al.: Two-dimensional copper nanosheets for electrochemical reduction of carbon monoxide to acetate. Nat. Catal. **2**, 423–430 (2019). https://doi.org/10.1038/s41929-019-0269-8
154. Clark, E.L., Wong, J., Garza, A.J., et al.: Explaining the incorporation of oxygen derived from solvent water into the oxygenated products of CO reduction over Cu. J. Am. Chem. Soc. **141**, 4191–4193 (2019). https://doi.org/10.1021/jacs.8b13201
155. Li, J., Che, F.L., Pang, Y.J., et al.: Copper adparticle enabled selective electrosynthesis of n-propanol. Nat. Commun. **9**, 1–9 (2018). https://doi.org/10.1038/s41467-018-07032-0
156. Zhuang, T.T., Pang, Y.J., Liang, Z.Q., et al.: Copper nanocavities confine intermediates for efficient electrosynthesis of C3 alcohol fuels from carbon monoxide. Nat. Catal. **1**, 946–951 (2018). https://doi.org/10.1038/s41929-018-0168-4
157. Pang, Y.J., Li, J., Wang, Z.Y., et al.: Efficient electrocatalytic conversion of carbon monoxide to propanol using fragmented copper. Nat. Catal. **2**, 251–258 (2019). https://doi.org/10.1038/s41929-019-0225-7
158. Costentin, C., Drouet, S., Robert, M., et al.: A local proton source enhances CO_2 electroreduction to CO by a molecular Fe catalyst. Science **338**, 90–94 (2012). https://doi.org/10.1126/science.1224581
159. Karunadasa, H.I., Montalvo, E., Sun, Y., et al.: A molecular MoS_2 edge site mimic for catalytic hydrogen generation. Science **335**, 698–702 (2012). https://doi.org/10.1126/science.1215868
160. Yin, Q., Tan, J.M., Besson, C., et al.: A fast soluble carbon-free molecular water oxidation catalyst based on abundant metals. Science **328**, 342–345 (2010). https://doi.org/10.1126/science.1185372
161. Torbensen, K., Joulié, D., Ren, S.X., et al.: Molecular catalysts boost the rate of electrolytic CO_2 reduction. ACS Energy Lett. **5**, 1512–1518 (2020). https://doi.org/10.1021/acsenergylett.0c00536
162. Boutin, E., Wang, M., Lin, J.C., et al.: Aqueous electrochemical reduction of carbon dioxide and carbon monoxide into methanol with cobalt phthalocyanine. Angew. Chem.-Int. Edit. **58**, 16172–16176 (2019). https://doi.org/10.1002/anie.201909257
163. Gong, M., Cao, Z., Liu, W., et al.: Supramolecular porphyrin cages assembled at molecular–materials interfaces for electrocatalytic CO reduction. ACS Central Sci. **3**, 1032–1040 (2017). https://doi.org/10.1021/acscentsci.7b00316
164. He, T.W., Kour, G., Mao, X., et al.: Cuδ+ active sites stabilization through Mott-Schottky effect for promoting highly efficient conversion of carbon monoxide into n-propanol. J. Catal. **382**, 49–56 (2020). https://doi.org/10.1016/j.jcat.2019.12.015
165. Li, Y.F., Qian, Y.M., Ji, Y.J., et al.: Improving selectivity of CO reduction via reducing the coordination of critical intermediates. J. Mater. Chem. A **7**, 24000–24004 (2019). https://doi.org/10.1039/c9ta06529f
166. Ma, T., Fan, Q., Li, X., et al.: Graphene-based materials for electrochemical CO_2 reduction. J. CO2 Util. **30**, 168–182 (2019). https://doi.org/10.1016/j.jcou.2019.02.001
167. Cui, H.J., Guo, Y.B., Guo, L.M., et al.: Heteroatom-doped carbon materials and their composites as electrocatalysts for CO_2 reduction. J. Mater. Chem. A **6**, 18782–18793 (2018). https://doi.org/10.1039/c8ta07430e
168. Huang, J., Mensi, M., Oveisi, E., et al.: Structural sensitivities in bimetallic catalysts for electrochemical CO_2 reduction revealed by Ag–Cu nanodimers. J. Am. Chem. Soc. **141**, 2490–2499 (2019)
169. Wang, L., Higgins, D.C., Ji, Y.F., et al.: Selective reduction of CO to acetaldehyde with CuAg electrocatalysts. Proc. Natl. Acad. Sci. U. S. A. **117**, 12572–12575 (2020). https://doi.org/10.1073/pnas.1821683117
170. Wang, X., Wang, Z.Y., Zhuang, T.T., et al.: Efficient upgrading of CO to C_3 fuel using asymmetric C–C coupling active sites. Nat. Commun. **10**, 1–7 (2019). https://doi.org/10.1038/s41467-019-13190-6
171. Martić, N., Reller, C., MacAuley, C., et al.: $Ag_2Cu_2O_3$—catalyst template material for selective electroreduction of CO to C_{2+} products. Energy Environ. Sci. **13**, 2993–3006 (2020). https://doi.org/10.1039/D0EE01100B
172. Pedersen, J.K., Batchelor, T.A.A., Bagger, A., et al.: High-entropy alloys as catalysts for the CO_2 and CO reduction reactions. ACS Catal. **10**, 2169–2176 (2020). https://doi.org/10.1021/acscatal.9b04343
173. Nellaiappan, S., Katiyar, N.K., Kumar, R., et al.: High-entropy alloys as catalysts for the CO_2 and CO reduction reactions: Experimental realization. ACS Catal. **10**, 3658–3663 (2020). https://doi.org/10.1021/acscatal.9b04302
174. Li, Y.L., Cheng, W.R., Su, H., et al.: Operando infrared spectroscopic insights into the dynamic evolution of liquid-solid (photo) electrochemical interfaces. Nano Energy **77**, 105121 (2020). https://doi.org/10.1016/j.nanoen.2020.105121
175. Gattrell, M., Gupta, N., Co, A.: A review of the aqueous electrochemical reduction of CO_2 to hydrocarbons at copper. J. Electroanal. Chem. **594**, 1–19 (2006). https://doi.org/10.1016/j.jelechem.2006.05.013
176. Schouten, K.J.P., Kwon, Y., van der Ham, C.J.M., et al.: A new mechanism for the selectivity to C1 and C2 species in the electrochemical reduction of carbon dioxide on copper electrodes. Chem. Sci. **2**, 1902 (2011). https://doi.org/10.1039/c1sc00277e
177. Pérez-Gallent, E., Figueiredo, M.C., Calle-Vallejo, F., et al.: Spectroscopic observation of a hydrogenated CO dimer intermediate during CO reduction on Cu(100) electrodes. Angew. Chem.-Int. Edit. **56**, 3621–3624 (2017). https://doi.org/10.1002/anie.201700580
178. Scott, S.B., Hogg, T.V., Landers, A.T., et al.: Absence of oxidized phases in Cu under CO reduction conditions. ACS Energy Lett. **4**, 803–804 (2019). https://doi.org/10.1021/acsenergylett.9b00172
179. Itaya, K.: In situ scanning tunneling microscopy in electrolyte solutions. Prog. Surf. Sci. **58**, 121–247 (1998). https://doi.org/10.1016/s0079-6816(98)00022-7
180. Kim, Y.G., Baricuatro, J.H., Javier, A., et al.: The evolution of the polycrystalline copper surface, first to Cu(111) and then to Cu(100), at a fixed CO_2RR potential: A study by operando EC-STM. Langmuir **30**, 15053–15056 (2014). https://doi.org/10.1021/la504445g
181. Kim, Y.G., Javier, A., Baricuatro, J.H., et al.: Regulating the product distribution of CO reduction by the atomic-level structural modification of the Cu electrode surface. Electrocatalysis **7**, 391–399 (2016). https://doi.org/10.1007/s12678-016-0314-1
182. Tsang, C.F., Javier, A.C., Kim, Y.G., et al.: Potential-dependent adsorption of CO and its low-overpotential reduction to CH_3CH_2OH on Cu(511) surface reconstructed from Cu(pc): Operando studies by seriatim STM-EQCN-DEMS. J. Electrochem. Soc. **165**, J3350–J3354 (2018). https://doi.org/10.1149/2.0451815jes
183. Baricuatro, J.H., Kim, Y.G., Korzeniewski, C.L., et al.: Tracking the prelude of the electroreduction of carbon monoxide via its interaction with Cu(100): Studies by operando scanning

tunneling microscopy and infrared spectroscopy. Catal. Today **358**, 210–214 (2020). https://doi.org/10.1016/j.cattod.2020.01.028
184. Wang, Y.X., Shen, H., Livi, K.J.T., et al.: Copper nanocubes for CO_2 reduction in gas diffusion electrodes. Nano Lett. **19**, 8461–8468 (2019). https://doi.org/10.1021/acs.nanolett.9b02748
185. Wang, Z.N., Yang, G., Zhang, Z.R., et al.: Selectivity on etching: Creation of high-energy facets on copper nanocrystals for CO_2 electrochemical reduction. ACS Nano **10**, 4559–4564 (2016). https://doi.org/10.1021/acsnano.6b00602
186. Loupe, N., Doan, J., Smotkin, E.S.: Twenty years of operando IR, X-ray absorption, and Raman spectroscopy: direct methanol and hydrogen fuel cells. Catal. Today **283**, 11–26 (2017). https://doi.org/10.1016/j.cattod.2016.06.012
187. Lewis, E.A., Kendrick, I., Jia, Q.Y., et al.: Operando X-ray absorption and infrared fuel cell spectroscopy. Electrochim. Acta **56**, 8827–8832 (2011). https://doi.org/10.1016/j.electacta.2011.07.091

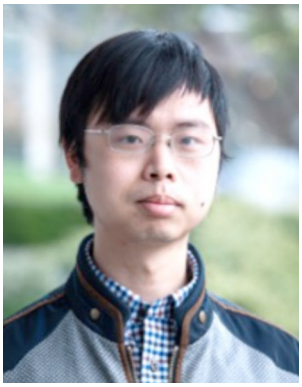

Jingfu He is currently an associate professor in School of Materials, Sun Yat-sen University. He received his PhD in 2012 from University of Science and Technology of China. He joined Berlinguette group at the University of British Columbia as a postdoctoral associate in 2015 and conducted research on CO_2 electrocatalysts and electrolyzer. His current research interests include photoelectrochemistry and electrochemistry for solar energy conversion.

Yuanli Li is currently a PhD candidate in National Synchrotron Radiation Laboratory, University of Science and Technology of China under the supervision of Prof. Shiqiang Wei and Prof. Qinghua Liu. She received her M.E. degree in 2011 from Sichuan University. She joined Southwest University of Science and Technology as an assistant professor in 2013. Her current research interests focus on (photo)electrochemistry of energy conversion nanomaterials and advanced in situ/operando synchrotron radiation experimental techniques.

Aoxue Huang is a PhD candidate in the Berlinguette group at the University of British Columbia. She received her B.S. degree in Chemistry from Wuhan University. Her current research interests include electrocatalysis and electrolyzer design.

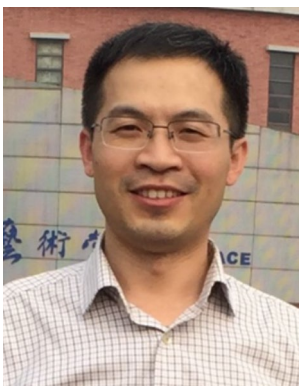

Prof. Qinghua Liu is currently a member of National Synchrotron Radiation Laboratory, University of Science and Technology of China (USTC). He received his PhD in 2009 from University of Science and Technology of China and then did research work on renewable energy conversion and synchrotron radiation experimental techniques. His current research interests focus on the synthesis and characterizations of advanced energy functional nanomaterials for photocatalytic, electrochemical, and photoelectrochemical applications and the development of advanced in situ/operando synchrotron radiation experimental techniques and their applications in energy storage and reaction mechanism.

Prof. Changli Li is an associate professor at the School of Materials, Sun Yat-sen University, China. He received his PhD degree in Mechanical Engineering from the University of Tokyo, Japan, in 2015. After postdoctoral studies at Tsinghua University and The University of British Columbia, he began his independent career as faculty member at Sun Yat-sen University. His research activities focus on the synthesis of nanostructured materials and semiconductor heterojunctions for electrochemical and photoelectrochemical energy conversion.